

AD-A196 876

UNCLASSIFIED

SECURITY CLASSIFICATION OF THIS PAGE (When Data Entered)

DTIC FILE COPY

1

REPORT DOCUMENTATION PAGE		READ INSTRUCTIONS BEFORE COMPLETING FORM
REPORT NUMBER AFIT/CI/NR 88-57	2. GOVT ACCESSION NO.	3. RECIPIENT'S CATALOG NUMBER
TITLE (and Subtitle) THE ION-ASSISTED DEPOSITION OF OPTICAL THIN FILMS		5. TYPE OF REPORT & PERIOD COVERED MS THESIS
AUTHOR(s) JAMES DONALD TARGOVE		6. PERFORMING ORG. REPORT NUMBER
PERFORMING ORGANIZATION NAME AND ADDRESS AFIT STUDENT AT: UNIVERSITY OF ARIZONA		8. CONTRACT OR GRANT NUMBER(s)
11. CONTROLLING OFFICE NAME AND ADDRESS		10. PROGRAM ELEMENT, PROJECT, TASK AREA & WORK UNIT NUMBERS
14. MONITORING AGENCY NAME & ADDRESS (if different from Controlling Office) AFIT/NR Wright-Patterson AFB OH 45433-6583		12. REPORT DATE 1988
		13. NUMBER OF PAGES 194
		15. SECURITY CLASS. (of this report) UNCLASSIFIED
16. DISTRIBUTION STATEMENT (of this Report) DISTRIBUTED UNLIMITED: APPROVED FOR PUBLIC RELEASE		15a. DECLASSIFICATION/DOWNGRADING SCHEDULE
17. DISTRIBUTION STATEMENT (of the abstract entered in Block 20, if different from Report) SAME AS REPORT		
18. SUPPLEMENTARY NOTES Approved for Public Release: IAW AFR 190-1 LYNN E. WOLAVER Dean for Research and Professional Development Air Force Institute of Technology Wright-Patterson AFB OH 45433-6583 19 Jan 88		
19. KEY WORDS (Continue on reverse side if necessary and identify by block number)		
20. ABSTRACT (Continue on reverse side if necessary and identify by block number) ATTACHED		

DTIC
ELECTE
AUG 03 1988
S D

DD FORM 1 JAN 73 1473

EDITION OF 1 NOV 65 IS OBSOLETE

UNCLASSIFIED

SECURITY CLASSIFICATION OF THIS PAGE (When Data Entered)

THE ION-ASSISTED DEPOSITION OF OPTICAL THIN FILMS

by

James Donald Targove

A Dissertation Submitted to the Faculty of the

Committee on Optical Sciences (Graduate)

In Partial Fulfillment of the Requirements
For the Degree of

DOCTOR OF PHILOSOPHY

In the Graduate College

THE UNIVERSITY OF ARIZONA



1987

Accession For	
NTIS CRA&I	<input checked="checked" type="checkbox"/>
DTIC TAB	<input type="checkbox"/>
Unannounced	<input type="checkbox"/>
Justification	
By _____	
Distribution _____	
Availability Codes	
Dist	Availability or Survival
A-1	

STATEMENT BY AUTHOR

This dissertation has been submitted in partial fulfillment of requirements for an advanced degree at The University of Arizona and is deposited in the University Library to be made available to borrowers under rules of the Library.

Brief quotations from this dissertation are allowable without special permission, provided that accurate acknowledgment of source is made. Requests for permission for extended quotation from or reproduction of this manuscript in whole or in part may be granted by the head of the major department or the Dean of the Graduate College when in his or her judgment the proposed use of the material is in the interests of scholarship. In all other instances, however, permission must be obtained from the author.

SIGNED: James Donald Fayart

THE UNIVERSITY OF ARIZONA
GRADUATE COLLEGE

As members of the Final Examination Committee, we certify that we have read
the dissertation prepared by James Donald Targove
entitled The Ion-Assisted Deposition of Optical Thin Films

and recommend that it be accepted as fulfilling the dissertation requirement
for the Degree of Doctor of Philosophy.

H. A. Macleod

6/29/87
Date

[Signature]

[Signature]
Date

[Signature]

6/29/87
Date

[Signature]

Date

[Signature]

Date

Final approval and acceptance of this dissertation is contingent upon the
candidate's submission of the final copy of the dissertation to the Graduate
College.

I hereby certify that I have read this dissertation prepared under my
direction and recommend that it be accepted as fulfilling the dissertation
requirement.

H. A. Macleod
Dissertation Director

6/29/87
Date

ACKNOWLEDGMENTS

This research would not have been possible without the assistance and support of a number of people. I am indebted to them for helping to make my stay at the Optical Sciences Center enjoyable and exciting (sometimes too exciting).

I first wish to thank my advisor, Angus Macleod, for his constant interest and support throughout this project. I was told before reaching the Optical Sciences Center that working for Angus would be a pleasure: I can only say that this was an understatement. I appreciate the extraordinary freedom which I was granted to determine the direction of this research and Angus' willingness to talk with me when I know that he had more pressing things to do.

Mike Jacobson has been a good friend throughout, providing companionship in the wee hours of the morning and helping to keep things running smoothly through bad times and good. His ruthless editing has greatly improved my products, including this dissertation.

A number of fellow students have collaborated in this research, and I am extremely grateful for their help and support. Steve Saxe and Mike Messerly taught me the arts of vacuum and thin film technology from scratch, enduring an often slow learning curve. Linda Lingg and John Lehan helped to perform most of the later research and shared gallons of coffee. Chang-Kwon Hwangbo, Bertrand Bovard (a post-doc), and Chang Cheng Weng (a visiting scholar from Taiwan) were also instrumental in carrying

out many of the experiments. This work could never have been performed without the efforts of all these people.

No experimental project is possible without a great deal of tooling and machining. Ross Potoff has built many items, without which this dissertation would not have been possible. His ability to design and fabricate solutions to many problems never ceases to amaze me, and I appreciate his assistance. Rick Swenson was similarly invaluable in helping me to characterize my samples, instructing me in the operation of various instruments and keeping them running long enough for me to perform the measurements.

I would particularly like to acknowledge Doctor Thomas Allen of OCLI for his interest in this work and his many insightful comments and suggestions. He has often helped us to overcome difficulties by performing measurements and supplying special substrates.

A number of other people have performed measurements, for which I am grateful. Charles Kennemore performed XPS measurements on several MgF_2 and LaF_3 films. Paul Arendt, Marion Scott, and Tom Cordi of the Los Alamos National Laboratory also carried out surface analysis on several samples. Wes Bilodeau of the Department of Geosciences analyzed dozens of films by x-ray diffraction, often on short notice. Professors John Leavitt and Larry McIntyre and their associates in the Department of Physics performed Rutherford backscattering analysis on innumerable films, providing invaluable results which are the crux of much of this work.

Finally, I take pleasure in thanking my wife Susan for her sufferance throughout the last three years. Being married to a student is trying at the best of times: Her

understanding of my erratic schedule and occasional singlemindedness made all this possible, and I love her very much.

This work was primarily sponsored by the Los Alamos National Laboratory under Contract 9-X56-0322C-1 and the Air Force Office of Scientific Research through the University Research Initiative Program. Additional support was provided by OCLI, GCA/Tropel, and TRW.

TABLE OF CONTENTS

	Page
LIST OF ILLUSTRATIONS	ix
LIST OF TABLES	xvi
ABSTRACT	xvii
 CHAPTER	
1. INTRODUCTION	1
2. ION-ASSISTED DEPOSITION	15
Ion Sources	17
Early IAD Research	22
Modification of Film Properties by IAD	24
Metal Oxides	24
Metal Fluorides	29
Metal Nitrides	31
Models for Ion-Assisted Deposition	32
Ion Sputtering of Compounds	32
Thermal Spikes	34
Collision Cascades	36
Ion-Stimulated Sorption	42
3. EXPERIMENTAL METHOD	44
Film Deposition	44
Thin Film Characterization	48
Measurements of Optical Constants	48
Humidity and Boiling Water Tests	56
X-Ray Diffraction	57
Rutherford Backscattering Spectrometry	61
Infrared Transmittance	62
X-Ray Photoelectron Spectroscopy	63

TABLE OF CONTENTS--Continued

	Page
4. THE ION-ASSISTED DEPOSITION OF MAGNESIUM FLUORIDE	67
Deposition Conditions	68
Unbombarded Films	69
Bombarded Films	69
Infrared Water Band Absorption	73
Rutherford Backscattering Analysis	73
Humidity and Boiling Water Tests	80
Color Centers in Magnesium Fluoride	81
5. THE ION-ASSISTED DEPOSITION OF CRYOLITE AND ALUMINUM FLUORIDE	86
Ion-assisted Deposition of Cryolite	87
Ion-assisted Deposition of Aluminum Fluoride	95
6. THE ION-ASSISTED DEPOSITION OF LANTHANUM AND LANTHANIDE (Ce, Nd) TRIFLUORIDES	104
Ion-Assisted Deposition of Lanthanum Fluoride	105
Deposition Conctions	105
Refractive Index and Packing Density	105
Extinction Coefficient	105
Rutherford Backscattering Analysis	112
X-Ray Diffraction	116
X-Ray Photoelectron Spectroscopy	119
Infrared Water Absorption Band	124
Multilayer Coatings	124
Conclusion	127
Ion-Assisted Deposition of Lanthanide Fluorides	130
Cerium Fluoride	131
Neodymium Fluoride	139
Conclusion	146
7. THE ION-ASSISTED DEPOSITION OF ALUMINUM OXIDE	150
Deposition Conditions	151
Unbombarded Films	152
Bombarded Films	153

TABLE OF CONTENTS--Continued

	Page
8. PREPARATION OF ALUMINUM NITRIDE AND OXYNITRIDE THIN FILMS BY ION-ASSISTED DEPOSITION	164
Deposition Conditions	165
Rutherford Backscattering Spectrometry	165
Optical Measurements	169
Annealing Studies	170
Oxynitride Deposition	175
Conclusions	176
9. CONCLUSIONS	178
Ion-Assisted Deposition of Metal Fluorides	178
Ion-Assisted Deposition of Aluminum Oxide	180
Ion-assisted Deposition of Aluminum Nitride	182
Suggestions for Further Research	183
LIST OF ACRONYMS	186
LIST OF REFERENCES	187

LIST OF ILLUSTRATIONS

	Page
1-1. Transmission electron micrograph of a cross-sectional replica of a ZnS-ThF ₄ multilayer structure	3
1-2. Schematic of vacuum chamber configured for DC diode sputtering	6
1-3. Schematic of vacuum chamber configured for RF diode sputtering	7
1-4. Schematic of vacuum chamber configured for RF magnetron sputtering	8
1-5. Schematic of vacuum chamber configured for triode sputtering	9
1-6. Schematic of vacuum chamber configured for ion-assisted deposition	10
1-7. Schematic of vacuum chamber configured for ion cluster beam deposition	11
1-8. Schematic of vacuum chamber configured for ion plating	12
2-1. Basic configuration for ion-assisted deposition	16
2-2. (a) Schematic and (b) electrical connections of a cold-cathode ion source	18
2-3. Energy distributions of ion beams from cold-cathode and hot-cathode ion sources	19
2-4. (a) Schematic and (b) electrical connections of Kaufman hot-cathode ion source	20

2-5. Refractive index at 550 nm of oxygen-ion bombarded ZrO_2 films as a function of ion beam current density	26
2-6. Refractive index at 550 nm of argon-ion bombarded ZrO_2 films as a function of ion beam current density	27
2-7. Various processes which occur during a linear collision cascade	37
2-8. Prevention of void formation by forward sputtering of overhanging atoms	39
2-9. Density of an IAD ZrO_2 film at three stages in its growth. The film is assumed to grow without ion bombardment until $t=0$	40
2-10. Density of IAD ZrO_2 films as a function of ion arrival rate, showing both experimental and calculated values	41
3-1. Schematic of the Optical Sciences Center Balzers BAK 760 box coater configured for ion-assisted deposition	45
3-2. Typical transmittance curve for a single-layer dielectric coating with the auxiliary T_{\min} and T_{\max} curves added	50
3-3. Typical output from a θ - 2θ x-ray diffractometer for a polycrystalline thin film on an amorphous substrate	59
3-4. Typical XPS spectrum, with each peak (or set of peaks) representing an electron orbital	65
4-1. Extinction coefficients of argon- and oxygen-bombarded MgF_2 films for ion fluxes of $20 \mu\text{A}/\text{cm}^2$, with the curve for an unbombarded film included as a reference	71
4-2. Extinction coefficients of argon- and oxygen-bombarded MgF_2 films for ion fluxes of $50 \mu\text{A}/\text{cm}^2$, with the curve for an unbombarded film included as a reference	72
4-3. Infrared transmittance of an unbombarded and an IAD MgF_2 film near the $3 \mu\text{m}$ water absorption band	74

LIST OF ILLUSTRATIONS--Continued

	Page
4-4. Fluorine to magnesium ratio x and anion to cation ratio $x+y$ for argon-bombarded MgF_2 films as a function of the ion to molecule arrival ratio γ	76
4-5. Fluorine to magnesium ratio x and anion to cation ratio $x+y$ for oxygen-bombarded MgF_2 films as a function of the ion to molecule arrival ratio γ	77
4-6. Ultraviolet transmittance of an IAD MgF_2 film after successive thermal anneals, showing the thermal bleaching of the color center absorption band	83
4-7. Ultraviolet transmittance of an IAD MgF_2 film deposited in the same batch with the film of Figure 4-5, showing the effects of a different set of thermal anneals on the transmittance	84
5-1. Ultraviolet transmittance of cryolite films bombarded with 300 eV argon ions	90
5-2. Ultraviolet transmittance of oxygen-bombarded cryolite films	91
5-3. Stoichiometries of IAD cryolite films as a function of ion current density for both oxygen and argon ion bombardment	92
5-4. Ratio of sodium atoms to aluminum atoms in IAD cryolite films as a function of ion beam current density for both oxygen and argon ion bombardment	93
5-5. The fluorine deficiency $(y+z)/(w+3x)$ and the anion deficiency (or surplus) $y/(w+3z)$ of IAD cryolite films as a function of ion beam current density for both oxygen and argon ion bombardment, with the stoichiometry expressed as $\text{Na}_w\text{Al}_x\text{F}_y\text{O}_z$	94
5-6. Transmittance in the visible region of unbombarded and 300 eV argon-bombarded AlF_3 films	98

LIST OF ILLUSTRATIONS--Continued

	Page
5-7. Infrared transmittance of unbombarded and 300 eV argon-bombarded AlF_3 films in the $3\text{ }\mu\text{m}$ water absorption band	99
5-8. Infrared transmittance of unbombarded and 200 eV argon-bombarded AlF_3 films in the $3\text{ }\mu\text{m}$ water absorption band	100
5-9. Transmittance in the visible region of 200 eV argon-bombarded AlF_3 films	101
5-10. Infrared transmittance in the $3\text{ }\mu\text{m}$ water absorption band of IAD AlF_3 films bombarded with $20\text{ }\mu\text{A}/\text{cm}^2$ of argon ions	102
5-11. Transmittance in the visible of IAD AlF_3 films bombarded with $20\text{ }\mu\text{A}/\text{cm}^2$ of argon ions	103
6-1. Index of refraction at 350 nm of LaF_3 films bombarded with 300 and 500 eV argon ions as a function of ion beam current density	107
6-2. Index of refraction at 350 nm of LaF_3 films bombarded with 300 eV argon and oxygen ions as a function of ion beam current density	108
6-3. Packing density of IAD LaF_3 films as a function of ion beam current density for bombardment by 300 eV argon ions	110
6-4. Packing density of IAD LaF_3 films as a function of ion beam current density for bombardment by 500 eV argon ions	111
6-5. Ultraviolet extinction coefficient of IAD LaF_3 films	113

LIST OF ILLUSTRATIONS--Continued

	Page
6-6. F-to-La ratio x and anion-to-cation ratio $x+y$ of IAD LaF_3 films bombarded with 300 eV argon ions as a function of ion beam current density, with the stoichiometry expressed as LaF_xO_y	114
6-7. F-to-La ratio x and anion-to-cation ratio $x+y$ of IAD LaF_3 films bombarded with 300 eV oxygen ions as a function of ion beam current density, with the stoichiometry expressed as LaF_xO_y	115
6-8. X-ray diffraction scans of unbombarded and 300 eV argon-bombarded LaF_3 films	118
6-9. Oxygen 1s XPS peak for an unbombarded LaF_3 film showing the deconvolution of the peak into two Gaussians	121
6-10. Oxygen 1s XPS peak for an IAD LaF_3 film bombarded with 60 $\mu\text{A}/\text{cm}^2$ of 300 eV argon ions showing the deconvolution of the peak into two Gaussians	122
6-11. Oxygen 1s XPS peak for an IAD LaF_3 film bombarded with 100 $\mu\text{A}/\text{cm}^2$ of 300 eV argon ions showing the deconvolution of the peak into two Gaussians	123
6-12. Transmittance of IAD LaF_3 films in the 3 μm water absorption band for varying argon ion beam energies and current densities. The transmittance scale is 45%-65% for each film	126
6-12. Air-to-vacuum shift of a 23-layer conventionally deposited $\text{LaF}_3/\text{MgF}_2$ stack	128
6-14. Air-to-vacuum shift of a 23-layer IAD $\text{LaF}_3/\text{MgF}_2$ stack deposited with the ion beam parameters of Table 1. The shift is less than 1 nm	129

LIST OF ILLUSTRATIONS--Continued

	Page
6-15. Refractive index of unbombarded and 300 eV argon-bombarded CeF_3 films as function of wavelength	133
6-16. Ultraviolet transmittance of unbombarded and 300 eV argon-bombarded CeF_3 films showing the 4f-5d absorption band	134
6-17. Refractive index of unbombarded and 300 eV oxygen-bombarded CeF_3 films as a function of wavelength	136
6-18. Ultraviolet transmittance of unbombarded and 300 eV oxygen-bombarded CeF_3 films showing the 4f-5d absorption band	137
6-19. Fluorine to cerium ratio x and anion to cation ratio x+y of 300 eV argon-bombarded CeF_3 films	138
6-20. X-ray diffraction scans of unbombarded and 300 eV argon-bombarded CeF_3 films	140
6-21. Transmittance of a NdF_3 film showing two 4f-4f absorption bands. There is also a band at 520 nm which is too small to show up in the figure, but which is evident in the original trace	141
6-22. Refractive index of 300 eV argon-bombarded NdF_3 films as a function of wavelength	143
6-23. Refractive index of 500 eV argon-bombarded NdF_3 films as a function of wavelength	144
6-24. Extinction coefficient k for the three NdF_3 films with measurable absorption. All films with smaller ion fluxes have extinction coefficients below the accuracy of the measurement . . .	145

LIST OF ILLUSTRATIONS--Continued

	Page
6-25. Infrared transmittance of 300 eV argon-bombarded NdF_3 films in the $3\text{ }\mu\text{m}$ water absorption band	147
7-1. Transmittance electron micrograph of an unbombarded Al_2O_3 film as deposited (400,000x magnification)	155
7-2. Transmittance electron micrograph of an unbombarded Al_2O_3 film after several minutes of electron bombardment in the electron microscope (400,000x magnification)	156
7-3. Infrared transmittance of unbombarded and IAD Al_2O_3 films in the $3\text{ }\mu\text{m}$ water absorption band	162
8-1. Stoichiometry of aluminum nitride films, expressed in the form AlN_x , as a function of the ratio of nitrogen to aluminum arrival rates γ	168
8-2. Transmittance of typical AlN films deposited by ion-assisted deposition	171
8-3. Transmittance of an AlN film deposited by IAD before and after annealing for 210 minutes at $500\text{ }^\circ\text{C}$	174
8-4. Transmittance of aluminum oxynitride films deposited by IAD	176

LIST OF TABLES

Table	Page
5-1. Densities of Argon-Bombarded IAD Cryolite Films	88
6-1. Deposition Conditions of an IAD $\text{LaF}_3/\text{MgF}_2$ Stack	125
7-1. Optical Constants of Unbombarded Al_2O_3 Films at 350 nm	154
7-2. Optical Constants of IAD Al_2O_3 Films at 350 nm (500 eV Argon Ion Bombardment)	158
7-3. Optical Constants of Al_2O_3 Films at 350 nm with 50% Ar/50% O_2 Bombardment	159
7-4. Optical Constants of IAD Al_2O_3 Films at 350 nm (500 eV Oxygen Ion Bombardment)	161
8-1. Stoichiometries of AlN Films (AlN_xO_y)	166
8-2. Refractive indices of AlN Films ($\lambda = 1\text{-}2\ \mu\text{m}$)	172
8-3. Effect of Annealing on Stoichiometry of AlN_xO_y Films (3.5 hours at 500 °C)	173



ABSTRACT

The columnar microstructure of most thermally evaporated thin films detrimentally affects many of their properties through a reduction in packing density. In this work, we have investigated ion-assisted deposition as a means of disrupting this columnar growth for a number of coating materials.

A Kaufman hot-cathode ion source bombarded thermally evaporated films with low-energy (< 1000 eV) positive ions during deposition in a cryopumped box coater. We have investigated MgF_2 , Na_3AlF_6 , AlF_3 , LaF_3 , CeF_3 , NdF_3 , Al_2O_3 , and AlN .

Argon ion bombardment of the fluoride coatings increased their packing densities dramatically. We achieved packing densities near unity without significant absorption for MgF_2 , LaF_3 , and NdF_3 , while Na_3AlF_6 , AlF_3 , and CeF_3 began to absorb before unity packing density could be achieved. Fluorine was preferentially sputtered by the ion bombardment, creating anion vacancies. The films adsorbed water vapor and hydroxyl radicals from the residual chamber atmosphere. These filled the vacancy sites, eliminating absorption in the visible, but the oxygen complexes caused increased absorption in the ultraviolet. For LaF_3 and NdF_3 , a sufficient amount of oxygen caused a phase transformation from the fluoride phase to an oxyfluoride phase. *These. Argon*

The refractive indices of Al_2O_3 films increased with ion bombardment. Values as high as 1.70 at 350 nm were achieved with bombardment by 500 eV oxygen ions. Since

all of the Al_2O_3 films had packing densities near unity and were amorphous, we postulate that the increase in refractive index was due to a change in amorphous networking.

Aluminum nitride was deposited by bombarding thermally evaporated aluminum with nitrogen ions. Films with N:Al ratios of 0.5-1.5 could be deposited by varying the deposition conditions. Films with low absorption for wavelengths longer than $1\text{ }\mu\text{m}$ could be deposited. Annealing the films at $500\text{ }^\circ\text{C}$ eliminated absorption at wavelengths longer than 500 nm .

CHAPTER 1

INTRODUCTION

Thin film coatings are an important part of the optics industry today, with literally acres of coatings deposited every year--mainly onto camera lenses and architectural glass (Baumeister 1985). These coatings, usually microns or less in thickness, are used to modify the optical properties of the materials onto which they are deposited.

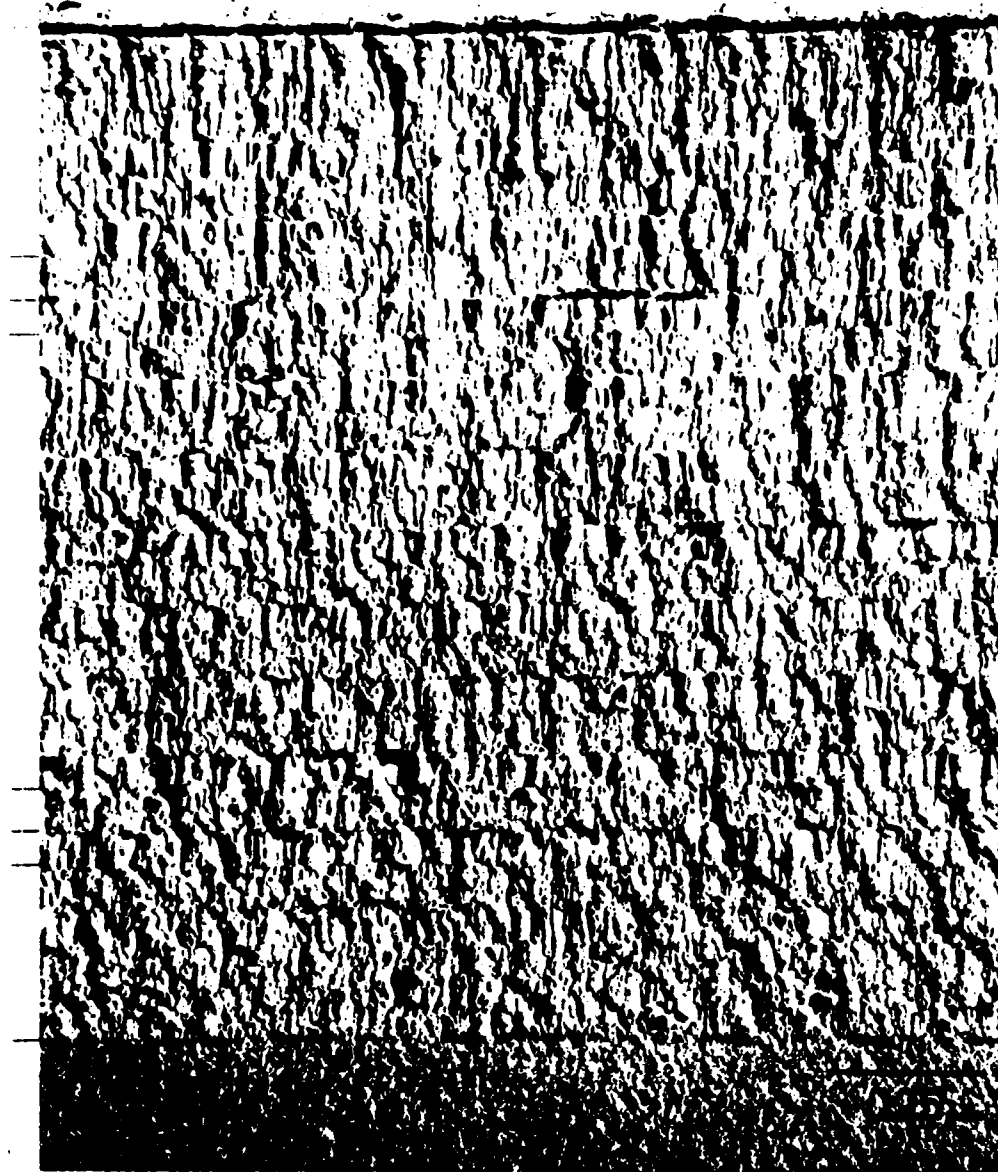
The great majority of these coatings are deposited by physical vapor deposition (PVD). The coating material is heated in high vacuum (10^{-5} mbar or less) to a temperature sufficient to raise its vapor pressure to 10^{-2} mbar (normally 1000-2500 °C). This material may evaporate from a liquid state or sublime from the solid. Substrates are then placed a distance less than or equal to the mean free path of the evaporant from the source. This evaporant then condenses on the substrates, forming a thin film.

An obvious question at this point is, "What is a thin film?" The optical thickness (physical thickness times refractive index) of a thin film is typically on the order of the wavelength of light in the spectral region of interest. This ensures that interference effects are present between the waves reflected from the interfaces, a necessary prerequisite if the film is to modify the light passing through, or reflected from, the

optic. For this reason, these coatings are often referred to as interference coatings. Many layers of different or alternating materials may be sequentially deposited onto the substrates to allow the spectral properties of the substrate-film system to be tuned very accurately.

These coatings are usually, to first order, designed under the assumption that they are composed of homogeneous slabs of coating material stacked one upon another. This assumption greatly simplifies thin film design. We know, however, that thin films are far from ideal. The most striking evidence are the superb transmission electron micrographs of Karl Guenther (Guenther and Pulker 1976). Figure 1-1 shows the cross-section of a typical multilayer thin film. We can see that the layers of the coating consist of vertical columns with void areas in between. These voids have a profound influence on all film properties.

When the coating chamber is vented to atmosphere after deposition, the voids partially fill with condensed water vapor. This fact alone has numerous implications. The water changes the effective refractive index of the thin film, a factor which must be taken into account during coating design. Changes in relative humidity can even change the refractive index after the film is exposed to air. The additional surface area subject to attack by moisture can also reduce the environmental stability of the coating, an important concern if a coating is to be inaccessible in a system such as an optical communications cable. Finally, adsorbed water may be of concern if the coating is subject to extreme photon fluxes, such as in laser resonator mirrors. The light may even couple into the water, lowering the damage threshold of the coating.



Cross-Section of a ZnS/ThF₄- $\lambda/4$ multilayer ($T_S \sim 30^\circ\text{C}$)

Figure 1-1. Transmission electron micrograph of a cross-sectional replica of a ZnS-ThF₄ multilayer structure (Guenther and Pulker 1976).

The above remarks assume a microstructure of columns and voids; we have not yet addressed the shape of the columns. If the columns were uniform in the direction perpendicular to the film surface, the effective refractive index of the coating would at least be uniform in that direction. We know from measurements, however, that the refractive index of thin films is inhomogeneous in this direction, suggesting that the packing density of the films is not uniform. While controlled inhomogeneity can lead to interesting thin film designs (Jacobsson, 1975), inhomogeneity is normally very undesirable; particularly since most thin film design programs cannot handle inhomogeneous layers.

What then can be done to improve PVD thin films? The key is to disrupt the columnar microstructure, densifying the films; the densification of the films will improve the homogeneity and decrease the water content of the films. A guide to this film modification is provided by the structure-zone model of Movchan and Demchishin (1969). It shows that films deposited onto substrates with temperatures below one-third of the evaporant melting temperature--the typical case for PVD--possess a columnar microstructure, while films deposited at higher temperature have a denser microstructure. While higher temperatures are not in general feasible, we can increase the effective energy of the growing film by a number of ion-based processes which increase the effective energy of the impinging species to 0.1 eV or more, equivalent to a temperature greater than 1000 K. Thornton (1974) has extended the structure-zone model to the case of sputtering by including the chamber pressure as a second parameter.

A great variety of these "high energy" deposition processes have been developed over the years. Figures 1-2 through 1-8 show typical chamber configurations for these methods. The goal of all these methods is to disrupt the columnar microstructure through the bombardment of the growing film by energetic particles: These particles can be either the film constituents or other species such as argon.

Most of these methods produce excellent films, although the various methods obviously have their own unique advantages and disadvantages. If a coating operation is to be started from scratch, many of these methods might be suitable. As stated above, however, an enormous capital base exists for thermal evaporation throughout the optics industry. While it may be possible to modify thermal evaporation equipment for sputtering, much of the evaporation knowledge base would then be irrelevant, sending the coater back to the bottom of a learning curve. It is therefore preferable to develop an energetic deposition process which can retain this evaporation knowledge base; ion-assisted deposition (IAD) fills this requirement.

Ion-assisted deposition involves the bombardment of a thermally evaporated film by an ion beam during deposition. In this way, the thermal evaporation data base is preserved while the ion bombardment modifies the film structure. Modifying a traditional coating plant for ion-assisted deposition simply requires the addition of an ion source, with its electrical and gas feedthroughs, in the chamber.

The first portion of this work deals with the ion-assisted deposition of a number of metal fluoride coating materials. Fluorides are useful optical materials, transmitting from the ultraviolet to the infrared (Pulker 1979). They can be evaporated by either

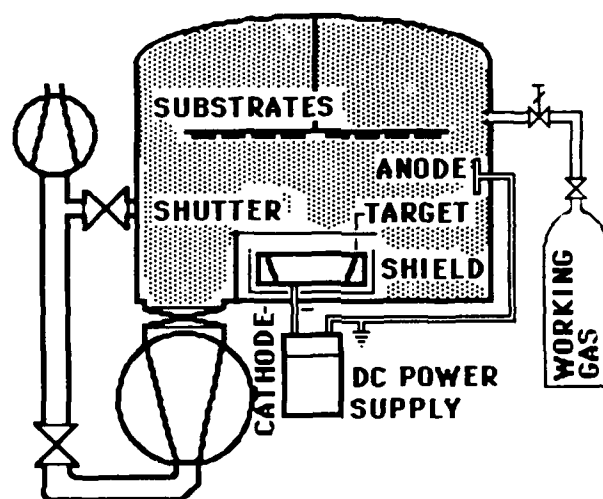


Figure 1-2. Schematic of vacuum chamber configured for DC diode sputtering (Jacobson 1987).

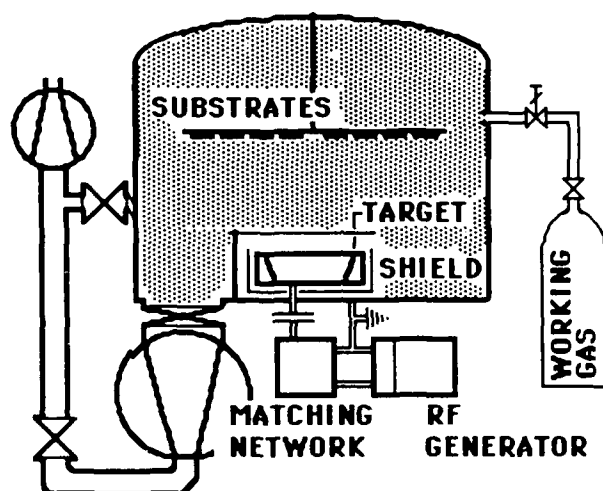


Figure 1-3. Schematic of vacuum chamber configured for RF diode sputtering (Jacobson 1987).

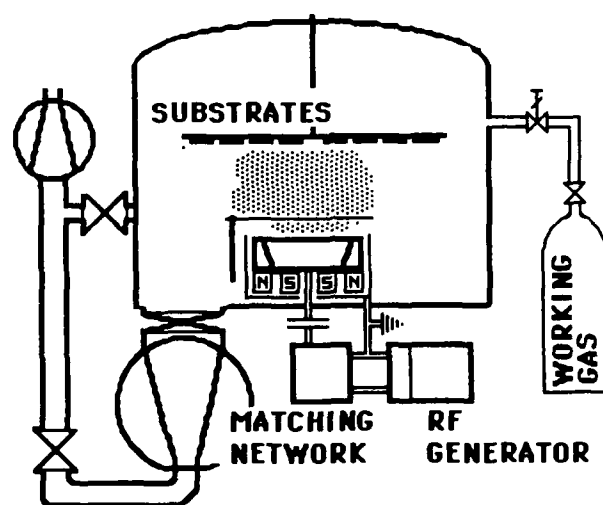


Figure 1-4. Schematic of vacuum chamber configured for RF magnetron sputtering (Jacobson 1987).

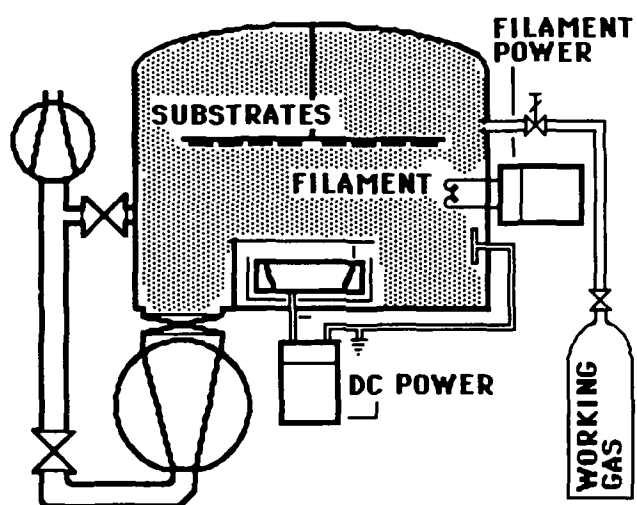


Figure 1-5. Schematic of vacuum chamber configured for triode sputtering (Jacobson 1987).

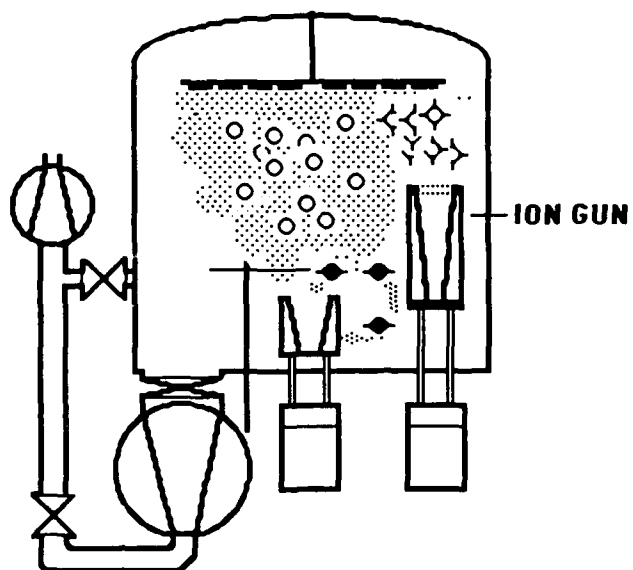


Figure 1-6. Schematic of vacuum chamber configured for ion-assisted deposition (Jacobson 1987).

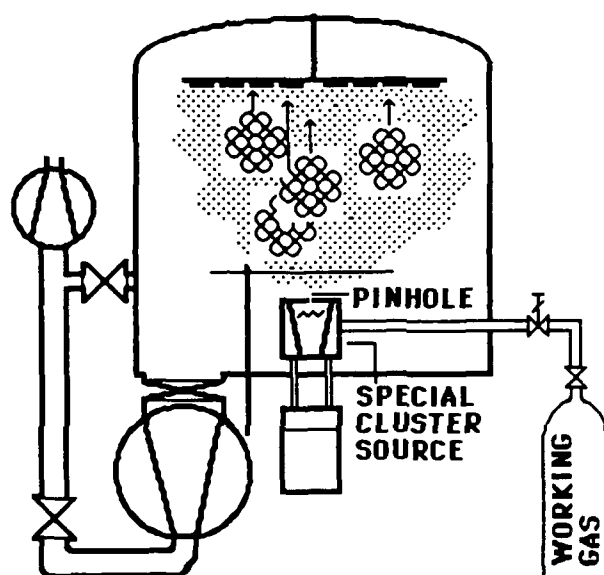


Figure 1-7. Schematic of vacuum chamber configured for ion cluster beam deposition (Jacobson 1987).

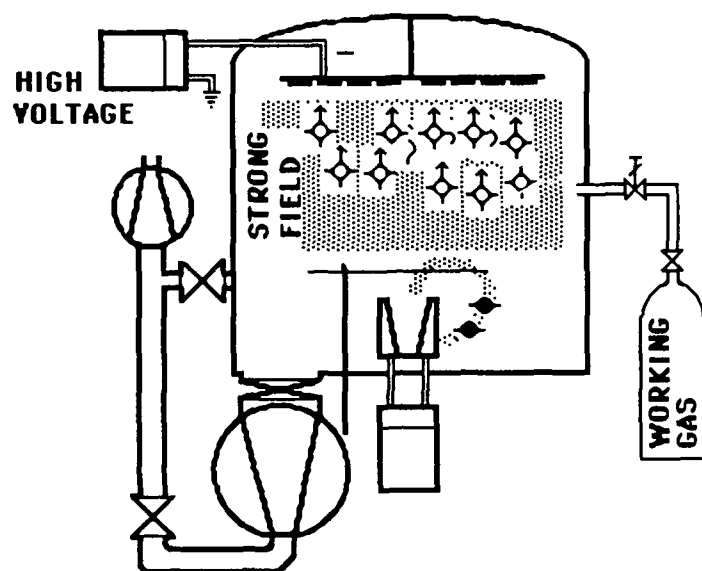


Figure 1-8. Schematic of vacuum chamber configured for ion plating (Jacobson 1987).

resistive or electron-beam evaporation. However, they suffer from two major problems:

1) Fluorides normally form films with packing densities of 80% or less when deposited onto substrates at room temperature (Ogura 1975). While packing density is increased by heating the substrates to several hundred degrees Celsius, this decreases the productivity of a coating plant; also, some types of substrates--including ultraflat surfaces and plastics--cannot safely be heated to high temperatures.

2) Thin films of many fluorides exhibit high tensile stress; magnesium fluoride is the classic example. Thicker films of these materials crack or delaminate from the substrate as a result, making these materials impractical for infrared applications where a quarter-wave film is a μm or more thick.

For this work, we have prepared MgF_2 , AlF_3 , Na_3AlF_6 , LaF_3 , CeF_3 , and NdF_3 films by IAD. We will show that many thin film properties can be improved by IAD; however, problems will also appear. The principal disadvantage is the additional absorption that appears in the ultraviolet when films are bombarded with large ion fluxes. This can always be alleviated by decreasing the ion flux or energy, but it may not then be possible to modify the film properties to the desired extent.

We next will discuss the ion-assisted deposition of aluminum oxide (Al_2O_3).

Aluminum oxide is an excellent coating material, with high transmittance from 200 nm to 7 μm (Pulker 1979). Aluminum oxide films are also very hard, and typically have packing densities near one. They do, however, sometimes suffer from poor moisture resistance (Rainer et al. 1985). An obvious question is, "Why deposit aluminum oxide

by IAD in the first place?" Aluminum oxide was investigated because a study by Ebert (1982) of the activated reactive evaporation of a number of oxides suggested that aluminum oxide was the only material which showed an increase in absorption when deposited in this manner. It was hoped that a thorough investigation would shed some light on this discrepancy. The work reported here continues that previously reported by Saxe (1985). We will see that IAD does have beneficial effects on aluminum oxide and that it can actually decrease absorption.

The previous topics involve the modification of compounds deposited by thermal evaporation. Another possibility for IAD is the synthesis of materials, such as nitrides, which cannot be deposited thermally. We will describe the synthesis of aluminum nitride by bombarding thermally evaporated aluminum with nitrogen ions during growth. Dielectric films were produced, but the optical properties were worse than films deposited by diode sputtering (Pawlewicz et al. 1986); annealing greatly improved these films.

CHAPTER 2

ION-ASSISTED DEPOSITION

Ion-assisted deposition (IAD) has been extensively examined as a means of modifying many properties of thermally evaporated thin films, including packing density, refractive index, stress, adhesion, and environmental stability. Many of these properties are manifestations of the porosity inherent in columnar microstructure. Ion bombardment apparently can disrupt this columnar structure, increasing the packing density of thin films (Macleod 1986).

Ion-assisted deposition is a very straightforward modification of thermal evaporation. An ion source is simply added to the vacuum chamber, bombarding the growing films (Figure 2-1). Our definition of IAD will include only that work done with broad-beam ion sources: a large body of work has also been performed at energies of tens of keV or higher using small-area sources. These discussions will necessarily be incomplete, but will summarize the current understanding of the IAD process and its capabilities. Several excellent reviews have appeared (Martin 1986; Macleod 1986; Gibson 1986; Martin and Netterfield 1986), and are recommended to the reader interested in a broader coverage of ion-based processes.

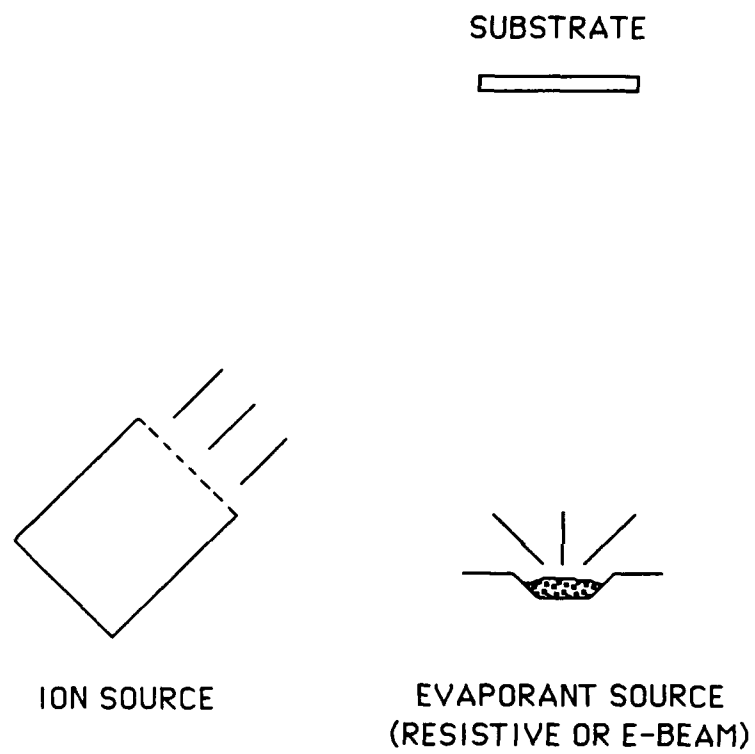


Figure 2-1. Basic configuration for ion-assisted deposition.

Ion Sources

The availability of compact, commercial ion sources has been instrumental to the interest in ion-assisted deposition. These sources by and large fall into two categories: cold-cathode and hot-cathode sources.

Much of the early IAD work was done with cold-cathode (also known as hollow-cathode) sources (Ebert 1982; Allen 1982). These generate a discharge between a cylindrical cathode and a wire filament anode (Figure 2-2) due to the potential gradient between the two, with the working gas admitted through a gap in the cathode. The ion beam is extracted through a hole in this discharge chamber by the electric field of the extraction electrodes. This source has the advantage of having no hot filaments, and therefore can run for indefinite periods with reactive gases such as oxygen. The main disadvantage is that the ion beam has an almost continuous energy distribution (Figure 2-3). This might be satisfactory in a production environment, but it makes careful experimentation very difficult. These sources have therefore been supplanted, at least in research laboratories, by hot-cathode sources.

The hot-cathode ion source was originally invented by Kaufman for NASA as a possible space propulsion system (Kaufman, Cuomo, and Harper 1982) and is therefore often called the "Kaufman" source. A heated metal filament cathode (usually tungsten or tantalum) emits thermal electrons in a discharge chamber formed by a cylindrical anode (Figure 2-4). The electrodes ionize the working gas atoms or molecules, creating a plasma. The ions produced in this form of discharge predominantly have a single positive charge, although some atoms are doubly-ionized. An optional magnetic field provided by

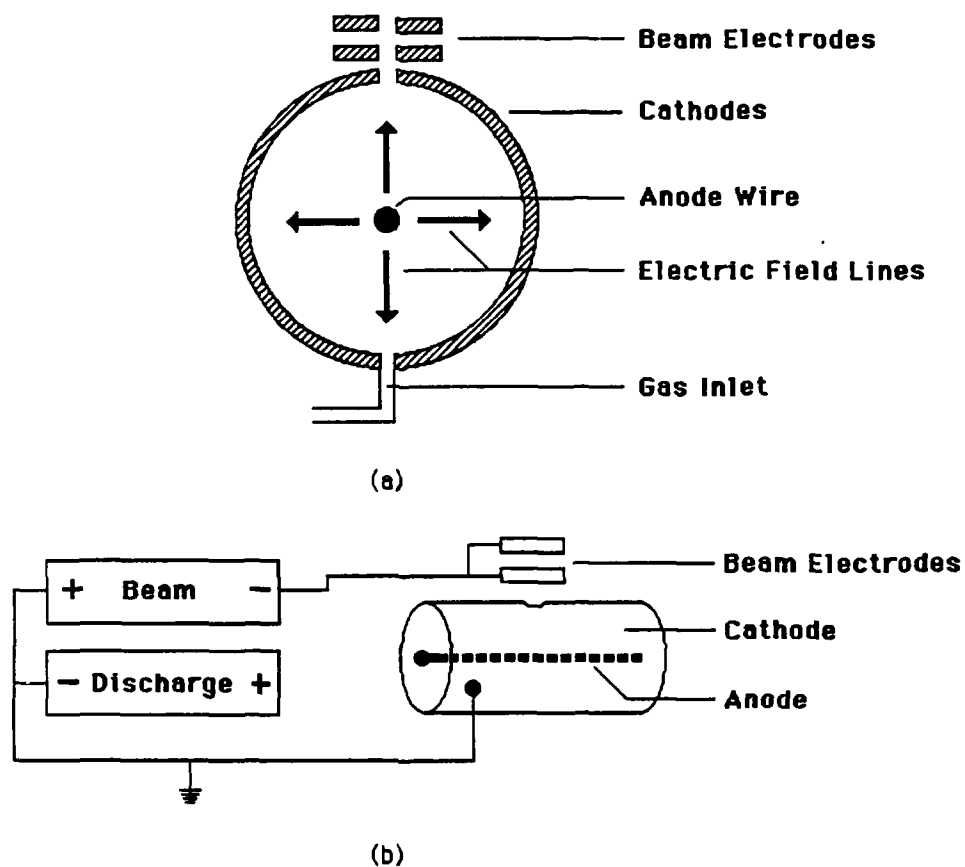


Figure 2-2. (a) Schematic and (b) electrical connections of a cold-cathode ion source (after Saxe 1985).

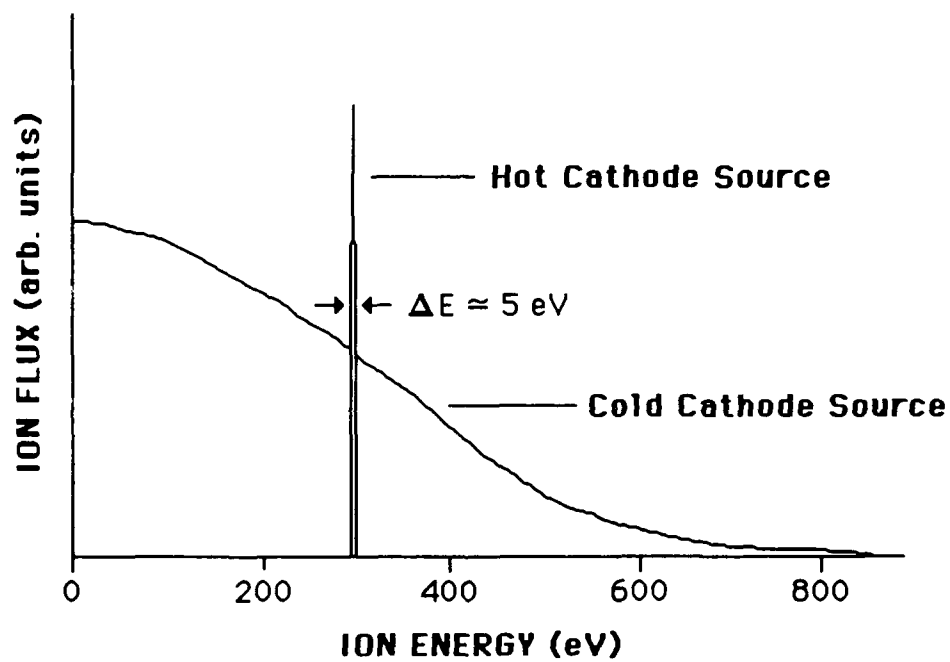
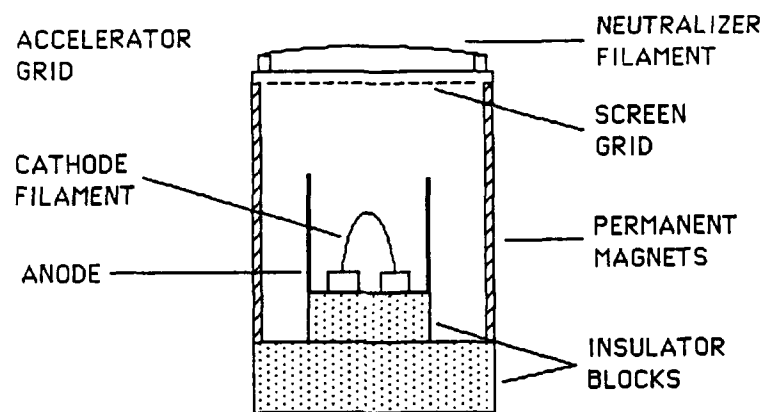
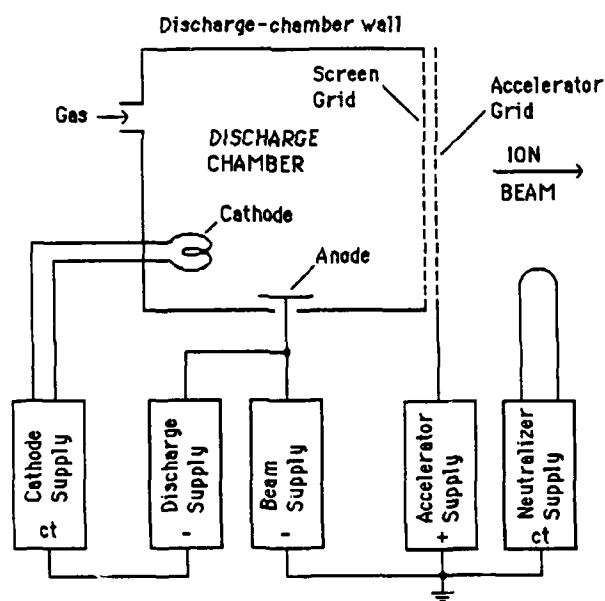


Figure 2-3. Energy distributions of ion beams from cold-cathode and hot-cathode ion sources (McNeil et al. 1984).



(a)



(b)

Figure 2-4. (a) Schematic and (b) electrical connections of Kaufman hot-cathode ion source (Kaufman 1984).

either permanent or electromagnets increases the time the electrons spend in the discharge chamber by deflecting their paths into spirals around the magnetic field lines, increasing their ability to ionize the working gas.

In the dual-grid source design used in this research, the ionized working gas exits the discharge through an electrically insulated screen grid. This grid is effectively at the discharge chamber voltage. The ions then are accelerated by the second, or accelerator grid, which is at a negative voltage relative to the discharge, to the desired beam energy. A second hot filament, called the neutralizer, emits electrons which give the beam a net neutral charge. It is important to note that the beam still consists of positive ions and electrons, but that equal numbers of the two are present. This neutralization prevents charging effects when insulating substrates and coating materials are used. Unfortunately, the filament must be immersed in the ion beam for proper neutralization to occur; otherwise, a space-charge layer forms at the edge of the plasma and limits the number of electrons which can enter the ion beam. Sputtering of the filament therefore is a source of film contamination. Hollow cathode and plasma bridge neutralizers have been developed to solve this problem by eliminating the filament.

The main disadvantage of the Kaufman source is the presence of hot metal filaments, which have drastically shortened lifetimes with reactive gases because of accelerated erosion, and which can cause heavy metal contamination in the films. The principal advantage of this source is the almost monoenergetic energy of the resultant ion beam. This well-characterized beam is very important for experiments on the nature of the IAD process.

A major concern with molecular gases is whether the resulting ions are atomic or molecular. Other groups have shown, with Kaufman sources similar to ours, that both oxygen (McNeil et al. 1984) and nitrogen (Van Vechten, Hubler, and Donovan 1986) ion beams are predominantly molecular in nature. We will use this result in our analysis, but will not verify it in our setup.

Early IAD Research

The first report on the ion-assisted deposition of optical thin films was probably the work of Hirsch and Varga (1978,1980). They observed that the bombardment by argon ions of thick germanium films grown on glass could relieve the cracking caused by germanium's large intrinsic stress. They concluded that the stress was relieved by an annealing process, and that the adhesion was being increased by an ion mixing process at the film-substrate interface. This work will be discussed further in the next section.

Three other groups reported IAD work in 1982 at a meeting of the Society of Photo-Instrumentation Engineers (SPIE). Ebert (1982) reported the activated reactive evaporation of metal oxides, with negatively-ionized oxygen being created by a hollow cathode ion source. The ionized oxygen, which generally had ion energies below 100 eV, was more effective than neutral oxygen in decreasing the absorption of the oxide films, usually by a factor of approximately three. The lone exception was Al_2O_3 , which showed an increase in absorption. Using this technique, a reflectivity of 99% was achieved at 193 nm with 35 layers of BeO and SiO_2 .

Herrmann and McNeil (1982) at the same meeting reported the ion-assisted deposition of durable MgF_2 films with slight absorption ($< 0.5\%$) in the visible. These films were deposited at a substrate temperature of approximately 50°C , with bombardment by $50 \mu\text{A}/\text{cm}^2$ of 700 eV argon ions. Also, 51-layer $\text{ThF}_4/\text{AlF}_3$ films with low absorption which did not delaminate were deposited with oxygen ion bombardment.

The third paper on IAD at the conference was by Allen (1982), who reported the IAD of TiO_2 and SiO_2 films with a hollow cathode ion source similar to Ebert's. The SiO_2 films decreased in refractive index as ion current increased, and both the bombarded and unbombarded films had no measurable absorption in the visible. Laser calorimetry at $1.06 \mu\text{m}$ showed a decrease in absorbance to only 10 ppm with bombardment. In contrast, the TiO_2 films displayed an increase in refractive index with increasing ion current, while the extinction coefficient of the films decreased from 1.5×10^{-3} to 1.5×10^{-4} at 550 nm with bombardment. Allen also performed attenuated total reflectance measurements of SiO_2 films in the infrared to study the packing densities of the films. The unbombarded film had an absorption band near $3 \mu\text{m}$ due to water in the film, while the bombarded film had virtually no absorption in this region.

The next major contribution in this field was by Martin et al. (1983). They surmised that ion bombardment might improve the mobility of condensing adatoms, promoting the growth of denser films (Macleod 1986). Although this mobility effect is no longer considered the most likely result of IAD, they succeeded in greatly improving

the properties of multilayers of SiO_2 and TiO_2 or ZrO_2 . They showed that $\text{ZrO}_2/\text{SiO}_2$ filters which exhibited no measurable vacuum-to-air shift upon venting the vacuum chamber could be deposited with ion bombardment.

Modification of Film Properties by IAD

Since 1983, there has been a flurry of activity in IAD research, including the work reported in this dissertation. Many groups have investigated the ion-assisted deposition of a wide range of materials, including a variety of metal oxides, fluorides and nitrides, as well as the metals themselves (Martin 1986). This work has shown that ion bombardment can improve some properties of almost all thin film materials; however, there has been relatively little investigation into the nature of the IAD process itself. In this section we will, in a necessarily incomplete manner, discuss the optical materials which have been investigated with IAD, and in so doing present the reported improvements in film properties. It is important to realize that much of this work has been published subsequent to the start of this dissertation research in 1984.

Metal Oxides

The bulk of the IAD literature has centered on the transition metal oxides, particularly ZrO_2 , TiO_2 , and SiO_2 , commonly used in the coating industry. ZrO_2 and TiO_2 are very prone to columnar growth, and IAD was therefore an obvious means of improving their properties.

Zirconium Dioxide. ZrO_2 has, as mentioned above, been studied by Martin et al.

(1983, 1984a). They showed that, for a ZrO_2 deposition rate of 0.8 nm/sec, the refractive indices of the films could be increased by 1200 eV oxygen ion bombardment to 2.18 at 550 nm, approximately the index of bulk ZrO_2 (Figure 2-5). This effect saturated for ion current densities greater than $100 \mu\text{A}/\text{cm}^2$. For 600 eV argon ion bombardment, the index could only be raised to 2.138 for an ion current density of $40 \mu\text{A}/\text{cm}^2$ (Figure 2-6). For higher current densities, the index decreased because of the preferential sputtering of oxygen and the implantation of argon in the films.

Titanium Dioxide. This is another high index coating material which is popular in the visible. It forms hard, transparent coatings, but is very difficult to deposit reproducibly. Allen's initial experiments with negative ions have been discussed above. His later experiments with a Kaufman ion source (Martin 1986) showed that the refractive index at 550 nm could be increased from 2.3 to 2.45 by bombardment with 300 eV oxygen ions at an arrival rate of 0.12 ions/molecule.

McNeil et al. (1984, 1985) have investigated the difference between low- and high-energy oxygen-ion bombardment using a Kaufman ion source. Both 60 and 500 eV oxygen ions were used to bombard films grown at 0.2-0.5 nm/sec onto ambient (50-100 °C) and 250 °C substrates. They observed that 500 eV ions were quite effective at 250 °C, increasing the index from 2.3 for no bombardment to 2.5 for $30 \mu\text{A}/\text{cm}^2$ of ions with virtually no increase in absorption. For ambient temperature substrates, however, 500 eV ions could only increase the index to 2.3, with the films

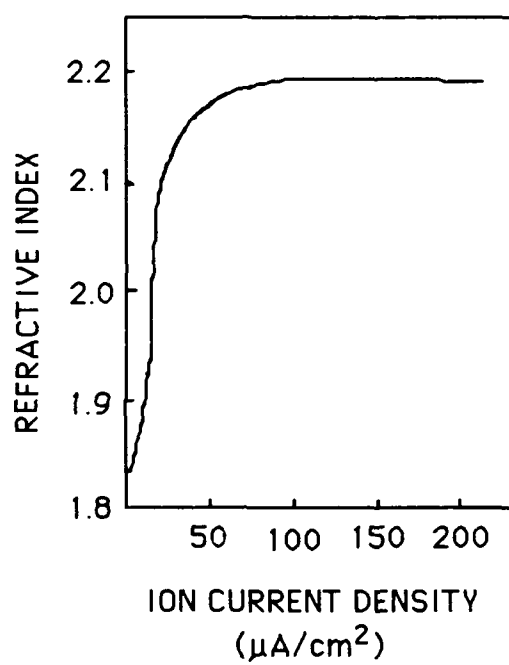


Figure 2-5. Refractive index at 550 nm of oxygen-ion bombarded ZrO₂ films as a function of ion beam current density (Martin 1986).

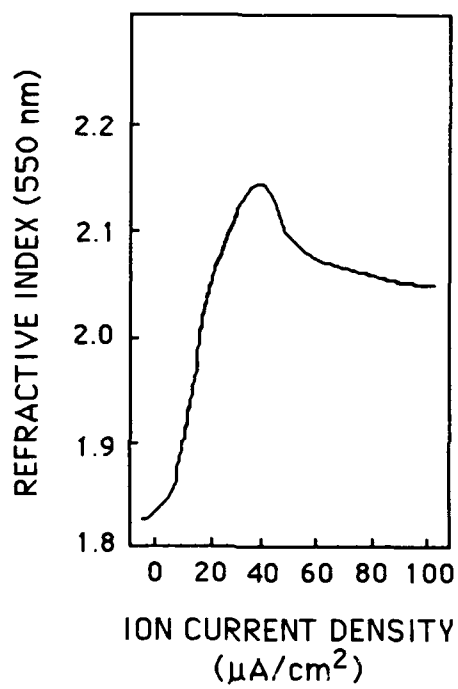


Figure 2-6. Refractive index at 550 nm of argon-ion bombarded ZrO_2 films as a function of ion beam current density (Martin 1986).

then beginning to absorb. 60 eV ions were then tried; at 250 °C, the index increased to 2.4 with no increase in absorption for an ion current density of $240 \mu\text{A}/\text{cm}^2$. At ambient temperature, however, the index increased to only 2.2 for an ion current density of $120 \mu\text{A}/\text{cm}^2$. Nuclear reaction analysis showed that the 500 eV ions significantly reduced the amount of hydrogen, and therefore water, in the films, while 60 eV ions had little effect. It therefore appears that, while low-energy ions increased the refractive index somewhat without an increase in absorption, they did not result in a packing density near unity. Higher-energy ions could cause absorption at ambient temperatures, but appear to increase packing density to a greater extent.

Silicon Dioxide. SiO_2 is the standard low-index material for oxide multilayer coatings in the visible and ultraviolet. Allen's hollow cathode work was mentioned above; his Kaufman source work (Martin 1986) shows that the refractive index could be raised from 1.45-1.5 to 1.55-1.6 by argon or oxygen ion bombardment. No added absorption was observed, suggesting that no appreciable preferential sputtering of oxygen occurred.

McNally, Williams, and McNeil (1986) have also examined SiO_2 deposited onto 275 °C substrates. They observed no change in refractive index with 300 and 500 eV oxygen ion bombardment, but observed a decreased transmittance shift after a humidity test when the films were ion-bombarded.

Other Metal Oxides. Similar results have been reported for CeO_2 (Netterfield et al. 1985), Al_2O_3 (McNally et al. 1986), and Ta_2O_5 (McNally et al. 1986) films. The

basic result in all these experiments was that the refractive indices could be increased markedly by oxygen ion bombardment.

Metal Fluorides

Metal fluoride films have been widely applied because many are transparent over a wide wavelength range, from the infrared to the ultraviolet. Because of their low packing densities and large stresses, however, their thicknesses must be limited; this situation can be improved by high temperature depositions. Herrmann and McNeil (1982) first attempted the ion-assisted deposition of fluorides, mentioning explicitly MgF_2 , AlF_3 , ThF_4 , and Na_3AlF_6 . No quantitative results were quoted. They simply reported that MgF_2 films bombarded with 700 eV argon ions withstood a humidity test which conventional films deposited at ambient temperature failed, and that a 51-layer $\text{AlF}_3/\text{ThF}_4$ multilayer was deposited without delamination.

Most of the literature on the IAD of fluorides has centered on magnesium fluoride. MgF_2 is a popular low-index material which commonly serves as a single-layer antireflection coating on glass in the visible. Unfortunately, substrates must be heated to approximately 300 °C before the coatings become sufficiently durable for commercial applications. Kennemore and Gibson (1985) first investigated the ion-assisted deposition of MgF_2 as a means of antireflecting plastics, which cannot be heated to sufficiently high temperatures for conventional deposition. The adhesion of films deposited onto ambient-temperature quartz substrates was greatly improved by

bombardment by $50 \mu\text{A}/\text{cm}^2$ of 150 eV argon ions. A similar bombardment (the exact deposition conditions were not stated) showed that the transmittance in the visible was not significantly affected, but that the ultraviolet absorption edge shifted to slightly longer wavelengths with ion bombardment. This would not be detrimental with plastic substrates whose own absorption edges would dominate the ultraviolet transmittance. They also pointed out that ion bombardment caused preferential sputtering of fluorine from the films, with $33 \mu\text{A}/\text{cm}^2$ of 150 eV argon ions reducing the stoichiometry to $\text{MgF}_{1.86}$, compared to $\text{MgF}_{1.93}$ for the unbombarded film.

From 1984 to 1985, our group at the Optical Sciences Center also investigated MgF_2 as a candidate material for ultraviolet laser optics. Saxe (1985) and Messerly (1987) have already published much of this data, with the remainder presented here in Chapter 4. Their conclusions were that bombardment with 300 eV oxygen or argon ions could increase the packing density of MgF_2 films to bulk values. Messerly actually measured the physical density of argon-bombarded films, showing that it agreed with the bulk value to within the uncertainty of the measurement.

Martin and Netterfield (1985) performed similar research, reporting that oxygen ions can increase the packing density of MgF_2 films without any increase in absorption in the visible, while argon ions caused approximately 1.5% absorption at 550 nm.

More recently, Gibson and Kennemore (1986) demonstrated that bombardment with freon (C_2F_6) can replace the fluorine sputtered from the films, thereby reducing

the absorption due to fluorine deficiency without increasing the oxygen content of the films. They also discovered that the use of a base vacuum lower than 5×10^{-7} torr greatly reduced the water incorporation in the films, but at the expense of increased absorption.

Martin et al. (1987) have very recently reported further work on the vacuum ultraviolet optical properties of MgF_2 films. They concluded that oxygen bombardment degraded the vacuum ultraviolet transmittance, while argon bombarded films were comparable to typical unbombarded MgF_2 films. They also showed, however, that unbombarded films deposited at 449°C had the best observed vacuum ultraviolet optical performance.

The work contained in Chapters 4, 5, and 6 of this dissertation continues this investigation of the ion-assisted deposition of fluorides.

Metal Nitrides

Nitride films cannot be deposited by traditional thermal evaporation: Ion-based processes are therefore employed. Martin, Netterfield, and colleagues have reported the ion-assisted deposition of both TiN (Martin et al. 1984b) and Si_3N_4 (Netterfield, Martin, and Sainty 1986). TiN is an important selective absorber for solar applications and forms a hard, wear-resistant coating. The films were synthesized by bombarding electron-beam evaporated titanium in a nitrogen atmosphere with either argon or nitrogen ions (Martin et al. 1984b). The substrates were maintained at room temperature or at 300°C . Films were deposited of the characteristic gold color

associated with TiN. The authors assumed that the mechanism for film formation was ion-stimulated sorption. This process will be discussed in the next section.

Si_3N_4 was deposited in the same way, with electron-beam evaporated silicon deposited in a nitrogen atmosphere with nitrogen ion bombardment (Netterfield et al. 1986). With bombardment by $30 \mu\text{A}/\text{cm}^2$ of 60 eV ions, a Si_3N_4 film with refractive index 1.934 and extinction coefficient $< 3.5 \times 10^{-6}$ was deposited at a rate of 0.08 nm/sec. Raising the ion energy to 100 eV raised the extinction coefficient to 5×10^{-4} .

We will discuss the ion-assisted deposition of aluminum nitride (AlN) in Chapter 8.

Models for Ion-Assisted Deposition

Ion-assisted deposition was first conceived as a means of increasing the adatom mobility of thermally evaporated films. Until very recently, however, there has been no consistent explanation of the dominant mechanisms at work during IAD. There are three principal regimes of ion-solid interaction which have been associated with IAD: Thermal spikes, collision cascades, and ion-stimulated sorption. Some of the basic tenets of sputtering theory are also relevant to the IAD process and will be discussed below.

Ion Sputtering of Compounds

While sputtering atoms from the thin film during IAD is not our intention, it is unavoidable with ion bombardment. A very successful theory has been developed by Sigmund (1969) for low-energy (1 keV and below) sputtering of elemental solids. The

sputtering yield (atoms sputtered/ion) can be expressed as

$$Y(E) = 0.3 \frac{m_1 m_2}{(m_1 + m_2)^2} \alpha \left(\frac{m_2}{m_1} \right) \frac{E_0}{U_0}$$

where m_1 and m_2 are the masses of the incident ion and target atom, respectively,

$\alpha(m_2/m_1)$ is a function valued between 0.15 and 1.5, E_0 is the ion energy, and U_0 is the binding energy of the target atom.

The sputtering of compounds is a much more difficult problem, and no successful analytical theory has been developed. In this work, the absolute sputtering yields of the constituent species are less important than their ratio. This ratio can be expressed in the form (Sigmund 1981)

$$\frac{Y_1}{Y_2} = \frac{c_1}{c_2} \left(\frac{m_2}{m_1} \right)^{2n} \left(\frac{U_{02}}{U_{01}} \right)^{1-2n}$$

where Y_i is the sputtering yield of the i 'th constituent, c_i is its atomic concentration

($\sum c_i = 1$), m_i is its mass, and U_{0i} is its surface potential in the compound. In a

compound, the ratio of potentials can be approximated by the ratio of coordination

numbers of the species. The exponent n is typically between 0 and 0.1 for ion energies below 1 keV. This formula predicts that there will be preferential sputtering of the lighter species, and also of the more loosely bound species. The binding energy effect is dominant at low ion energies because of the small value of n . For all the fluoride compounds studied in this work, both criteria predict that the anion will be preferentially sputtered away. IAD therefore often leads to substoichiometric films, which may or may not be a problem in any particular application. A common solution is to bombard the film with the anion species itself; for example, bombarding an oxide with oxygen ions. Implantation of the ions can then compensate for the preferential sputtering.

Thermal Spikes

Thermal spikes are typically associated with high-energy (tens of keV or more) ion-solid interactions. The ions penetrate the solid, are slowed by atomic collisions, and are captured, with the remaining kinetic energy deposited in 10^{-12} sec or less. This energy can either excite lattice vibrations, an effect known as a displacement spike (Brinkman 1954), or melt the solid over a small region, known as a thermal spike (Seitz and Koehler 1956). If the lattice melts, it is assumed to anneal upon cooling, increasing the density of the solid. The simple analysis of Seitz and Koehler predicted the number of atoms rearranged during the lifetime of the spike as

$$n_T = 0.016 \rho \left(\frac{Q}{E_0} \right)^{\frac{5}{3}}$$

where E_0 is the activation energy of the process, Q is the energy deposited into the spike by the incident ion, and ρ is a material-dependent parameter usually in the range 1-10. Of course, the question arises whether thermal spikes are still relevant at ion energies of 1000 eV or less.

The work of Hirsch and Varga (1978,1980) has already been mentioned. They observed that argon ion bombardment of growing germanium films on glass substrates eliminated film cracking associated with intrinsic stress. To isolate the effects of adhesion enhancement from reduction in the intrinsic stress, 100 nm of unbombarded germanium was deposited, followed by 2 μm of IAD material. For an assortment of ion energies between 65 and 3000 eV, the critical current density I_c at which film cracking began was measured. This data was fit very well by the relationship

$$I_c \approx \frac{6.2 \times 10^3}{E^{3/2}} \frac{\mu A}{\text{cm}^2} = \frac{3.9 \times 10^{16}}{E^{3/2}} \frac{\text{ions}}{\text{cm}^2 \cdot \text{sec}}$$

where E is the ion energy. As stated above, Seitz and Koehler (1956) derived a $E^{-5/3}$ dependence for the number of atoms rearranged by a thermal spike. At an ion flux of I_c ions $\text{cm}^{-2} \text{sec}^{-1}$, the total rate of atomic rearrangement would then be $I_c n_T$ atoms $\text{cm}^{-2} \text{sec}^{-1}$. Hirsch and Varga then assumed that the total number of atoms needing rearrangement to reduce the intrinsic stress sufficiently to prevent cracking was

constant. This would require that $I_c \propto E^{-5/3}$. Since $5/3 \approx 3/2$, they assumed that they were actually observing a "thermal annealing" effect. Saxe (1975), however, has pointed out that the accuracy of their data is sufficient to rule out the $-5/3$ power law dependence. This result must therefore be viewed with a certain degree of skepticism.

More recently, Müller (1986a) has performed a Monte Carlo simulation to model the effect of thermal spikes during IAD. Using a two-dimensional film geometry, he deposited atoms and introduced ions in fixed proportions, with the locations of the incident particles chosen randomly. The evaporant atoms struck the growing film and stuck, with the film then undergoing a relaxation process simulating the thermal diffusion expected in any solid. A thermal spike model developed by Sigmund and Claussen (1981) was used. This model assumes that the spike vaporizes a spherical region around the point of ion incorporation, with a Boltzmann gas present in the cavity. The spike cools and grows with time until the temperature cools sufficiently for the material to solidify. The conclusion of this work was that IAD does not densify thin films, although it may cause the voids between columns to be sealed near the film surface.

Collision Cascades

The simplest model of ion-solid interaction is the kinetic "billiard-ball" model. An incident ion collides with atoms, displacing the atoms and deflecting the ion. Figure 2-7 shows the various effects which can be expected. The number of options greatly complicates the problem. If the ion is sufficiently energetic, the rearrangement of the

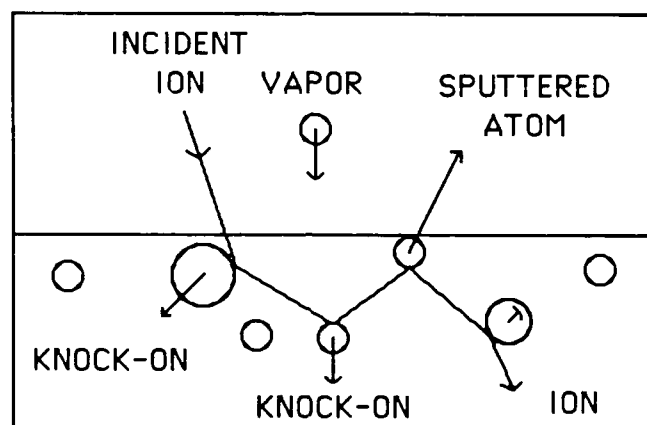


Figure 2-7. Various processes which occur during a linear collision cascade (Müller 1986b).

solid can be significant. Collision cascades are traditionally considered in the keV energy range, but knock-on effects are possible even at low energies.

Harper et al. (1984) have proposed that forward sputtering can eliminate void formation by dislodging overhanging atoms which might create a void (Figure 2-8). This model was supported by evidence from non-normal incidence bombardments of films growing over a step in the substrate.

Collision cascades have recently been studied by Müller (1986b), again using a Monte Carlo approach. He started with a Monte Carlo code called TRIM developed by Biersack (Biersack and Eckstein 1984) to model the ion-atom interaction. To simulate ion-assisted deposition, Müller alternately deposited a thin layer of pristine material on the top of the film and bombarded the film with ions. This alternation was assumed to simulate the simultaneous processes.

The results of this simulation present a coherent picture of IAD. Surface atoms are knocked deeper into the film through recoil implantation. This results in the densification of a layer approximately 1 nm below the film surface and the formation of a depletion layer on the surface. Since the sub-keV ions used in IAD have ranges of at most tens of nm in dielectric materials, the bombardment can only affect the near-surface region. Therefore, as the film grows, it is progressively densified. This model predicts that a depleted surface layer should remain when the deposition is complete. Figure 2-9 shows a typical growth simulation from Müller's work.

Müller then compared these results with data for the density of ZrO_2 films bombarded with 600 eV O^+ ions (Figure 2-10). For low ion fluxes, the agreement

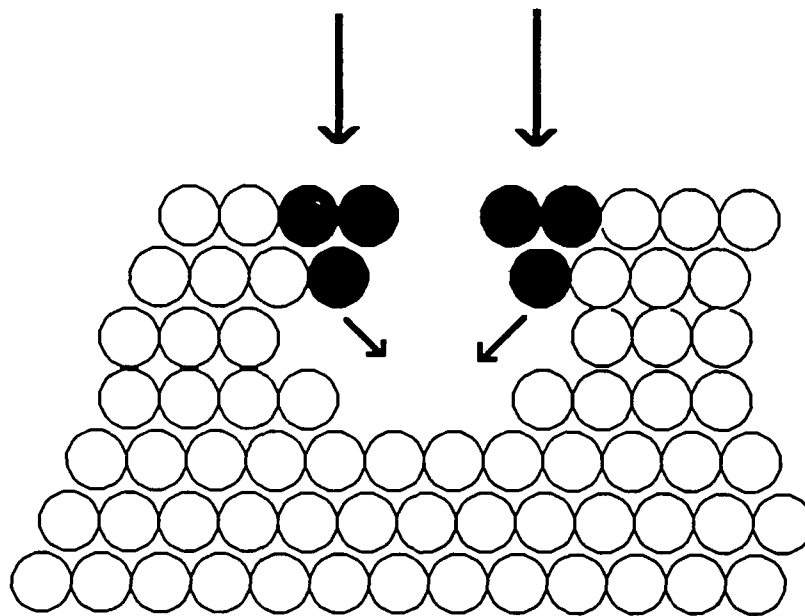


Figure 2-8. Prevention of void formation by forward sputtering of overhanging atoms (Harper et al. 1984).

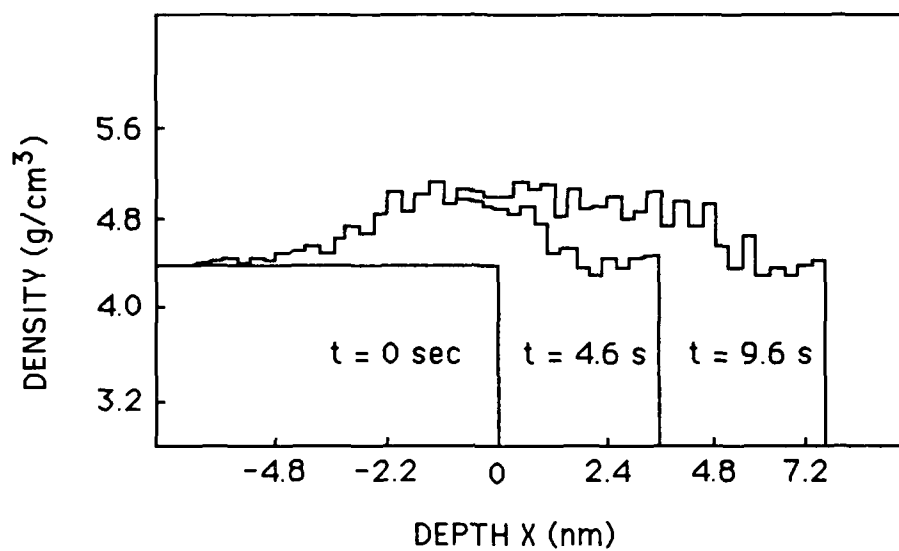


Figure 2-9. Density of an IAD ZrO_2 film at three stages in its growth. The film is assumed to grow without ion bombardment until $t = 0$ (Müller 1986b).

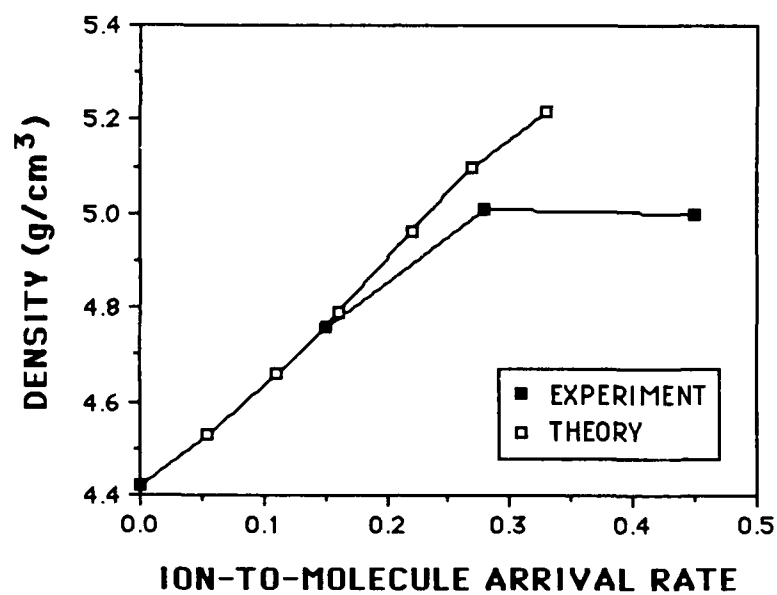


Figure 2-10. Density of IAD ZrO₂ films as a function of ion arrival rate, showing both experimental and calculated values (Müller 1986b).

between experiment and theory is very good. For higher fluxes, the theory predicts higher densities than are observed because the TRIM code does not keep track of actual lattice sites. There is therefore no limitation on the possible density of the films, allowing the model to predict densities larger than the bulk value.

This model, which suggests that recoil implantation is the primary cause of the densification observed in IAD, is very appealing. Recent experiments appear to reveal a surface depletion layer during the ion etching of ZrO_2 (Netterfield 1986), strengthening the credibility of the model.

Ion-Stimulated Sorption

When reactive metals are deposited in a background of reactive gas, some gas is incorporated into the film. However, if the metal is bombarded during growth by either inert or reactive ions, the incorporation rate of the reactive gas into the film can be greatly increased. As an example, Grigorov and Martev (1986) have reported that they could deposit Ti-N films with a N:Ti ratio of 3:1 by bombarding titanium with argon ions in a nitrogen background. In this way, they could form a number of nonequilibrium compounds as well as the stoichiometric material TiN. The suggested mechanism for this ion-stimulated sorption is the creation of ion-induced defects in the film which are then filled with reactive gas atoms. This theory was supported by a study of the effects of different noble gases on the sorption process; both the amount of adsorbed nitrogen and the number of ion-induced defects in the films peaked for argon bombardment.

Martin, Netterfield, and colleagues (Martin et al. 1984b) have also deposited TiN films by ion-assisted deposition. They explicitly attributed the formation of stoichiometric TiN to ion-stimulated sorption, since argon bombardment was as effective as nitrogen bombardment.

CHAPTER 3

EXPERIMENTAL METHOD

Film Deposition

The thin films studied in this work were deposited at the Thin Films Laboratory of the Optical Sciences Center in a Balzers BAK 760 box coater (Figure 3-1). This system consists of a 1000 x 900 x 900 mm box-shaped vacuum chamber evacuated by a mechanical pump and Roots blower down to 5×10^{-2} mbar and then cryopumped to base pressures as low as 4×10^{-7} mbar. Most of this work, however, was performed in the low 10^{-6} mbar range.

Two resistive and two electron-beam sources were located at the base of the chamber. Tungsten, tantalum, and molybdenum boats resistively evaporated some materials; others were electron-beam evaporated from molybdenum or intermetallic (for aluminum evaporation) crucible liners. A 6 kV electron beam evaporated fluorides and metals, while a 10.5 kV beam handled the refractory oxides.

The deposition rate from these sources was normally controlled automatically by a microprocessor-based system, with a quartz crystal monitor in the center of the chamber measuring the rate. Alternately, the sources could be manually set at specific power levels. The chamber was also equipped with a sophisticated optical monitoring system consisting of two wideband scanning monochromators (Van Milligen et al. 1985), but this system was not used in this research.

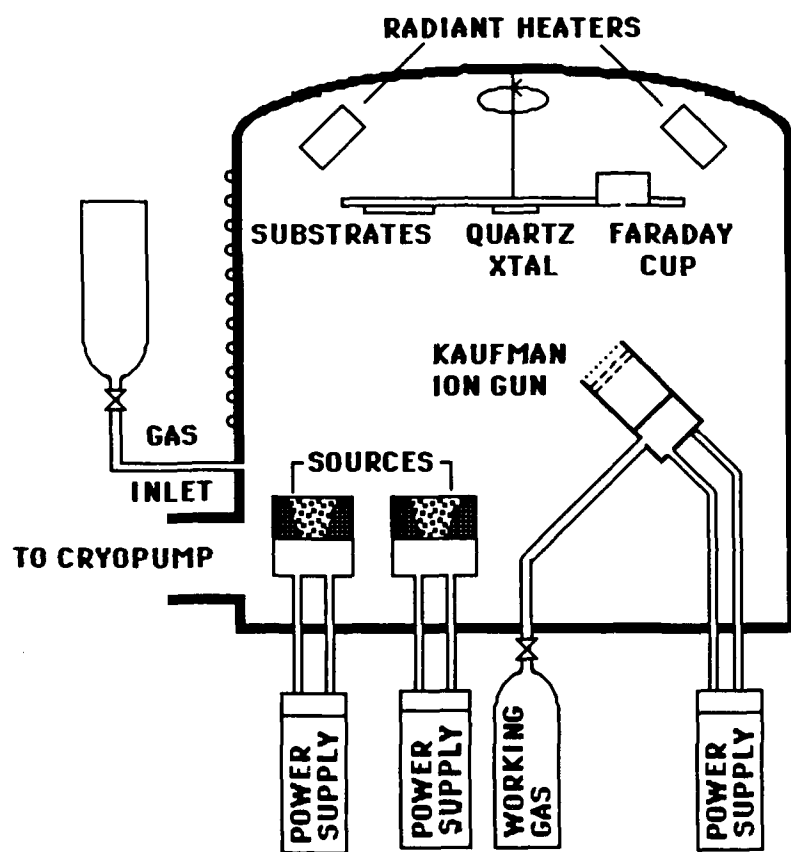


Figure 3-1. Schematic of the Optical Sciences Center Balzers BAK 760 box coater configured for IAD.

The chamber could be heated as high as 300 °C using four tungsten lamps mounted at the top of the chamber above the substrate holder. A thermocouple mounted on a baffle in the rear of the chamber just below the substrate level measured the substrate temperature. This thermocouple and the substrates were approximately equidistant from the electron-beam sources, the major source of undesired chamber heating. These sources could heat the chamber from room temperature to more than 100 °C during the deposition of 1 µm of refractory oxide material. The resistive sources caused much less superfluous heating, raising the chamber temperature only 20-30 °C above ambient after the deposition of 1.5 µm of fluoride coating material.

Gas could be added to the chamber through an automatic valve mounted in the side of the plant. This valve automatically adjusted the flow to maintain a constant pressure on an ionization pressure gauge.

For ion assisted deposition, a Commonwealth Sciences Corporation 3-cm aperture ion source was mounted in the center of the chamber on a mount with two axes of adjustment. This source is of the Kaufman hot-cathode variety discussed in Chapter 2. Dual graphite grids and tungsten filaments were used with the gun in this research, generating beam energies of 150 to 1000 eV. A needle valve metered the working gas (argon, oxygen, or nitrogen in this work) into the bottom of the gun. Two different gases could also be simultaneously fed into the gun through a T-fitting in the feed line with separate needle valves for each gas. Since manual needle valves, instead of flow controllers, set the flow through this line, these valves were set for a total chamber pressure of 8×10^{-5} mbar, which allowed the ion source to operate properly. When two

gases were mixed, a lower chamber pressure was first reached with one gas and the line with the second gas was then opened until 8×10^{-5} mbar was reached.

The actual ion beam current density striking the substrates was measured using a Faraday cup arrangement which could be rotated into the sample position before and after deposition. A -45 V bias on the cup prevented the measurement of neutralization electrons. The substrates were mounted on a rotating substrate dome with four sample positions at 90° intervals. Three of the positions contained substrates, while the fourth contained the Faraday cup. These positions were mounted parallel to the bottom of the chamber so that the ion beam struck them at a $15\text{-}30^\circ$ angle of incidence.

An assortment of substrates accommodated the various analysis techniques. Float glass was used for experiments in which substrate transmittance was not a factor, such as humidity testing. Spectrosil B grade synthetic fused silica was used for optical measurements because published values of refractive index were available (Malitson 1965). A measurement of the Spectrosil refractive index at the sodium D line with a Bausch & Lomb Abbe refractometer agreed with the literature value, at least at this wavelength, to three decimal places. Silicon and germanium substrates were used for infrared transmittance measurements, and graphite substrates were used for Rutherford backscattering analysis.

Thin Film Characterization

Measurement of Optical Constants

The optical properties of a thin film can be described by a number of pairs of optical constants. We have chosen the refractive index n and the extinction coefficient k . For dielectric coatings, the refractive index describes the dispersive nature and the extinction coefficient the absorptive nature of light propagation through the medium, although the separation is not rigorously complete. An accurate determination of the optical constants is essential in characterizing the optical behavior of a thin film.

Numerous methods based on different optical measurements have been developed to calculate optical constants (Arndt et al. 1984). In our laboratory, the most accurate instrument available is a Cary 14 double-beam spectrophotometer. A chopper divides a monochromatic beam into two beams which alternately pass through a sample and a reference compartment, after which they fall upon a common photomultiplier tube. If the reference compartment is empty, the ratio of the two signals at the photomultiplier gives the absolute transmittance of a sample. These measurements can be performed to an accuracy of better than 0.5% over a wavelength range of 0.2-2.5 μm . Absolute reflectance can be measured using a V-W reflectance attachment in the sample compartment and a variable attenuator in the reference path, but accurate measurements require samples larger than the 25.4 x 25.4 mm squares used for most of this work. A reflectance relative to an aluminum standard can be measured using single-bounce reflectance attachments in both compartments, but these measurements in our instrument can only be considered accurate to approximately 1% in the visible and

ultraviolet (Swenson 1987). We have therefore chosen an analysis technique which only requires transmittance measurements.

The extrema of transmittance and reflectance curves make very convenient inputs into optical constants programs. Our knowledge of the optical thickness (the product of refractive index and physical film thickness) at each extremum provides an additional variable not available in other methods using the same data. In particular, an independent measurement of the film thickness is not required. This advantage has led to several "envelope" methods for optical constant calculation. In all these techniques, two auxiliary curves are derived for each spectrophotometer trace--one curve passing through the quarter-wave points and another passing through the half-wave points. These two envelopes then provide two data points at each wavelength of interest for each trace. Using only a transmittance measurement, we have three independent variables--half- and quarter-wave transmittance and optical thickness--at each extremum. Therefore, this data is sufficient to calculate n , k , and the physical thickness d at these wavelengths.

An envelope technique due to Manifacier, Gasiot, and Fillard (1976) assumes that the film is homogeneous and weakly absorbing. This method was chosen for this work because it only requires a spectral transmittance measurement at normal incidence of a single-layer film on a transparent substrate. Figure 3-2 shows a typical transmittance curve for a high-index material with the two envelopes drawn. The T_{\max} envelope shows what the transmittance of the film at any given wavelength would be if the optical thickness of the film were some even number of quarter-waves at that wavelength

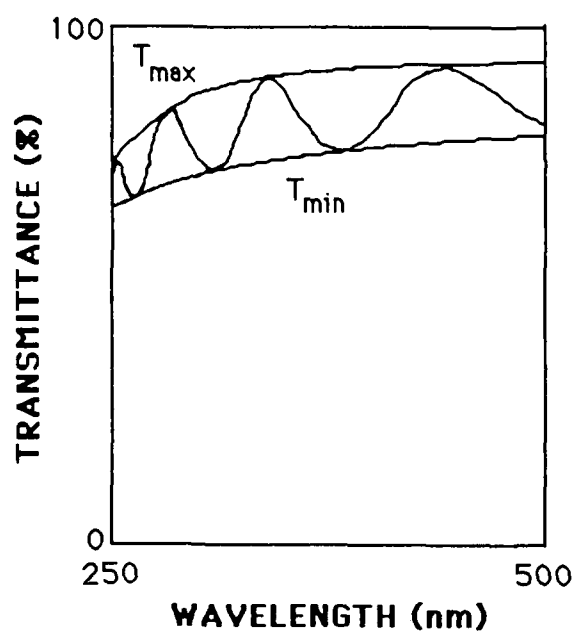


Figure 3-2. Typical transmittance curve for a single-layer dielectric coating with the auxiliary T_{\min} and T_{\max} curves added.

rather than its actual thickness. Similarly, T_{\min} shows what the transmittance would be if the film's optical thickness were an odd number of quarter-waves thick at that wavelength. The variables T_{\min} , T_{\max} , and m --the order of the extremum at the measurement wavelength--are adequate to calculate unambiguously n , k , and d at the wavelength of the extremum.

The mathematics involved in this method is presented in the literature and will not be duplicated here. However, the basic framework of the argument is helpful in appreciating the application of the method. The following development follows directly from Manifacier et al. (1976).

The transmittance of a weakly absorbing, homogeneous, single-layer film of index n , extinction coefficient k , and thickness d on a semi-infinite substrate is given by

$$T = \frac{16 n_0 n^2 \alpha}{C_1^2 + C_2^2 \alpha^2 + 2 C_1 C_2 \alpha \cos\left(\frac{4\pi n d}{\lambda}\right)}$$

where n_0 and n_1 are the refractive indices of the incident medium and substrate,

respectively, $C_1 = (n+n_0)(n_1+n)$, $C_2 = (n-n_0)(n_1-n)$, and $\alpha = e^{-4\pi k d/\lambda}$. Letting

$4\pi n d/\lambda = m\pi$ at the extrema, it is easily shown that the two envelopes are given by

$$T_{\max} = \frac{16n_0 n_1 n^2 \alpha}{(C_1 + C_2 \alpha)^2}$$

and

$$T_{\min} = \frac{16n_0 n_1 n^2 \alpha}{(C_1 - C_2 \alpha)^2}$$

These equations are then inverted to give

$$\alpha = \frac{C_1 \left[1 - \sqrt{\frac{T_{\max}}{T_{\min}}} \right]}{C_2 \left[1 + \sqrt{\frac{T_{\max}}{T_{\min}}} \right]}$$

and

$$n = \sqrt{N + \sqrt{N^2 - n_0^2 n_1^2}}$$

where

$$N = \frac{n_0^2 + n_1^2}{2} + 2n_0 n_1 \frac{T_{\max} - T_{\min}}{T_{\max} + T_{\min}}$$

The reliance of this method on extrema in T places a requirement on the film thickness. Typically, at least five extrema are desirable in the spectral range of interest. We obtain transmittance values for the envelopes between the data points by performing a Cauchy interpolation of the form (Garcia 1986)

$$T(\lambda) = T(\lambda_1) + \frac{(\lambda - \lambda_1)[T(\lambda_2) - T(\lambda_1)]}{(\lambda_2 - \lambda_1)}$$

where λ_1 and λ_2 are the wavelengths of two adjacent known data points and λ is the interpolation wavelength.

A major problem with this method (and most spectrophotometric methods, for that matter), is that the error in the calculation increases rapidly as $T_{\max} - T_{\min}$ gets small. It is therefore difficult to get good results for low index materials on fused silica. In fact, we have been unable to measure the refractive indices of low-index films accurately enough by this method to observe meaningful changes with ion bombardment. Changes in the extinction coefficient are normally much larger (in percentage terms), and therefore can still be calculated meaningfully by this method for low-index films. The accuracy of the method could be improved somewhat by using higher-index

substrates such as sapphire, but the increase in transmittance contrast between extrema would only be approximately 1%. Given the cost of sapphire substrates with the optical axis oriented so as to avoid birefringence in the measurement, this slight increase in sensitivity was not considered worthwhile for this work.

Once the index has been calculated at each turning point, the optical thickness (nd) at the turning points can be divided by the calculated refractive index n at that wavelength to give the physical thickness of the film d . The calculated values of d at each turning point can then be averaged to give an estimate of the film thickness. For a well-behaved calculation, the thickness calculations at the turning points typically showed a spread of $\pm 50 \text{ \AA}$ or less.

Macleod (Arndt et al. 1984) extended this method to the inhomogeneous film case by making use of the characteristic matrix for a weakly absorbing, inhomogeneous film. An analysis analogous to that of Manifacier et al. then shows that, while the expressions for T_{\max} , T_{\min} , R_{\max} , and R_{\min} do not lead explicitly to solutions for the optical constants, an iterative method is possible. Thus, at the cost of requiring a reflectance as well as a transmittance measurement, the degree of inhomogeneity of the film can be determined as well as the mean index and the extinction coefficient. As mentioned above, however, making accurate reflectance measurements on the available samples with the available instruments was very difficult. Therefore, we modified the Manifacier method to analyze films which showed measurable inhomogeneity--that is, whose half-wave transmittance was greater than the bare substrate transmittance.

This modified method is based on the similarities between the reflectance extrema of homogeneous and inhomogeneous films in the absence of absorption. It has been shown in the literature (Borgogno, Lazarides, and Pelletier 1982) that the quarter-wave reflectance of a weakly-absorbing inhomogeneous film is almost identical to that of a homogeneous film of index $\sqrt{(n_a n_b)}$, where n_a and n_b are the film refractive indices at the air-film and substrate-film interfaces, respectively. For a nonabsorbing film, the equivalence is exact. This suggests a simple modification of the Manifacier method--in spectral regions of negligible absorption, keep the measured quarter-wave transmittance values and replace the half-wave transmittance values with the bare substrate transmittance which a nonabsorbing homogeneous film would have. This procedure approximates the slightly inhomogeneous film by an effective homogeneous film with the same mean index. This is an excellent assumption for nonabsorbing films and obviously degrades with increasing absorption as the assumption that the half-wave transmittance equals the substrate transmittance becomes more and more inaccurate. Since most of the coatings analyzed in this study are highly transparent in the visible, this approximation has generally been applied over the 300-700 nm wavelength range for films which have obvious inhomogeneity, that is, whose half-wave transmittances are greater than the substrate transmittance. A combination of inhomogeneity and the proper amount of absorption could lower the half-wave transmittance of an inhomogeneous film to that of the bare substrate and thus mask the inhomogeneity, but this is obviously an exceptional case which is unlikely to be encountered.

Humidity and Boiling Water Tests

A thin film's utility in everyday use is often determined by its resistance to attack by atmospheric moisture. In some cases, optical coatings are expected to perform for years in humid environments with little or no optical degradation. Ideally, coatings would be aged in air for their rated lifetime to get an accurate measure of their actual performance; however, it is obviously impractical in most cases to conduct such testing over periods of months or years. As a result, an accelerated testing procedure is required. A typical standard test is that specified by MIL-SPEC-C-675, which involves placing the films for at least 24 hours in an environmental chamber (often called a humidity chamber) at 48 °C with 95% to 100% relative humidity. The films are then rubbed with an eraser and examined for scratching. The result of the test is a pass or fail rating. We employ a similar test in this work; after the humidity test, we examine the films by Nomarski microscopy at approximately 200x magnification to detect degradation. Nomarski microscopy, which reveals changes in the slope of the wavefront reflected from the sample (Klein 1970), is much more sensitive to surface degradation than conventional optical microscopy, particularly for single layer dielectric films. The eraser test was avoided because of the great difficulties involved in standardizing the rubbing procedure from sample to sample.

Two basic problems affect humidity testing: First, water droplets can condense on the film surface and cause more severe damage than the moist air itself; second, durable films might take weeks to degrade in a conventional humidity test. The latter is certainly no problem in a production facility, but can be in a research environment

where we seek to observe small differences in film properties caused by changes in the deposition process. To accelerate the tests, we have subjected some coatings to a boiling water test, placing the films in boiling deionized water for a specified length of time. Since the films were completely immersed in water, they were subject to a much more uniform attack. To protect the films from agitation by rising bubbles, the samples were placed in a beaker at an incline with the coated side of the substrate facing upwards. This is a very severe test, and damage can often be detected in films after only minutes.

X-Ray Diffraction

The degree of long-range order present is an important property of any optical material, as it can have a major effect on the optical properties. Solids can be amorphous, with minimal order beyond adjacent atoms, or crystalline, with order extending over even macroscopic distances. While thermally deposited thin films typically consist of vertical columns (Macleod 1982), the material within a column can still display crystallinity, or more likely polycrystallinity, with crystallites having different orientations.

The crystallinity of many of our thin film samples has been measured by Mr. Wes Bilodeau of the University of Arizona Department of Geosciences using a Siemens $\theta-2\theta$ x-ray diffractometer with the $\text{Cu K}\alpha_1$ line at $\lambda = 1.54051 \text{ \AA}$ and the $\text{Cu K}\alpha_2$ line at $\lambda = 1.54433 \text{ \AA}$ as the source radiation. Weighting these wavelengths by the relative intensities of the two lines gives an average $\text{Cu K}\alpha$ wavelength of 1.54178 \AA . When a sample is crystalline, the x-ray reflectivity increases sharply at an incident angle

specified by Bragg's Law (Kittel 1976). Light is coherently reflected in phase by successive crystalline planes at angles of incidence (with 0° representing grazing rather than normal incidence) satisfying

$$2d \sin \theta = n \lambda$$

where d is the interplanar spacing in the crystal, θ is the angle of incidence, λ is the x-ray wavelength, and n is an integer (usually one in these experiments). By determining the angles θ at which sharp x-ray reflections occur, the interplanar spacing of the crystallites in the film can be measured. Figure 3-3 illustrates a typical x-ray diffraction spectrum showing a number of peaks due to different crystalline orientations in a film. The broad reflection background observed is due to the amorphous fused silica substrate rather than the film itself. If the film is amorphous, we observe only this substrate background. The abscissa is labelled 2θ because the detector is scanned through twice the rotation angle of the sample; this satisfies the law of reflection for the x-ray source and detector.

It is important at this point to draw a distinction between different crystalline phases (hexagonal and monoclinic, for example) and different orientations of the same phase. Phases represent fundamentally different relationships between the atoms in the crystalline lattice: *Orientations describe crystallites of the same phase facing in different directions with respect to the substrate surface.*

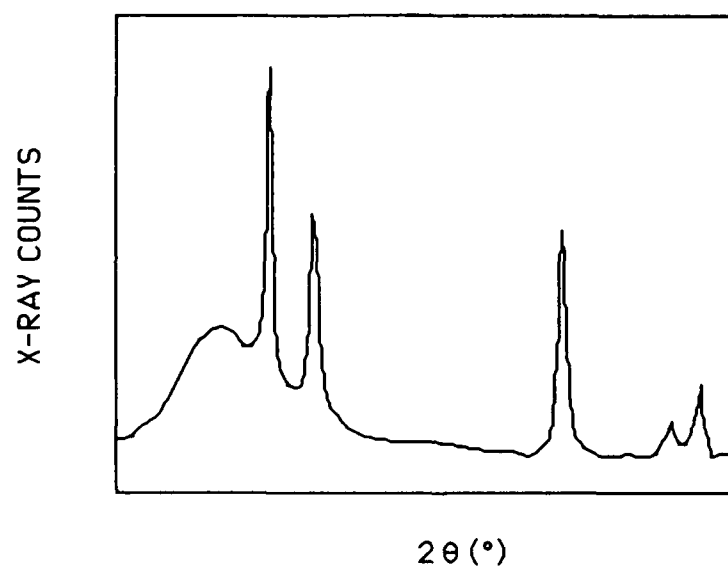


Figure 3-3. Typical output from a θ - 2θ x-ray diffractometer for a polycrystalline thin film on an amorphous substrate.

The Joint Committee on Powder Diffraction Standards (JCPDS) of the American Society for Testing and Materials publishes a compendium of x-ray diffraction data for most common materials in powder form (JCPDS 1967). For each crystalline phase of each material, this collection lists the interplanar spacing and relative intensity of each crystalline orientation. The x-ray diffraction measurements therefore tell us which crystalline phases and which crystallite orientations of each phase are present.

The size of the crystallites in a film can also be measured from the width of the x-ray diffraction peaks using the Scherrer equation

$$p = \frac{k\lambda}{b \cos \theta}$$

where p is the average projected crystallite diameter parallel to the film surface, K is the Scherrer constant (which is usually taken as one), b is the width of the x-ray diffraction lines (measured here as the full width at half maximum of the diffraction peak) minus the instrumental broadening, and θ is again the angle of incidence (Langford and Wilson 1978). The instrumental linewidth of the diffractometer was determined by measuring the width of the $2\theta=28^\circ$ peak in a silicon reference standard with large crystallites. Theoretically, this line should have negligible linewidth, so the measured linewidth can be directly attributed to the instrumental line broadening. This broadening was measured at 0.2° for typical operating conditions of the diffractometer.

Rutherford Backscattering Spectrometry

Rutherford backscattering spectrometry (RBS) has proven to be an excellent tool for studying compositional changes within thin films as a result of IAD. Messerly (1987) contains a detailed discussion of RBS and its application to thin film analysis, as well as as a discussion of many of our RBS results. I will simply provide a brief overview of the technique and refer the interested reader to Messerly (1987) or the seminal work by Chu, Mayer, and Nicolet (1978).

Our RBS measurements have been performed on the Van de Graaff accelerator of the Ion Beam Analysis Facility of the University of Arizona Physics Department by Professors John Leavitt and Larry McIntyre and their co-workers. Michael Messerly and John Lehan reduced the data.

In RBS, high-energy (1.892 MeV in this work) singly-ionized helium ions from a Van de Graaff accelerator are scattered by a thin sample in vacuum. The measured number of scattered helium ions per unit solid angle per incident helium ion, combined with known scattering cross sections, provides the absolute number of each atomic species in the film in units of atoms per unit area. Film stoichiometries can thus be measured to an accuracy of better than one percent. Graphite substrates are necessary because the silicon and oxygen peaks from glass substrates overwhelm the peaks from lower Z elements, including any film constituents with $Z < 14$, decreasing measurement accuracy and complicating the analysis. Thin film thicknesses must also be chosen to prevent adjacent elemental backscattering peaks from overlapping. This requires fluoride films to be at most 1000 Å thick.

Rutherford backscattering, a nuclear scattering process, is insensitive to the nature of the chemical bonding in the films. In particular, the oxygen content of the films cannot be divided between oxygen atoms and water or OH^- complexes. With a little intuition, however, useful conclusions can be drawn about the chemistry of the films when the data from RBS and other analysis methods are combined.

Infrared Transmittance

The infrared transmittance of a thin film is obviously of interest in terms of its optical performance, but it can also be used to qualitatively compare the packing densities of two thin films. Bradford, Hass, and McFarland (1972) have shown that thin films display an absorption band centered around $3\text{ }\mu\text{m}$ due to absorption by the water trapped in the film. The strength of this water band therefore provides a qualitative measure of the water content of the film and, if we assume that the water is filling the voids in the film, the packing density as well. An absorption band at $2.7\text{ }\mu\text{m}$ due to OH^- radicals is also present in some films. In many cases, however, this band falls on the tail of the water band, making it very difficult to observe the OH^- band.

Measurements of coatings on silicon and germanium substrates were made at the Optical Sciences Center with an Analect FX-6200 Fourier Transform Infrared (FTIR) Spectrometer and at the Optical Coating Laboratory Incorporated (OCLI) on a Perkin-Elmer 983 FTIR Spectrometer. The Analect instrument measures transmittance over the $400\text{--}4400\text{ cm}^{-1}$ ($2.3\text{--}25\text{ }\mu\text{m}$) region. The Perkin-Elmer spectrometer is capable of measuring over a wider spectral region, but measurements were not made over this extended range. The sample compartment of the Analect instrument contains

ambient air, introducing atmospheric absorption bands. Dividing the sample spectra by a reference spectrum taken without the sample largely removed these bands, but atmospheric fluctuations between the two measurements resulted in noise of one percent in the worst case, although most measurements were significantly less noisy. This noise varied from run to run and was the primary reason for having some samples measured at OCLI. The Perkin-Elmer spectrometer is purged with dry nitrogen and therefore does not suffer from atmospheric absorption bands.

X-Ray Photoelectron Spectroscopy

A previous section pointed out the capabilities of Rutherford backscattering (RBS) but also indicated a number of limitations as well. These disadvantages include: (1) the lack of chemical information from the analysis, (2) the need for thin samples in some cases, and (3) the difficulty of determining stoichiometry accurately on glassy substrates. All three of these disadvantages can be addressed by x-ray photoelectron spectroscopy (XPS), although there is a new set of disadvantages inherent to this technique.

XPS involves the irradiation of a sample by a monoenergetic beam of x-rays in an ultra-high vacuum environment (typically 10^{-9} torr or better). The x-rays cause the photoionization of core electrons in the sample atoms. The difference in energy between the incident x-ray and the photoelectron gives the binding energy of the original electron state. In this way, atomic species can be detected with high sensitivity. In addition, this technique is very surface sensitive because photoelectrons can only escape from the sample if excited near the surface. This means that the measurement is

insensitive to the substrate composition, and that depth profiling of the film requires ion beam sputtering of the film. This sputtering can change the nature of the film through ion mixing, thus confusing the analysis. Therefore, we concentrated on another property of XPS--its ability to give chemical bonding information.

The use of XPS to obtain bonding information, often known as Electron Spectroscopy for Chemical Analysis (ESCA), depends on the fact that the binding energy of a core electron state is perturbed slightly by the valence electrons through electron-electron interactions. These perturbations are typically on the order of several electron volts. If the valence state of an atom changes, the perturbation energy therefore changes as well, resulting in a "chemical shift" in the XPS peak. It is therefore possible to discern information about chemical bonding from XPS analysis. This has been our principle use of XPS, with the bonding information supplementing the RBS analysis. In some cases, it is possible to correlate peaks directly with particular valence states; in our case, however, most of the interesting species were impurities in the samples, complicating the analysis. We were at least able to tell if a particular atomic species was present in more than one bonding configuration in the films.

Figure 3-4 shows a typical XPS spectrum. The sharp peaks represent photoelectrons which escape the film without energy loss, while the background is due to photoelectrons which undergo collisions before leaving the film.

Our XPS measurements were carried out by two groups. The Materials Sciences Division of the Los Alamos National Laboratory provided measurements taken with their

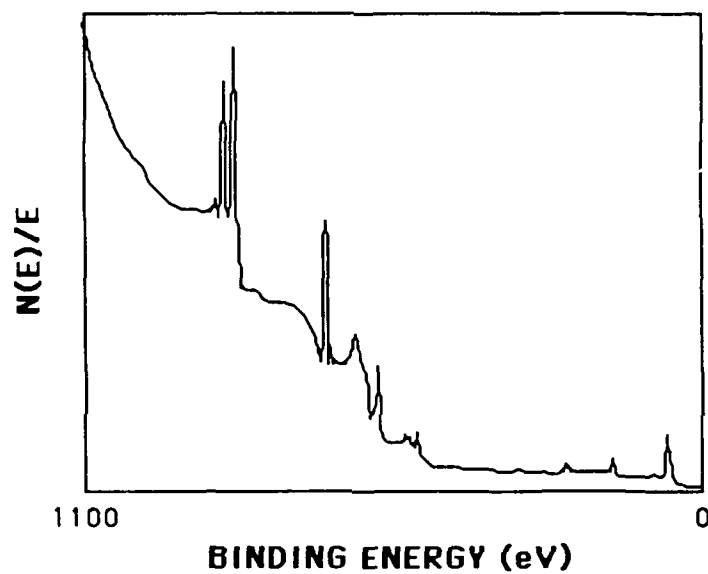


Figure 3-4. Typical XPS spectrum, with each peak (or set of peaks) representing an electron orbital.

Physical Electronics system, and the Optical Materials Group here at the Optical Sciences Center has taken data with their Perkin-Elmer 5100 system.

CHAPTER 4

THE ION-ASSISTED DEPOSITION OF MAGNESIUM FLUORIDE

Magnesium fluoride (MgF_2) is one of the mainstays of the optical coating industry. It evaporates easily by either resistive or electron-beam heating and has an index in the visible of approximately 1.38. It forms tough, water-resistant coatings on glass when deposited at high temperatures; these make an excellent AR coating on glass with a minimum reflection of slightly over one percent. For these reasons, literally acres of single-layer MgF_2 coatings are deposited annually onto mass-production optics such as camera lenses (Baumeister 1985). Perhaps more relevant to this study, MgF_2 has exceptional ultraviolet optical properties, with a transmittance cutoff near 110 nm (Pulker 1979). MgF_2 was therefore a natural starting point for us.

Several properties of MgF_2 films suggested that they would be improved by ion-assisted deposition. First, the deposition of hard coatings requires a substrate temperature of approximately 300 °C. Coatings deposited onto ambient temperature substrates are quite fragile and therefore are not suitable for many applications. Second, the refractive index and packing density of MgF_2 films also increase with increasing substrate temperature up to approximately 270-350 °C (Hacman 1970). Materials

whose properties show a strong temperature dependence are usually well suited for IAD.

Third, MgF_2 films suffer from very high tensile stress (Pulker 1982). This stress causes thick films to crack, preventing a quarter-wave of MgF_2 from being deposited for wavelengths greater than 3 or 4 μm . Hoffman and Gaertner (1980) have shown that IAD reduces the stress of chromium films and it was therefore hoped that we would observe the same effect.

Kennemore and Gibson, as discussed in Chapter 2, have extensively investigated the ion-assisted deposition of MgF_2 onto ambient temperature substrates (Kennemore and Gibson 1984; Gibson and Kennemore 1986). Their work, at least in the early phases, differed in emphasis from ours, although the projects converged in later stages. Portions of our research have already been reported by my colleagues, Saxe (1985) and Messerly (1987). My analysis here will deal with aspects of the problem not discussed in their work or will present differing interpretations of data previously reported, although their results will obviously be mentioned below to interrelate the various data where applicable.

Deposition Conditions

The MgF_2 films were electron-beam evaporated from a molybdenum crucible at a rate of 0.6 nm/sec using powdered starting material from Bendix. This material had to be warmed up very slowly to avoid blowing the powder out of the crucible, but once the powder melted the deposition progressed very smoothly with the automatic controller

maintaining the deposition rate to better than 0.1 nm/sec. All of the depositions, with the exception of one reference sample deposited at 300 °C, were conducted at ambient temperature (20-25 °C). The chamber temperature increased very little during the runs because of the low e-beam power required to evaporate MgF_2 .

Unbombarded Films

Before discussing the effects of ion bombardment on MgF_2 films, it is obviously important to know the behavior of unbombarded samples. We first attempted to deposit a film 700 nm thick on fused silica for an optical constant calculation using the Manifacier method. This film showed severe cracking which was visible in reflection to the naked eye. This cracking is undoubtedly due to excessive tensile stress in the film. A thinner sample approximately 400 nm in thickness was then deposited. This film has a very weak absorption edge in the ultraviolet which is quantified in Figure 4-1. RBS measurements of unbombarded films approximately 100 nm thick on graphite substrates show that the unbombarded films are slightly fluorine deficient, with the fluorine-to-magnesium ratio ranging from 1.94 to 2.00 (Messerly 1987).

Bombarded Films

MgF_2 films were deposited initially with argon ion bombardment. Argon has successfully been used by Kennemore and Gibson (1984) and presumably does not alter the films chemically. An ion energy of 300 eV was initially chosen as a compromise between two extremes: high energies might cause severe damage to the growing film,

while low energies might not significantly increase the packing density. Once the effectiveness of this energy was demonstrated, we continued it largely through inertia and to preserve the continuity of the data.

Ion-bombarded films 700 nm thick were grown on fused silica for transmittance measurements. These films showed no sign of cracking, demonstrating qualitatively that the ion bombardment decreased the tensile stress and/or increased the adhesion of the films. The errors in the refractive index calculations for these films were several percent. This is because of the small difference between the quarter- and half-wave transmittances of low-index films on fused silica. No useful information can be drawn from these calculations. The 0.5 % transmittance accuracy of our spectrophotometer is just not accurate enough. Better measurements might be possible in the future if sapphire substrates are used because of the increased index contrast between the film and substrate, but they were not used here. In addition, the fact that the index of the material is relatively close to that of water means that a porous coating with water in its voids is optically very similar to a dense film with few voids. In fact, Pulker (1979) reported that a porous MgF_2 film with a vacuum index of 1.32 had an index of 1.38 after being exposed to air. Therefore, we cannot draw any useful conclusions from these index measurements.

The extinction coefficients, on the other hand, are more significant because only one digit of accuracy is required for typical applications. Figures 4-1 and 4-2 show that mild argon ion bombardment in fact reduced the absorption of the films below that of the unbombarded film. This result is rather unusual and may simply suggest an anion

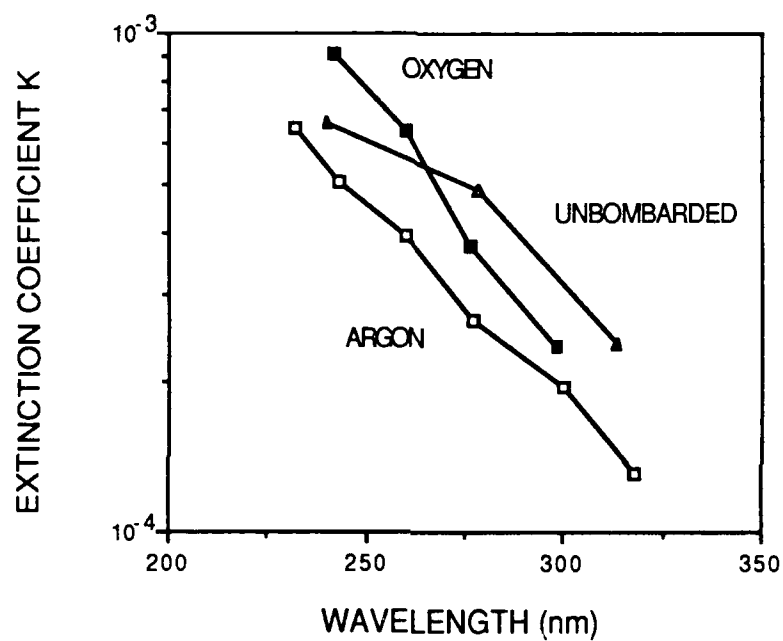


Figure 4-1. Extinction coefficients of argon- and oxygen-bombarded MgF_2 films for an ion flux of $20 \mu\text{A}/\text{cm}^2$, with the data for an unbombarded film included as a reference.

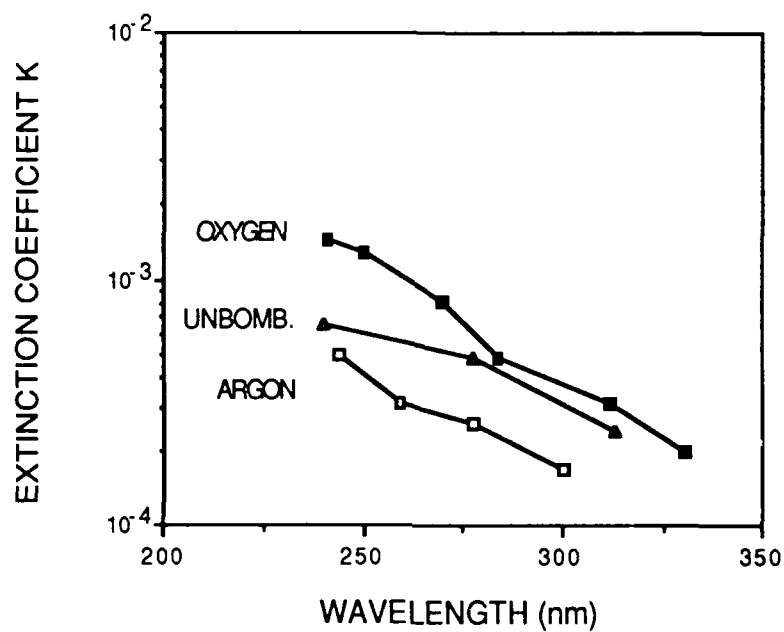


Figure 4-2. Extinction coefficients of argon- and oxygen-bombarded MgF_2 films for an ion flux of $50 \mu\text{A}/\text{cm}^2$, with the data for an unbombarded film included as a reference.

deficiency in the conventional film. In any case, the bombarded films have minimal absorption down to a wavelength of 250 nm. For each ion flux, the oxygen-bombarded film shows a stronger absorption edge than the argon-bombarded film. This behavior is explained by the changes in film stoichiometry with bombardment.

Infrared Water Band Absorption

An unbombarded film and a film bombarded with $20 \mu\text{A}/\text{cm}^2$ of 300 eV argon ions were deposited onto silicon wafers to examine the effect of IAD on the packing densities of the films. The transmittance of the films was then measured in the region of the $3 \mu\text{m}$ water absorption band. The unbombarded film showed a significant absorption band in this area (Figure 4-3), demonstrating its high porosity. The IAD film showed virtually no absorption, indicating that its packing density is very close to one. The absolute difference between the measured transmittances is due to the back surface of the wafers being unpolished, not to any absorption in either film.

Rutherford Backscattering Analysis

Film stoichiometries are greatly influenced by ion bombardment. These stoichiometries were determined by Rutherford backscattering. The raw data is due to Messerly (1987), but the interpretation given here is sufficiently different from his to warrant a repetition. We analyzed 100 nm thick films deposited onto graphite substrates. Neglecting the argon content of the films (which is typically 0.5 to 2 at.% for argon bombardment), film stoichiometry can be expressed in the form MgF_xO_y . A particularly stoichiometric unbombarded film has $x=2.005$ and $y=0.12$. The oxygen

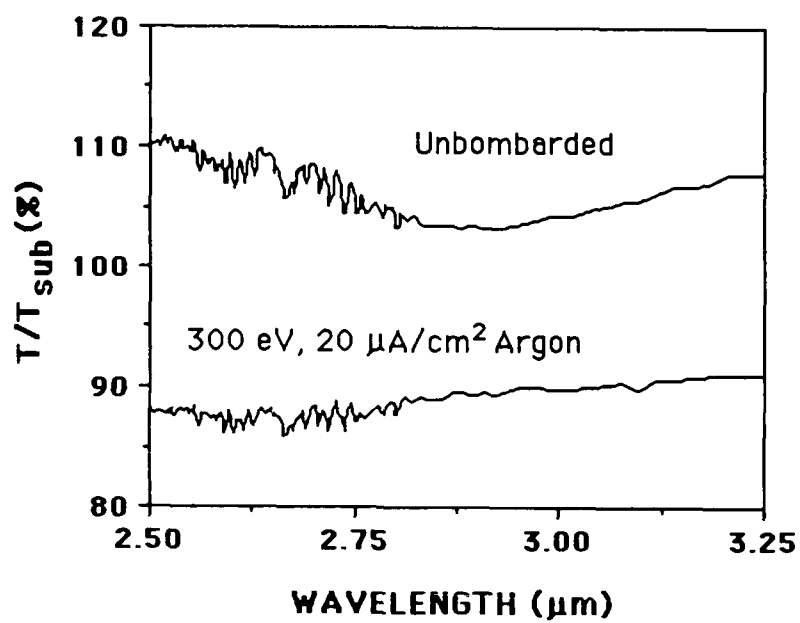


Figure 4-3. Infrared transmittance of an unbombarDED and an IAD MgF₂ film near the 3 μm water absorption band.

content probably comes from the residual oxygen in the vacuum chamber. Since RBS does not give chemical bonding information, it is impossible to determine how many of these oxygen atoms are actually present in the form of water or hydroxyl radicals.

With argon bombardment, preferential sputtering of fluorine by the incident ions reduces x below 2.0, with the fluorine deficiency increasing with increasing ion flux (Figure 4-4). The residual oxygen in the vacuum chamber compensates for the fluorine deficiency at low ion fluxes, but the oxygen content also decreases with ion flux because of the preferential sputtering of oxygen (Figure 4-4). The films thus begin to absorb slightly in the ultraviolet when the ratio of ions to arriving evaporant molecules γ surpasses 0.15. At this ion flux, the oxygen content of the film just compensates for the fluorine deficiency. For higher ion fluxes, the uncompensated anion vacancies cause increased ultraviolet absorption. The $\gamma=0$ films in Figure 4-4 were deposited in an argon atmosphere, so this data will not be repeated in Figure 4-5.

With oxygen bombardment, the fluorine deficiency is greater (Figure 4-5), probably due to the more efficient energy transfer from oxygen to fluorine atoms than from argon to fluorine atoms. It was shown in Chapter 2 that energy transfer is greater when the two bodies have similar masses. The oxygen content increases, however, as oxygen from the ion beam is implanted in the film (Figure 4-5). There is now enough oxygen in the films to compensate for the fluorine deficiency even for $\gamma=0.2$.

Combining the absorption and RBS data, we can draw several conclusions. First, fluorine is being preferentially sputtered out of the films, as would be expected from simple sputtering theory (see Chapter 2). Second, oxygen or oxygen compounds

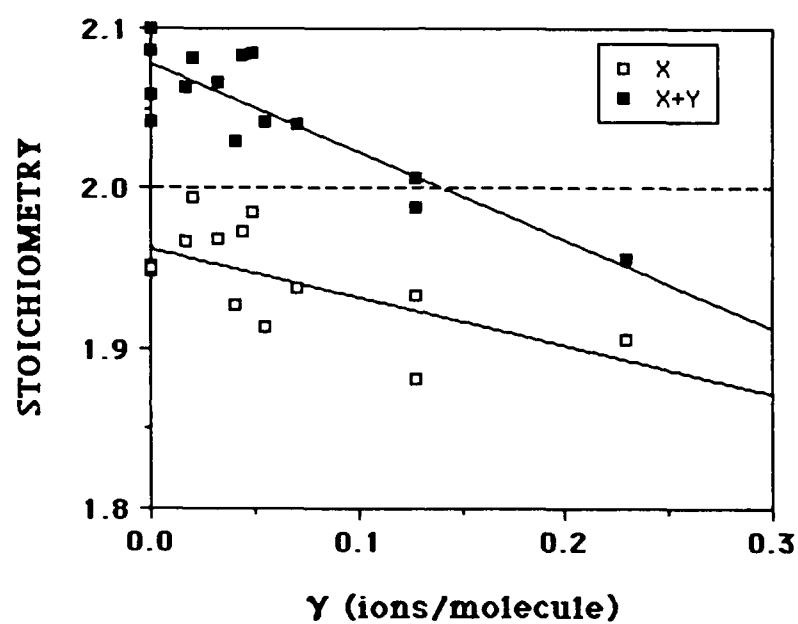


Figure 4-4. Fluorine to magnesium ratio x and anion to cation ratio $x+y$ for argon-bombarded MgF_2 films as a function of the ion to evaporant molecule ratio γ .

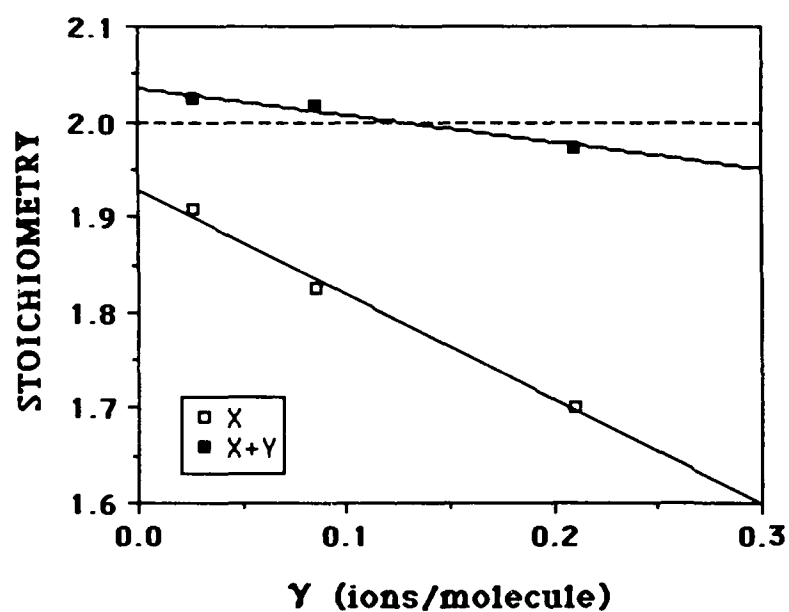


Figure 4-5. Fluorine to magnesium ratio x and anion to cation ratio $x+y$ for oxygen-bombarded MgF_2 films as a function of the ion to molecule arrival ratio γ .

(probably water or hydroxyl radicals) are incorporated into the films from the residual vacuum in the chamber or by ion implantation during oxygen bombardment. For unbombarded films, the amount of oxygen incorporated into the film exceeds the number of fluorine vacancies present. At some critical ion flux, however, the oxygen incorporation cannot compensate for the fluorine vacancies. We may assume that the film then contains anion vacancies.

These vacancies can cause ultraviolet absorption due to dangling bonds on the neighboring atoms. For MgF_2 , these vacancies also can capture an electron to form an F center (Kittel 1976). Messerly has shown that the onset of strong ultraviolet absorption for argon-ion bombarded MgF_2 films occurs when the anion-to-cation ratio in the films first drops below two (Messerly 1987). The absorption edge in heavily argon-bombarded films can therefore be attributed to the creation of anion vacancies by the preferential sputtering of fluorine.

With oxygen bombardment, the oxygen concentration in the films increases significantly as the ion flux is increased. There are two possibilities for how the oxygen is incorporated into the films. First, the oxygen may be located interstitially. Ion implantation would be likely to inject some interstitial atoms, but interstitials would probably not quench the vacancy absorption seen with argon bombardment. Second, the oxygen may be incorporated into the material lattice, filling fluorine vacancies. Of course, both cases might be present at the same time.

There is one other complication which we must consider. We do not know whether the basic lattice structure of the magnesium fluoride is changed by oxygen incorporation. It is quite possible that the lattice in some crystalline grains first transforms into an oxyfluoride phase as the oxygen content of the film increases. We have observed just such a behavior with IAD LaF_3 and NdF_3 (see Chapter 6). We have performed x-ray diffraction on a number of MgF_2 films. Only one of the 700 nm thick films showed any x-ray diffraction peaks at all, and these peaks were very small. Martin et al. (1987) have recently reported the results of electron diffraction and bright-field transmission electron microscopy of MgF_2 films. They observed crystallites approximately 10 nm in size in both conventional and IAD films. It is therefore likely that our films are crystalline, but with crystallites too small to detect by x-ray diffraction.

Whatever the precise nature of the oxygen in the lattice, it appears to cause an oxide-like absorption edge beginning at approximately 250 nm. Magnesium oxide is known to have its transmittance cutoff near 250 nm (Pulker 1979). We may therefore picture the oxygen as filling the fluorine vacancies in the films and quenching the vacancy absorption, but at the price of a growing oxide-like absorption edge. Martin and Netterfield (1985) have reported that MgF_2 bombarded with oxygen shows less absorption in the visible than argon-bombarded MgF_2 , in agreement with our results.

Humidity and Boiling Water Tests

The 3000-7000 Å thick MgF_2 films on glass substrates were subjected to a 24 hour humidity test at 40 °C and 95% relative humidity to test their moisture resistance. Unbombarded films deposited at room temperature and at 300 °C and argon-bombarded films deposited at room temperature showed no damage under Nomarski microscopy. Oxygen-bombarded films, however, showed microscopic pitting. Gibson and Kennemore (1986) have observed a similar effect, attributing it to the poor moisture resistance of MgO . Some variant of this explanation is probably valid, as our later results with LaF_3 (Chapter 6) indicated that an oxyfluoride phase formed in those films.

To differentiate between the films which were undamaged by the humidity testing, 15 minute boiling water tests were conducted on 1000 Å thick samples. An unbombarded film deposited onto a 25 °C substrate was completely removed by the test, while an unbombarded film deposited at 300 °C and an IAD sample using a 300 eV, 10 $\mu\text{A}/\text{cm}^2$ argon beam suffered only minor microscopic damage. When the ion current density was increased to 50 $\mu\text{A}/\text{cm}^2$, however, the test cracked the sample catastrophically. IAD thus appears to improve the moisture resistance of the films deposited onto room temperature substrates when low ion current densities are used, but is less effective at higher current densities. A plausible argument can be made for this behavior on the basis of film stress. MgF_2 films are known to have tensile stress, which we have shown is reduced by ion bombardment. In addition, water is known to reduce the tensile stress of thin films (Pulker 1982). It is therefore possible that the more

heavily bombarded film only had a small tensile stress after deposition, which became compressive during the boiling water test. Excessive compressive stress could then have caused the cracking. If this is indeed the failure mechanism, then this test would have little bearing on the utility of the $50 \mu\text{A}/\text{cm}^2$ film for everyday use, as the stress would only become compressive during immersion in water.

Color Centers in Magnesium Fluoride

Saxe (1985) and Messerly (1987) have previously reported our observation of F center formation in IAD MgF_2 thin films. F centers are electrons trapped in anion vacancies which then exhibit bound electron transitions (Kittel 1976). The F center absorption band in bulk MgF_2 crystals is centered at 260 nm and has a half-width of approximately 40 nm (Sibley and Facey 1968). We have observed a broader absorption band centered around 270 nm (Saxe 1985) which can be bleached out by a thermal anneal in air as atmospheric oxygen diffuses into the films, filling the anion vacancy sites (Messerly 1987). Rather than repeat these results, I will address the temperature dependence of this bleaching effect.

Figures 4-6 and 4-7 show the ultraviolet transmittance of two IAD MgF_2 films deposited in the same coating run and designated 202B1 and 202B2. These films were bombarded by $130 \mu\text{A}/\text{cm}^2$ of 300 eV argon ions. This absorption band is typical of that observed for IAD MgF_2 films bombarded with an excessive ion flux. These films were

then subjected to a series of thermal anneals in a tube furnace, with the film transmittance measured after each anneal.

We began by annealing sample 202B2 at 200 °C (Figure 4-6). The absorption decreased significantly, indicating that there is a diffusion mechanism for oxygen through the films at temperatures below 200 °C. Increasing the temperature to 350 °C had very little additional impact. 375 °C was more effective, suggesting that there is possibly a second diffusion mechanism becoming significant in this temperature range. Finally, the absorption was totally bleached in the 400-500 °C range. These results suggest that there are at least two, and possibly three, different oxygen diffusion processes in this sample.

The anneal of sample 202B1 (Figure 4-7) showed that the low temperature mechanism saturates quickly at a temperature below 300 °C, with a 200 °C anneal no longer increasing the transmittance after the 300 °C treatment. The final diffusion mechanism, which totally bleached the absorption band, now occurred at or below 400 °C. The appearance of a short-wavelength absorption edge after the final 400 °C anneal suggests that enough oxygen had now diffused into the film to cause an oxide-like absorption edge.

A common rule of thumb for thermally activated processes is to assume that the activation energy of the process is $25kT$, where T is the temperature at which the

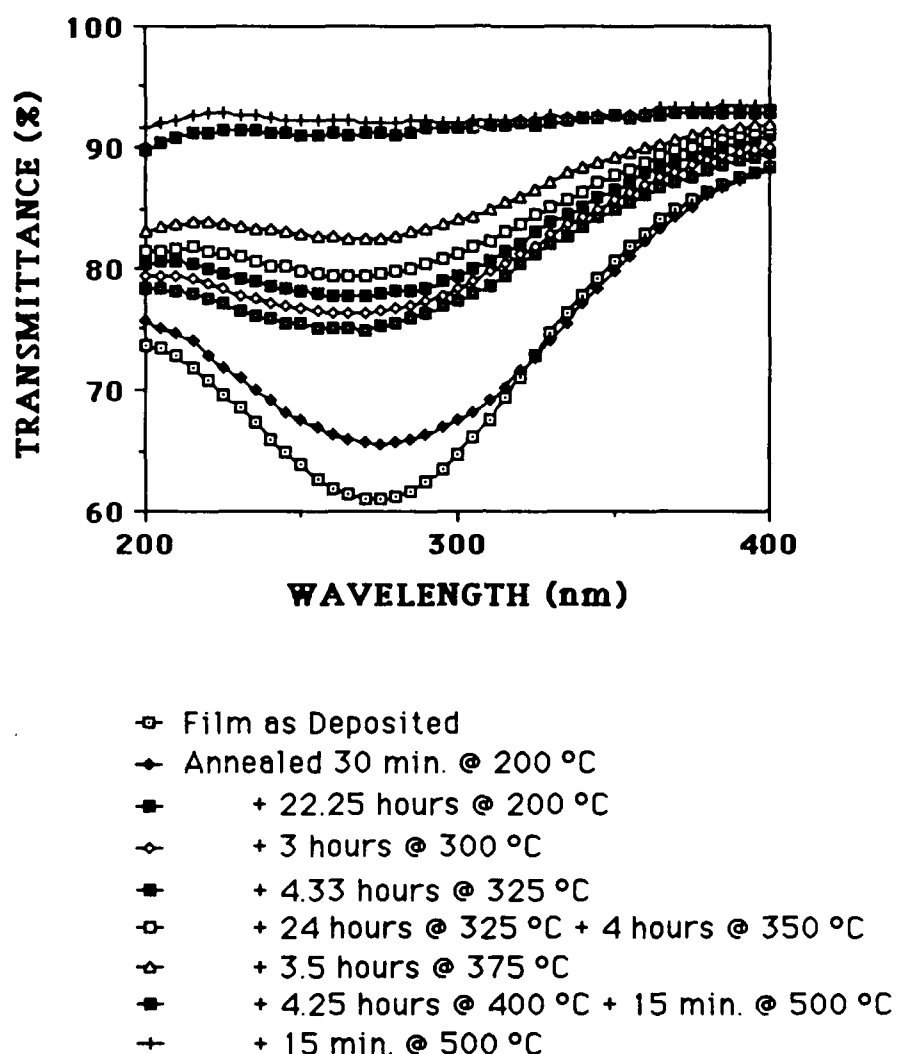


Figure 4-6. Ultraviolet transmittance of an IAD MgF_2 film after successive thermal anneals, showing the thermal bleaching of the color center absorption band.

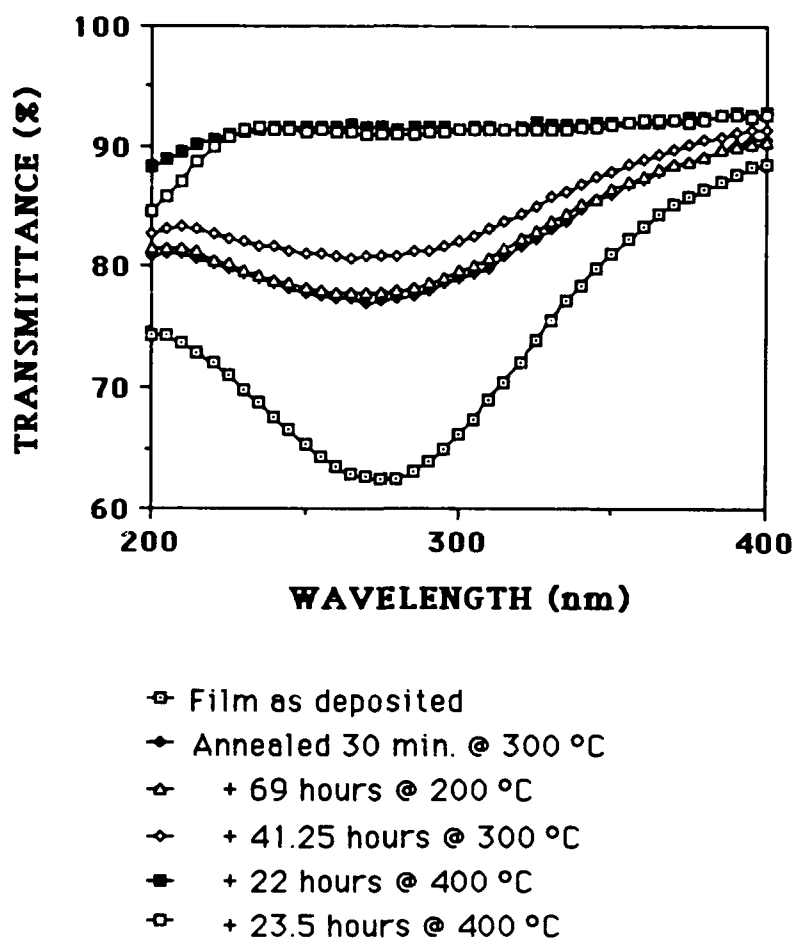


Figure 4-7. Ultraviolet transmittance of an IAD MgF_2 film deposited in the same batch with the film of Figure 4-5, showing the effects of a different set of thermal anneals on the transmittance.

process becomes significant and k is Boltzmann's constant (Townsend, Kelly, and Hartley 1976). A temperature of 500 °C thus corresponds to an activation energy of 1.5 eV. Catlow, James, and Norgett (1976) theoretically studied vacancy diffusion through crystalline MgF_2 and determined activation energies for vacancy diffusion between the differing anion sites. The calculated values are 0.03, 0.31, and 1.53 eV. The former two energies correspond to cryogenic temperatures, while the third agrees surprisingly well with our result that the absorption bleaches for anneals between 400 and 500 °C. These calculated values are for vacancy diffusion, but we may assume that the activation energies for anion diffusion are similar.

CHAPTER 5

THE ION-ASSISTED DEPOSITION OF CRYOLITE AND ALUMINUM FLUORIDE

Cryolite (Na_3AlF_6) is a very popular low-index coating material for applications in which the coating can be protected from atmospheric moisture, such as in cemented beamsplitters. A solid solution of aluminum fluoride (AlF_3) and sodium fluoride (NaF) in a 1:3 ratio, it is extremely hygroscopic (Weast 1978) and degrades quickly if left unprotected in air. We therefore decided to see if ion-assisted deposition might increase the water resistance of the material by increasing the packing density. According to Bourg (1962), cryolite deposited at room temperature has a packing density of 88%. In retrospect, this packing density is surprisingly high and suggests that the hygroscopicity dominates the microstructure of the film, but at the time of this experiment we felt that an improvement in microstructure could be beneficial.

Aluminum fluoride (AlF_3) is a very similar material to cryolite. Also a hygroscopic low-index material, conventional AlF_3 films deposited onto ambient temperature substrates have a packing density below 60% (Heitmann 1970). It should therefore be possible to densify AlF_3 films by IAD, but the hygroscopic nature of the material will be a serious problem.

Ion-Assisted Deposition of Cryolite

We evaporated CERAC 99.9% pure cryolite material resistively from tantalum boats at a rate of approximately 6 Å/sec. Bourg (1962) has previously shown that the refractive index of cryolite varies substantially with substrate temperature, but stabilizes above approximately 100 °C. We have therefore chosen 100 °C as our chamber temperature for these depositions. Both oxygen and argon bombardment have been tried.

We first investigated argon bombardment of cryolite. Argon bombardment at 300 eV does not cause additional absorption in the visible, but the ultraviolet absorption edge definitely degrades (Figure 5-1). Density measurements made with RBS and optical profilometry by Michael Messerly show that argon bombardment under these conditions actually decreases the film density (Table 5-1). Unfortunately, index measurements could not be made with any accuracy because of the low fringe contrast of cryolite on fused silica.

When oxygen bombardment was used, the results are similar to those observed with MgF₂. 40 μA/cm² of 300 eV oxygen ions can be used with no additional absorption in the visible, and a mild degradation in the ultraviolet transmittance (Figure 5-2).

The Rutherford backscattering results for the cryolite films bombarded by 300 eV ions are highly unusual (Figure 5-3). There appears to be little variation in stoichiometry with ion current density; the major difference is between the films deposited in argon or oxygen atmospheres. The sodium to aluminum ratio is approximately 2.0-2.3 for oxygen and 1.5-1.8 for argon, as opposed to the

TABLE 5-1. Densities of Argon-Bombarded IAD Cryolite Films

Beam Parameters	Density (g/cm ³)
Unbombarded	3.14
300 eV, 40 $\mu\text{A}/\text{cm}^2$	3.07
300 eV, 80 $\mu\text{A}/\text{cm}^2$	2.63

stoichiometric value of three (Figure 5-4). Pulker and Zaminer (1970) have shown that the ratio of NaF to AlF_3 molecules in a cryolite film is a function of the source material temperature, as the temperature dependences of the vapor pressures of the two molecules are different. An excess of aluminum over sodium in their experiment occurred for a source temperature of approximately 1000 °C, with more sodium present at lower temperatures. This suggests that we could have improved the sodium to aluminum ratio--if a ratio of three is indeed preferable--by lowering the deposition rate, thus reducing the source temperature. The fluorine deficiency increases very slightly with increasing ion flux (Figure 5-5), but this deficiency is less than that observed for other fluorides. The anion to cation ratio indicates that there is an excess of oxygen present, and that tightly bound oxygen is presumably present in the films.

A humidity test was performed to determine if ion-assisted deposition could mitigate the hygroscopic nature of the cryolite. An unbombarded film and an IAD film bombarded with $15 \mu\text{A}/\text{cm}^2$ of 100 eV oxygen ions were subjected for thirty minutes to 50 °C with 80% relative humidity. Both films were covered after the test with microscopic patches some tens of microns across. These patches covered approximately half the surface area of the films and each appeared to surround a central pit which apparently was the site of moisture penetration. The poor performance of these films in such a mild test suggested that the hygroscopicity of the films was too great to allow for any noticeable packing density effects.

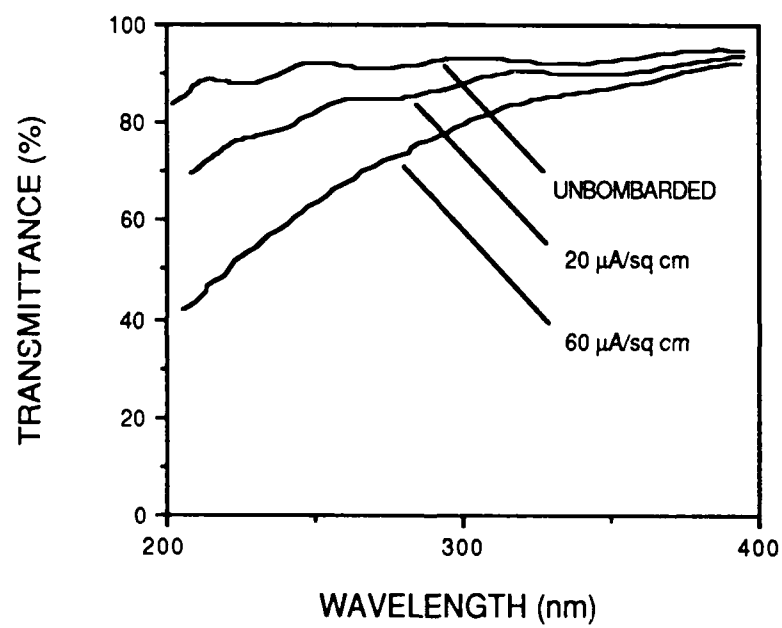


Figure 5-1. Ultraviolet transmittance of cryolite films bombarded with 300 eV argon ions.

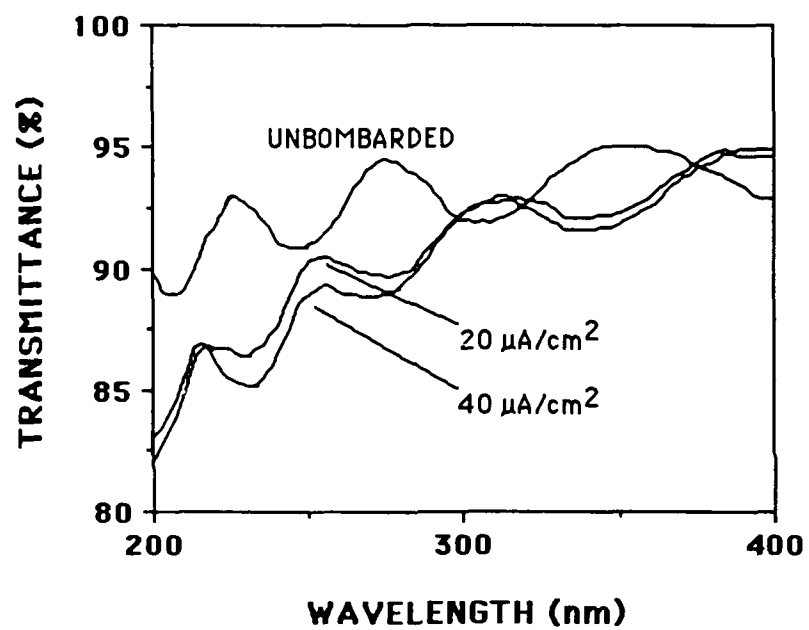


Figure 5-2. Ultraviolet transmittance of oxygen-bombarded cryolite films.

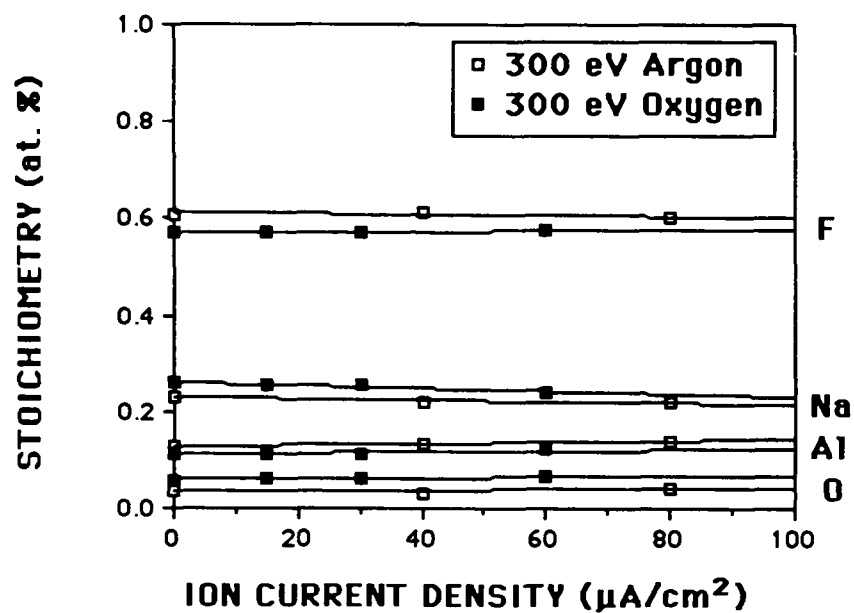


Figure 5-3. Stoichiometries of IAD cryolite films as a function of ion current density for both oxygen and argon ion bombardment.

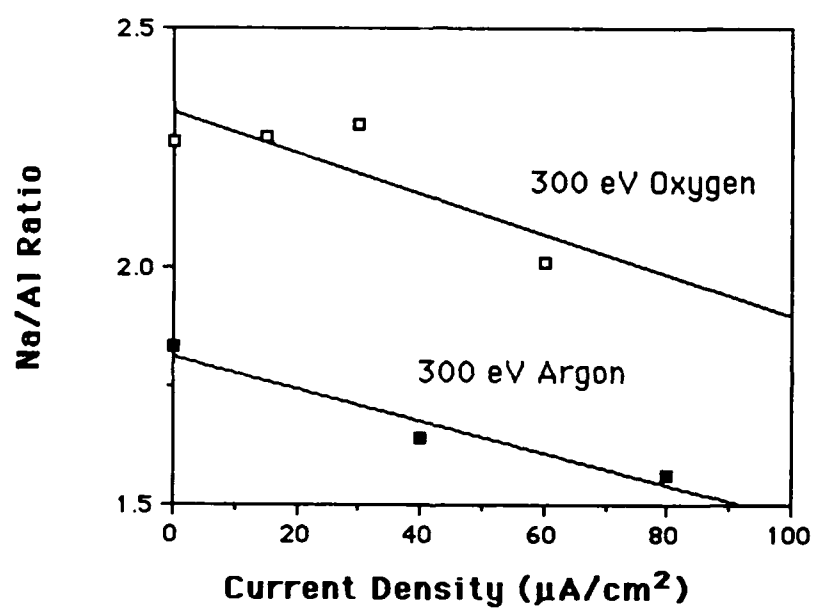


Figure 5-4. Ratio of sodium atoms to aluminum atoms in IAD cryolite films as a function of ion beam current density for both oxygen and argon ion bombardment.

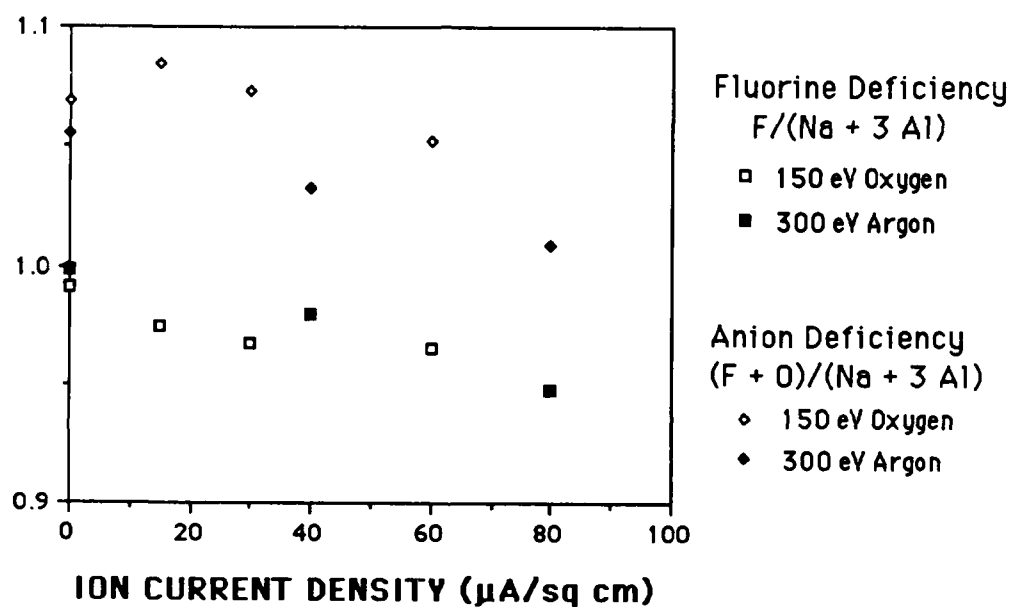


Figure 5-5. The fluorine deficiency $y/(w+3x)$ and the anion deficiency (or surplus) $(y+z)/(w+3x)$ of IAD cryolite films as a function of ion beam current density for both oxygen and argon ion bombardment, with the stoichiometry expressed as $\text{Na}_w\text{Al}_x\text{F}_y\text{O}_z$.

From the cryolite results, we conclude that IAD offers no advantage for such profoundly hygroscopic materials. In any case, cryolite forms surprisingly dense films in the first place, leaving little room for densification through IAD.

Ion-Assisted Deposition of Aluminum Fluoride

We resistively evaporated CERAC 99.5% pure AlF_3 from molybdenum boats at a rate of 6 Å/sec with the chamber at ambient temperature. Films approximately 5000 Å thick were deposited onto fused silica, silicon, and graphite substrates. The CERAC material outgassed badly, raising the chamber pressure to $1-2 \times 10^{-5}$ mbar; this pressure did not decrease noticeably with time, so we deposited the films under these conditions. The residual gas analyzer was not operational during this period, so we could not positively identify the gases. Water would be the most likely contaminant: We have seen similar behavior from old CaF_2 material, with newer material behaving normally. The AlF_3 material was purchased approximately one year before this experiment, but was stored in an unopened metal tin until these experiments. So, while it is possible that the material took up moisture during storage, it was certainly unexpected.

An unbombarded AlF_3 film was highly transparent across the visible (Figure 5-6) but showed large infrared absorption in the 3 μm water band, suggesting that the film was very porous. Films were first deposited with heavy bombardment by 300 eV ions in an effort to increase the packing density to unity. Figure 5-7 shows that 60 $\mu\text{A}/\text{cm}^2$ bombardment decreased the depth of the 3 μm absorption band to 2% in

transmission, as opposed to the 9% of the unbombarded film; however, the absorption of the film in the near UV increased noticeably (Figure 5-6). Raising the current density to $100 \mu\text{A}/\text{cm}^2$ eliminated the $3 \mu\text{m}$ band, suggesting that the packing density was indeed near one, but the absorption in the near UV increased even more and became appreciable in the visible region. We were thus able to increase the packing density with 300 eV argon bombardment, but at the expense of increased visible absorption as we disrupted the film structure. It is interesting to note that once the $3 \mu\text{m}$ water band is eliminated, the $2.7 \mu\text{m}$ OH^- band becomes discernible, suggesting that OH^- radicals are incorporated into fluorine vacancies during the deposition.

We next attempted a milder bombardment with 200 eV argon ions to seek a compromise between packing density and absorption. We found that an ion current density of $30 \mu\text{A}/\text{cm}^2$ did not cause absorption in the visible (Figure 5-9), but was still ineffective in eliminating the water in the films (Figure 5-8). As a final attempt, we lowered the ion beam current density to $20 \mu\text{A}/\text{cm}^2$ and raised the ion energy to 300, 400, and 500 eV in the hope that this would allow densification without increased absorption. Figures 5-10 and 5-11 show that the water band did not improve significantly above 300 eV, but the visible absorption again increased.

The films were finally subjected to a humidity test at 50°C and 95% relative humidity for two hours to check their moisture resistance. All the coatings were severely damaged by this test. The hygroscopic nature of the AlF_3 is obviously more important than the porosity of the films, so an increase in packing density does not have any noticeable impact on the moisture resistance of the films.

To summarize this study, we have succeeded in increasing the packing density of AlF_3 films to near-unity by bombardment with a 300 eV, $100 \mu\text{A}/\text{cm}^2$ argon ion beam, but only at the expense of absorption in the visible region. We have not investigated oxygen bombardment of AlF_3 , but our results with cryolite suggest that the packing density could be increased with only a minimal increase in absorption. The only negative feature would then be the large oxygen content in the films as a result of oxygen ion implantation. This would increase the index of the films, as aluminum oxide has a refractive index above 1.60 in the visible (see Chapter 7). The material would then be less attractive as a low index layer on glass or fused silica, and the hygroscopicity of the AlF_3 would still jeopardize the integrity of the films.

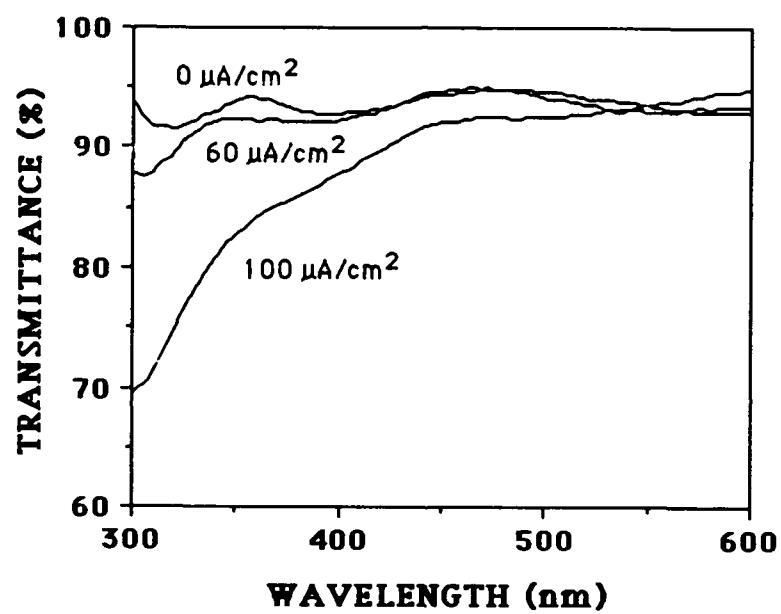


Figure 5-6. Transmittance in the visible region of unbombarded and 300 eV argon-bombarded AlF₃ films.

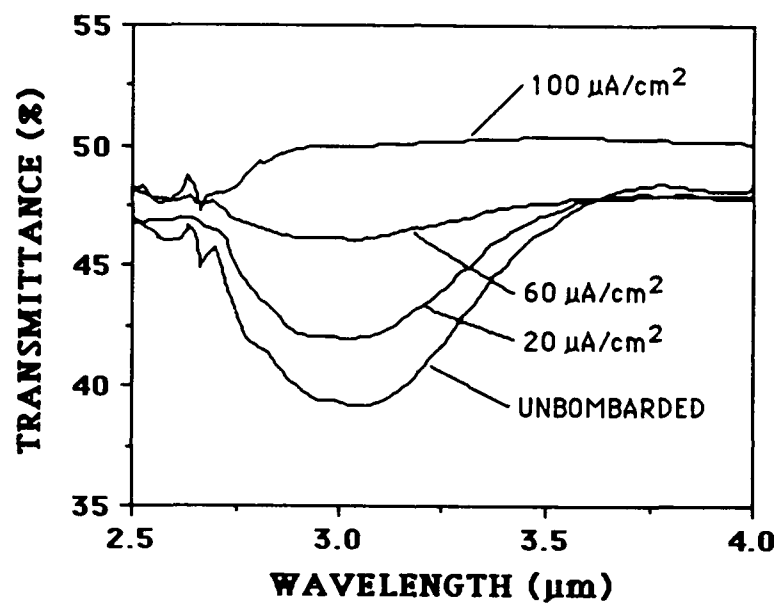


Figure 5-7. Infrared transmittance of unbombarded and 300 eV argon-bombarded AlF_3 films in the 3 μm water absorption band.

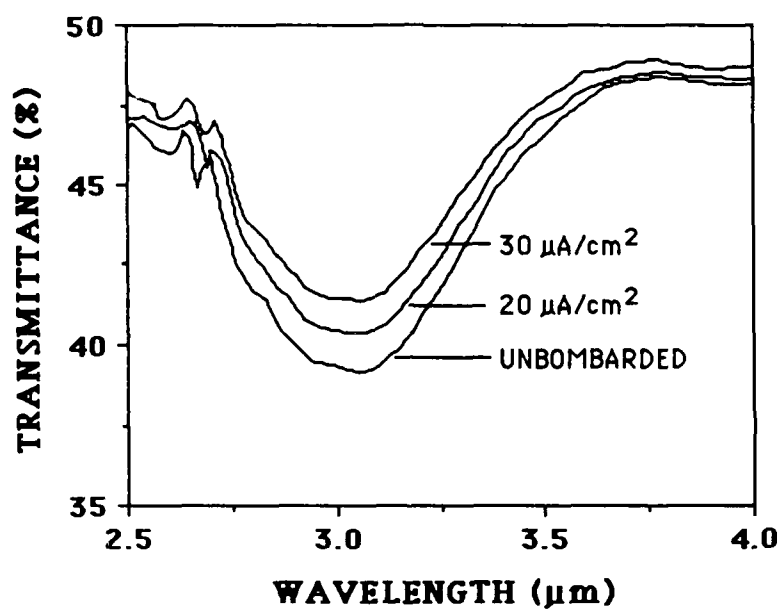


Figure 5-8. Infrared transmittance of unbombarded and 200 eV argon-bombarded AlF₃ films in the 3 μm water absorption band.

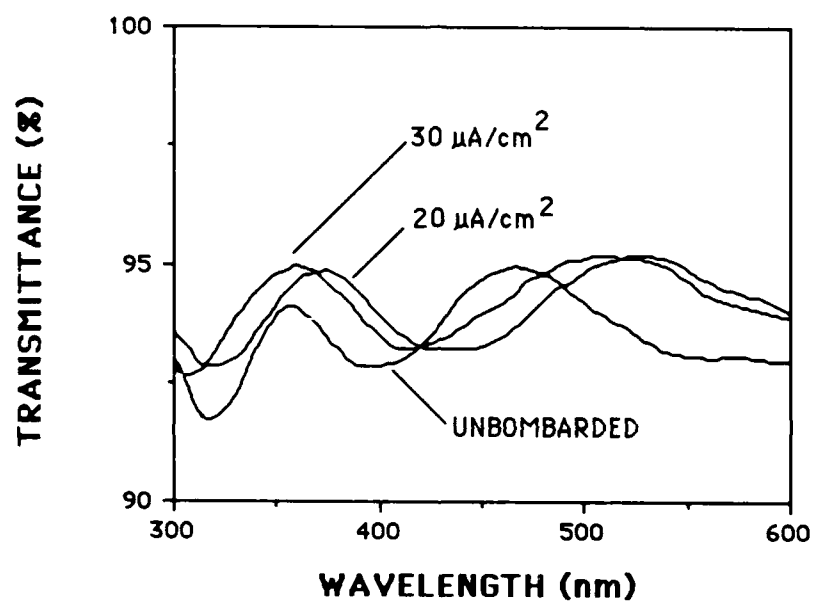


Figure 5-9. Transmittance in the visible region of 200 eV argon-bombarded AlF_3 films.

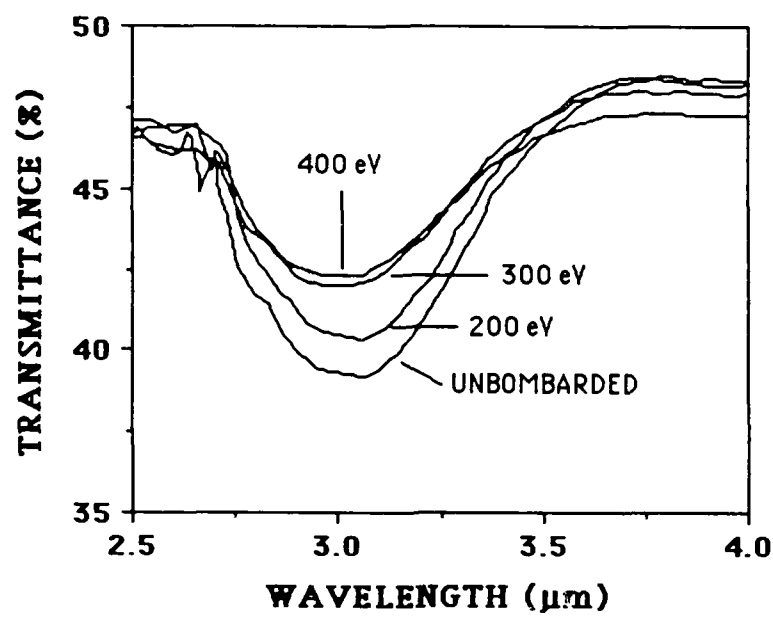


Figure 5-10. Infrared transmittance in the 3 μm water absorption band of IAD AlF_3 films bombarded with $20 \mu\text{A}/\text{cm}^2$ of argon ions.

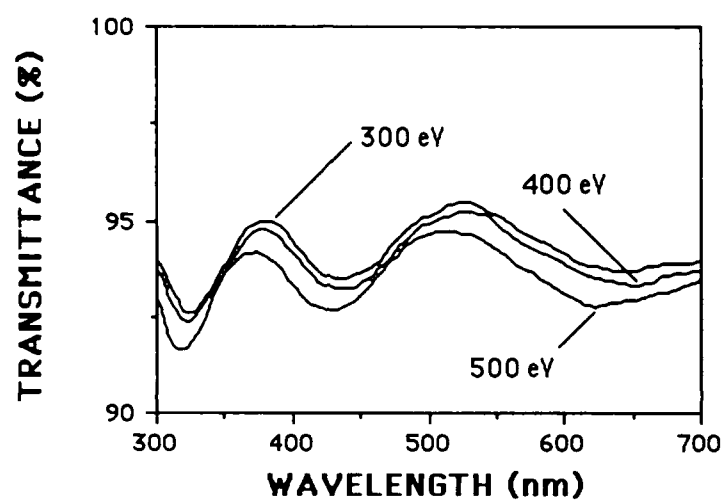


Figure 5-11. Transmittance in the visible of IAD AlF₃ films bombarded with 20 $\mu\text{A}/\text{cm}^2$ of argon ions.

CHAPTER 6

THE ION-ASSISTED DEPOSITION OF LANTHANUM AND LANTHANIDE (Ce,Nd) TRIFLUORIDES

Rare earth fluoride thin films are of great interest because of their excellent transmission from the ultraviolet (even the vacuum ultraviolet) to the infrared (Pulker 1979). LaF_3 is a popular material in this family; it is transparent from approximately 130 nm to 10 μm and has a very high laser damage threshold (Rainer et al. 1985). However, like most fluorides, it suffers from large tensile stress (Rainer et al. 1985) and has a packing density of only 0.80 when deposited onto ambient temperature substrates (Ogura 1975). We have therefore investigated ion-assisted deposition as a means of improving lanthanum fluoride coatings. In the next section, we will discuss the ion-assisted deposition of two closely related lanthanide fluorides (lanthanum is not a member of the lanthanide family), NdF_3 and CeF_3 .

The following discussion of the ion-assisted deposition of LaF_3 thin films is an expanded version of a paper submitted to Applied Optics (Targove et al. 1987). The style of presentation therefore differs somewhat from the rest of this dissertation.

Ion-Assisted Deposition of Lanthanum Fluoride

Deposition Conditions

All LaF_3 coating runs were performed at room temperature with a residual pressure of $1.5\text{--}3 \times 10^{-6}$ mbar and at a deposition rate of 6 Å/sec. The LaF_3 films were resistively evaporated from molybdenum boats at a rate of 6 Å/sec using CERAC 99.9% pure starting material. LaF_3 evaporates nicely in this manner, and the deposition rates were very uniform throughout the runs.

Refractive Index and Packing Density

The increase in packing density caused by ion-assisted deposition can be calculated from the increase in refractive index (Ogura 1975). We calculated the refractive index and extinction coefficient of single layer coatings using the envelope method of Manifacier, Gasiot, and Fillard (1976) as described in Chapter 3. The refractive index data are then fit by least-squares to a dispersion relation of the form

$$n^2 = A + B/\lambda^2$$

which is a first-order approximation to the Sellmeier dispersion relation away from resonance (Smith and Baumeister 1979). The index of refraction is then converted into packing density using a linear formula for refractive index as a function of packing

density which assumes that the film is a mixture of columns and voids (Kinosita and Nishibori 1969):

$$n_f = p n_s + (1 - p) n_v$$

where

n_f = the measured refractive index of the film,

n_s = the refractive index of the material in the film columns,

n_v = the refractive index of the film voids,

and

p = the packing density of the film.

We assume here that the columns have the bulk index of the material and that the voids are filled with water. These assumptions and the choice of the linear model together result in an estimate for the packing density which is a lower bound on the true value.

The variation in refractive index at a wavelength of 350 nm with ion beam current density is shown in Figures 6-1 and 6-2 for bombardment of films with a physical thickness of 500 nm by 300 and 500 eV argon and 300 eV oxygen ions. The bulk index is taken to be 1.624 at 350 nm, an average of the ordinary and extraordinary bulk refractive indices (Driscoll 1978). These curves show that the refractive index,

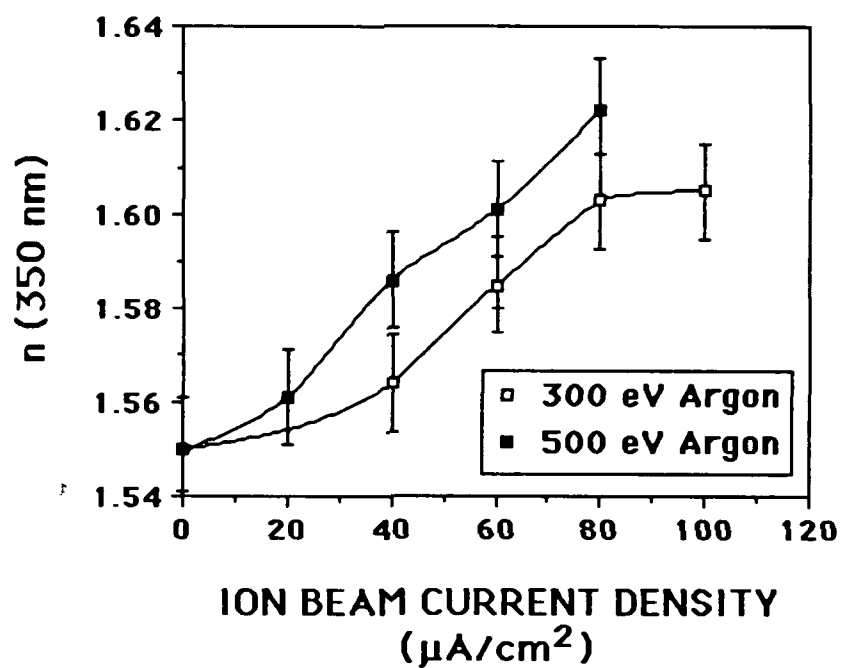


Figure 6-1. Index of refraction at 350 nm of LaF_3 films bombarded with 300 and 500 eV argon ions as a function of ion beam current density.

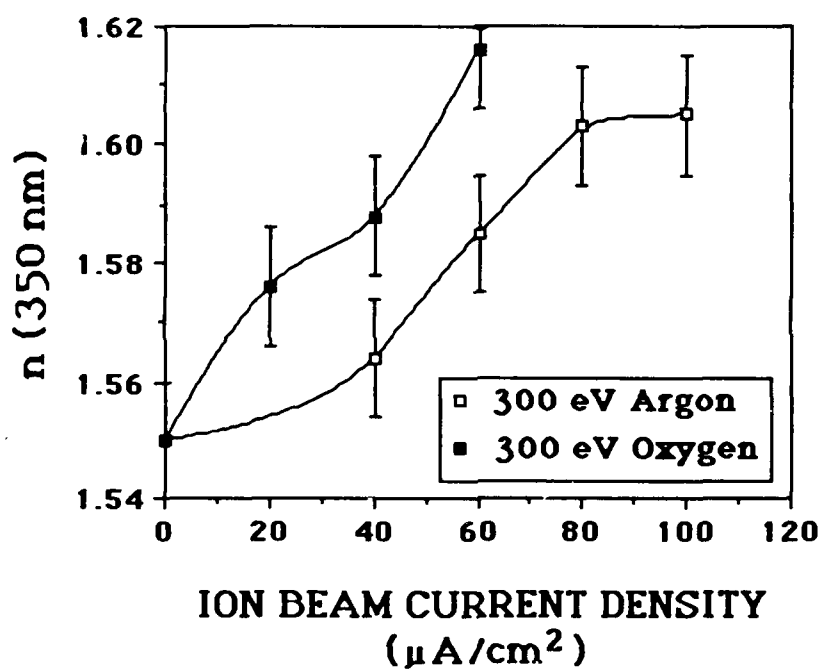


Figure 6-2. Index of refraction at 350 nm of LaF_3 films bombarded with 300 eV argon and oxygen ions as a function of ion beam current density.

and thus the packing density, is substantially increased by argon bombardment at both 300 and 500 eV. The indices of the oxygen-bombarded films cannot be related to packing density in a similar manner: n_s probably lies between the refractive indices of LaF_3 and La_2O_3 because of the implanted oxygen in the coatings.

The packing densities of the argon-bombarded films are then calculated by substituting the data from Figure 6-1 into the linear interpolation, with the refractive index of the water in the voids taken to be 1.35 at 350 nm (Lauer and Miller 1947). Packing densities have been calculated from the refractive index data assuming a bulk index for n_s (Figures 6-3 and 6-4). However, Ogura pointed out (Ogura 1975) that n_s is not necessarily the bulk index and substituted 1.59 at 500 nm; we have also tried this value at 500 nm. These results are compared in Figures 6-3 and 6-4. The packing densities obtained using $n_s=1.59$ agree closely with Ogura's value of 0.80 for conventional coatings deposited onto ambient temperature substrates and exceed those obtained with a bulk column index by 0.04-0.06. We achieved unity packing density by bombardment at 500 eV with a current density of $80 \mu\text{A}/\text{cm}^2$ (the calculated value was actually 1.02 with the bulk value for n_s , which has been graphed as 1.0 for clarity), and a packing density greater than 90% was reached for 300 eV, $100 \mu\text{A}/\text{cm}^2$ bombardment.

Extinction Coefficient

The extinction coefficients of the single layer films were also calculated with the Manifacier method. The argon-bombarded films all have extinction coefficients at

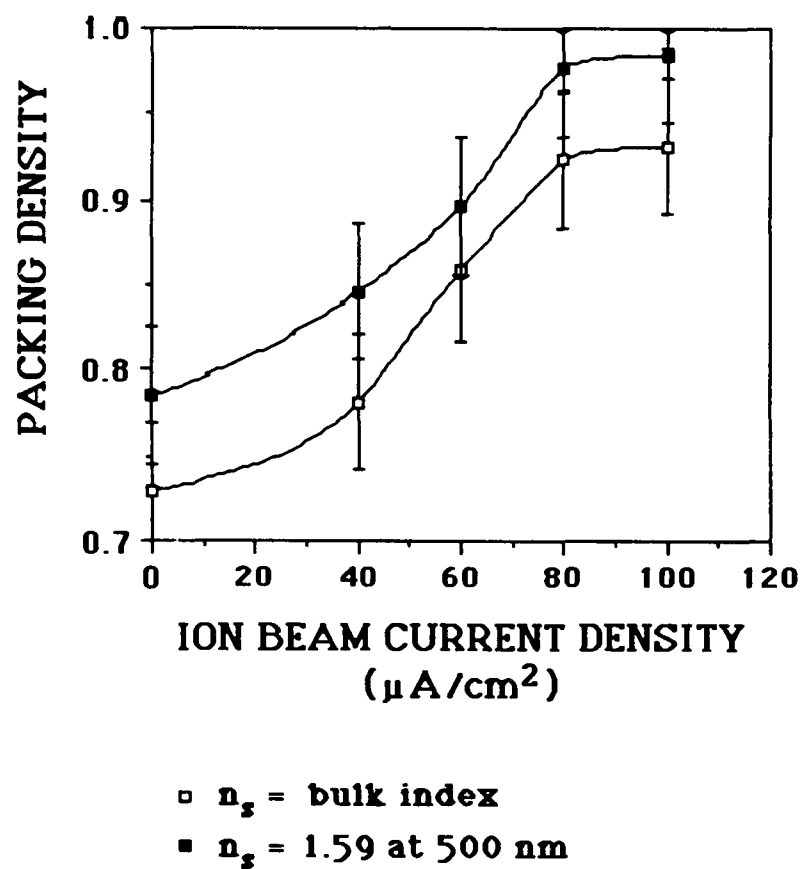


Figure 6-3. Packing density of IAD LaF₃ films as a function of ion beam current density for bombardment by 300 eV argon ions.

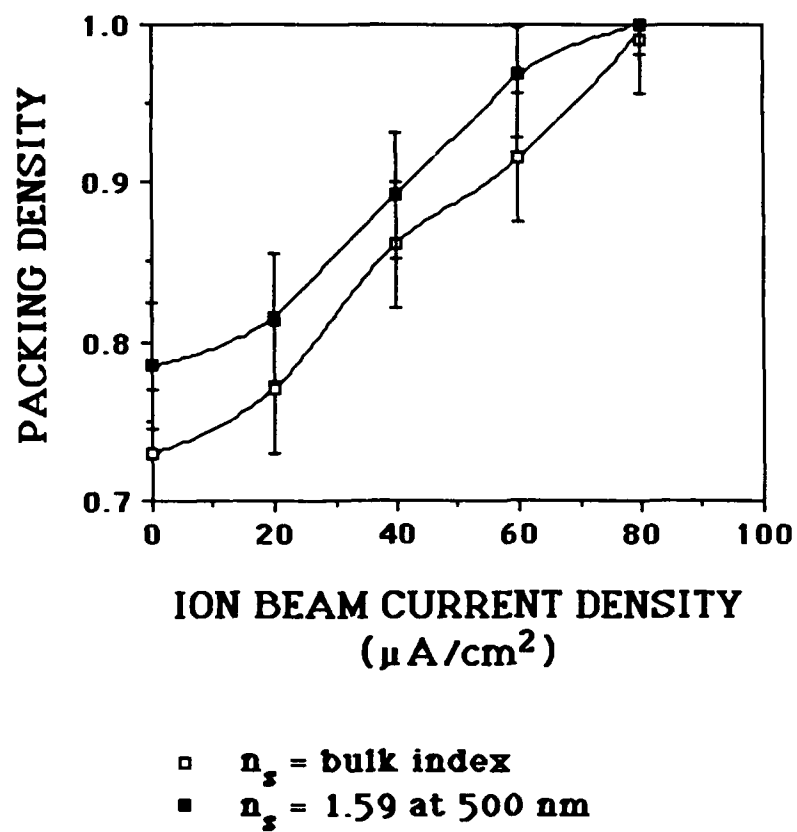


Figure 6-4. Packing density of IAD LaF₃ films as a function of ion beam current density for bombardment by 500 eV argon ions.

$\lambda = 250$ nm below the accuracy of the calculation (approximately 3×10^{-4}), with the exception of the 500 eV, $80 \mu\text{A}/\text{cm}^2$ bombardment. This film is therefore the only argon-bombarded one included in Figure 6-5. With oxygen bombardment, however, the films begin to show a short-wavelength absorption edge characteristic of lanthanum oxide (Figure 6-5) (Hass, Ramsey, and Thun 1959). This absorption edge shifts towards longer wavelengths as the ion beam current density increases because of increasing oxygen implantation.

Rutherford Backscattering Analysis

We have analyzed with RBS films bombarded with 300 eV argon and oxygen ions. These samples are approximately 100 nm thick; for thicker films, the rear of the fluorine peak would overlap the front of the oxygen peak. Writing the film stoichiometries as LaF_xO_y , a perfectly stoichiometric film would have $x=3$ and $y=0$. Our unbombarded films have $x=2.91-3.00$ and $y=.11-.15$. We have previously noted that unbombarded MgF_2 films of good optical quality sometimes are slightly fluorine deficient (Messerly 1987). Figures 6-6 and 6-7 show that all the bombarded films suffer a preferential sputtering of fluorine over lanthanum, as expected from simple sputtering theory (Betz and Wehner 1983). The argon-bombarded films contain a fairly constant amount of oxygen, probably a result of residual water vapor in the chamber. When oxygen ions are used, ion implantation sharply increases the oxygen content of the films. This extra oxygen compensates for the larger fluorine deficiency in the oxygen-bombarded films and explains their lack of absorption in the visible.

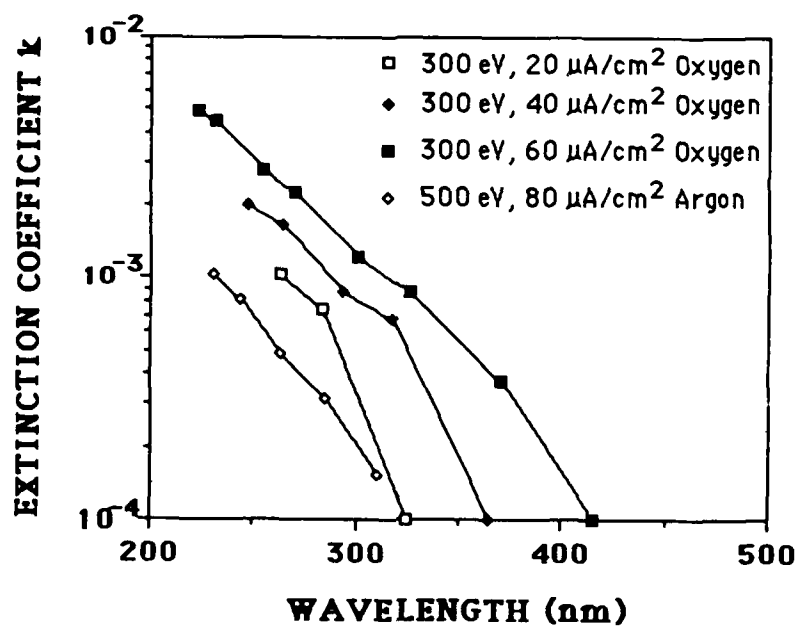


Figure 6-5. Ultraviolet extinction coefficient of IAD LaF_3 films.

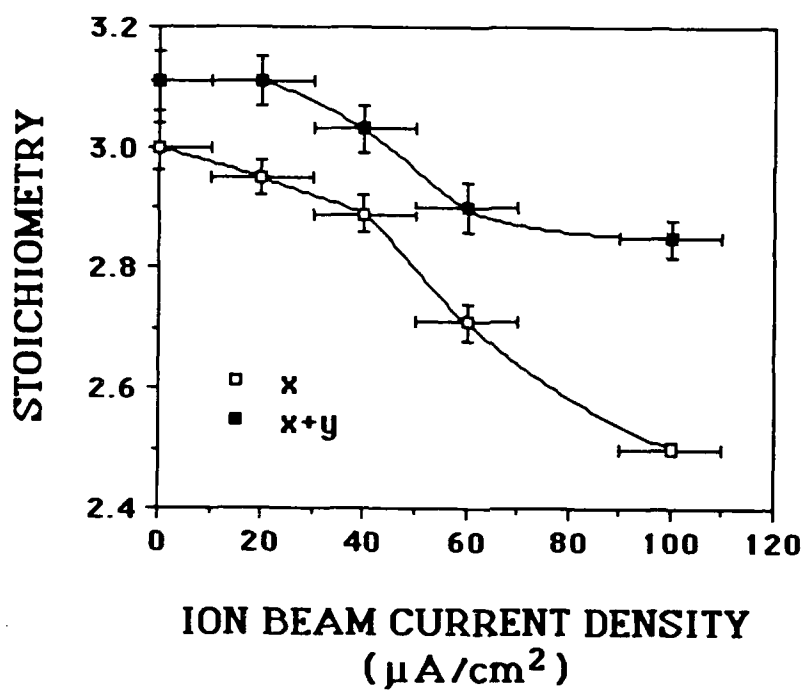


Figure 6-6. F-to-La ratio x and anion-to-cation ratio $x+y$ of IAD LaF_3 films bombarded with 300 eV argon ions as a function of ion beam current density, with the stoichiometry expressed as LaF_xO_y .

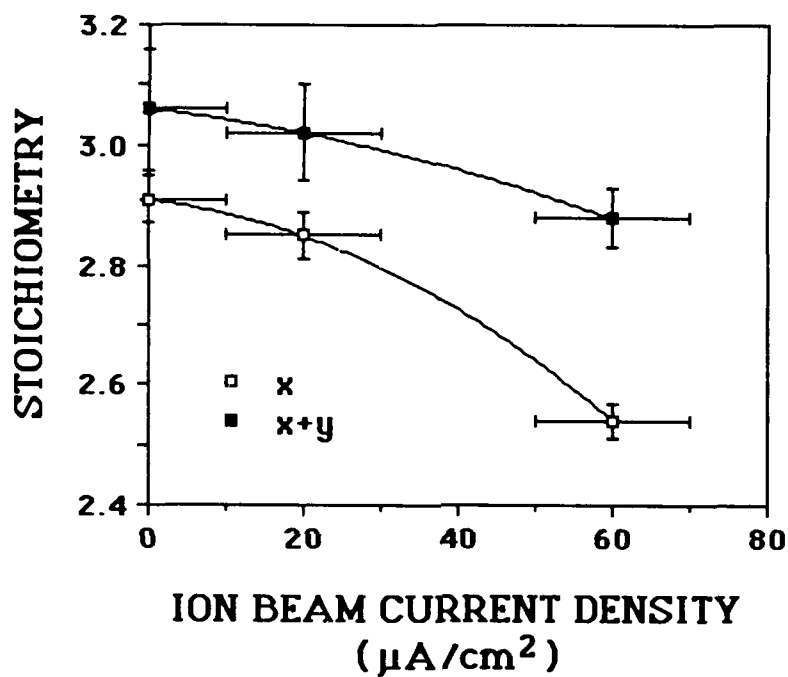


Figure 6-7. F-to-La ratio x and anion-to-cation ratio $x+y$ of IAD LaF_3 films bombarded with 300 eV oxygen ions as a function of ion beam current density, with the stoichiometry expressed as LaF_xO_y .

The anion-to-cation ratio $x+y$ is also plotted in Figures 6-6 and 6-7. The unbombarded films have a ratio greater than three, suggesting that more water molecules are adsorbed from the residual gases in the chamber than are needed to fill the fluorine vacancies in the film. With an ion current density of 20 or 40 $\mu\text{A}/\text{cm}^2$, the anion-to-cation ratio remains greater than three. Films deposited with these ion beam parameters do not show the sharp ultraviolet transmission cutoff typical of anion vacancies (Gibson and Kennemore 1986). This suggests that most of the anion vacancies caused by the preferential sputtering are filled by oxygen atoms or complexes; but, as mentioned above, oxygen-bombarded films do show an oxide-like transmission cutoff because of the oxygen implanted into the films. For 60 $\mu\text{A}/\text{cm}^2$ argon bombardment, however, $x+y$ is approximately 2.9 and the films begin to show a slight ultraviolet absorption due to anion vacancies not filled by oxygen or water. This absorption increases with larger current densities as the anion-to-cation ratio in the films decreases further. The bombarded samples all have a tungsten concentration of less than 0.02 at. % due to erosion and sputtering from the tungsten filaments of the ion gun. In addition, argon-bombarded films contain 0.4-2 at. % argon implanted by the ion bombardment. As shown above, these impurities appear to be much less important than oxygen content to the optical properties.

X-Ray Diffraction

Lanthanum fluoride is an unusual material in that coatings deposited onto ambient temperature substrates are highly crystalline. The identification of the single observed phase has been a topic of continued discussion for fifty years (Greis and Haschke

1982); currently, LaF_3 is thought to have a trigonal unit cell of the tysonite type (Greis and Haschke 1982). This structure surrounds each lanthanum atom with 9 nearest-neighbor fluorine atoms, with two fluorine atoms slightly further away.

X-ray diffraction measurements have been made with the films on fused silica used for the optical measurements above. The unbombarded film shows three strong lines at 2θ values of 24.8° , 27.6° , and 43.7° which correspond to the (110), (111), and (300) orientations of the LaF_3 crystal (JCPDS 1967, Plate 8-461). Figure 6-8 shows x-ray diffraction data for films bombarded with 300 eV argon ions. The orientations of the LaF_3 grains change, with the (111) orientation disappearing for current densities of $80 \mu\text{A}/\text{cm}^2$ and a new peak appearing at 26.5° which does not correspond to any LaF_3 orientation. For $120 \mu\text{A}/\text{cm}^2$ bombardment, this is the predominant orientation in the film. Since the RBS results above show that the oxygen content of the films is increasing with ion current density, it is natural to assume that the new phase is either lanthanum oxide or oxyfluoride. According to the JCPDS compendium, lanthanum oxide has a hexagonal crystalline structure with the (100) orientation having a line at 26.1° (JCPDS 1967, Plate 5-0602), far enough from 26.5° to eliminate La_2O_3 from consideration. The tetragonal phase of lanthanum oxyfluoride has a 26.6° line from the (101) orientation which shifts to smaller angles as the crystal becomes more fluorine deficient, while the rhombohedral phase has a 26.5° line from the (222) orientation (Zachariasen 1951). Of the three phases, only the tetragonal lanthanum oxyfluoride

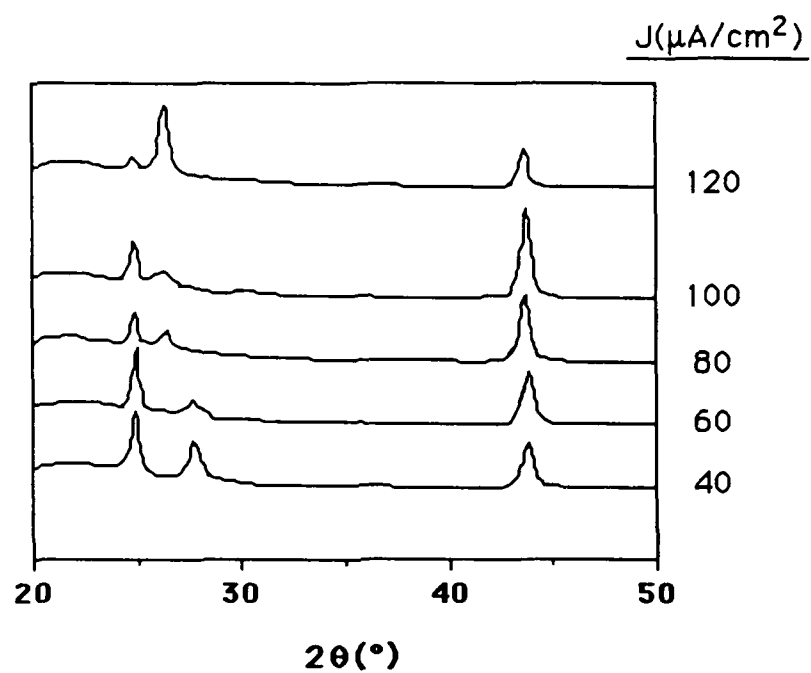


Figure 6-8. X-ray diffraction scans of unbombarded and 300 eV argon-bombarded LaF_3 films.

phase has its strongest powder diffraction line near 26.5° . With only one x-ray line, we can conclude that the oxygen or oxygen complexes in the film are distorting the crystalline lattice sufficiently to cause a phase transition from the fluoride phase to an oxyfluoride phase for some percentage of the grains in the films. The full width at half maximum of the 26.5° line for the 300 eV, $120 \mu\text{A}/\text{cm}^2$ argon-bombarded sample is 0.5° , corresponding to an average grain size of approximately 200 Å. This is approximately the same grain size observed in the unbombarded LaF_3 film, suggesting that we are indeed oxidizing entire crystalline grains with heavy bombardment.

To bring out more x-ray lines, the 300 eV, $120 \mu\text{A}/\text{cm}^2$ argon-bombarded sample was annealed in air for two hours at 500°C . After this anneal, the 44.7° line shifted to 44.3° . The possible identifications for this new line are the (200) tetragonal LaOF peak at 44.3° , the (332) rhombohedral LaOF peak at 44.2° , and the (110) La_2O_3 peak at 44.9° . This confirms our decision to rule out lanthanum oxide, suggesting that the observed phase transition involves the formation of an oxyfluoride phase. There is still insufficient data to choose between the two different oxyfluoride phases.

X-Ray Photoelectron Spectroscopy

XPS can provide very important insights into chemical bonding. Several of the LaF_3 samples on fused silica were examined with XPS at the Optical Sciences Center. These samples were also examined optically on the Cary 14 and with x-ray diffraction, allowing us to correlate the various measurements.

The XPS peak corresponding to the oxygen 1s orbital is particularly interesting. For $60 \mu\text{A}/\text{cm}^2$ of 300 eV argon ion bombardment (Figure 6-10), the O 1s peak appears to be a closely spaced doublet. The other samples appear to have wide peaks centered at different binding energies; however, these peaks can be resolved into two Gaussian peaks spaced 2-2.5 eV apart. Figures 6-9, 6-10, and 6-11 show the resolved Gaussians which best fit the experimental data. We can now see that the unbombarded sample predominantly has oxygen atoms with the lower binding energy (Figure 6-9). As the ion flux increases, a growing percentage of the atoms possess the higher O 1s binding energy. There is thus a fundamental change in the oxygen atom binding with increasing ion flux.

This change can be correlated with the x-ray diffraction data (Figure 6-8), which shows that increasing ion flux also causes a phase transition of crystallites from a fluoride to an oxyfluoride phase, and the RBS data which shows that the oxygen content of the films increases with increasing ion flux. The lower binding energy peak predominant in the unbombarded film is probably due to oxygen in water molecules, while the higher energy peak probably represents oxygen incorporated into the crystalline lattice of the films. This is consistent with the fact that 300 eV, $100 \mu\text{A}/\text{cm}^2$ films have a larger oxygen content than the unbombarded films, but contain almost no water. We thus have a coherent explanation of the nature of the IAD LaF_3 films which explains the XPS, RBS, and x-ray diffraction data.

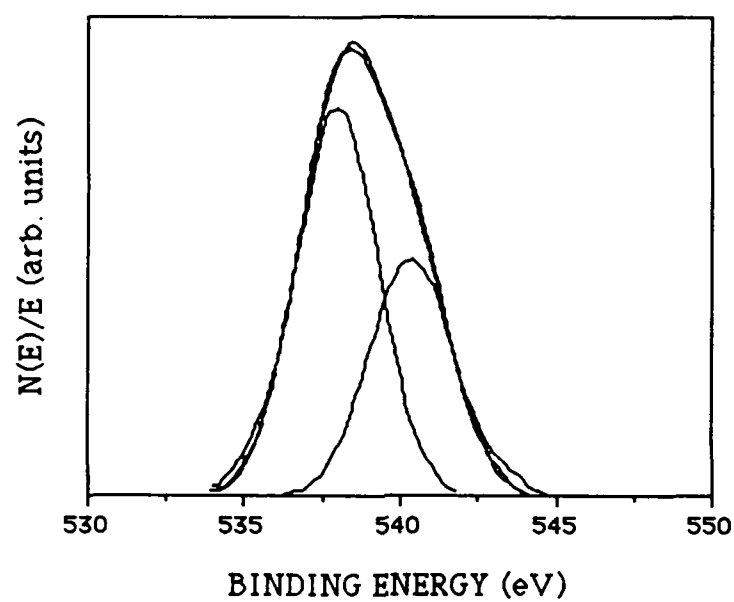


Figure 6-9. Oxygen 1s XPS peak for an unbombarded LaF_3 film showing the deconvolution of the peak into two Gaussians.

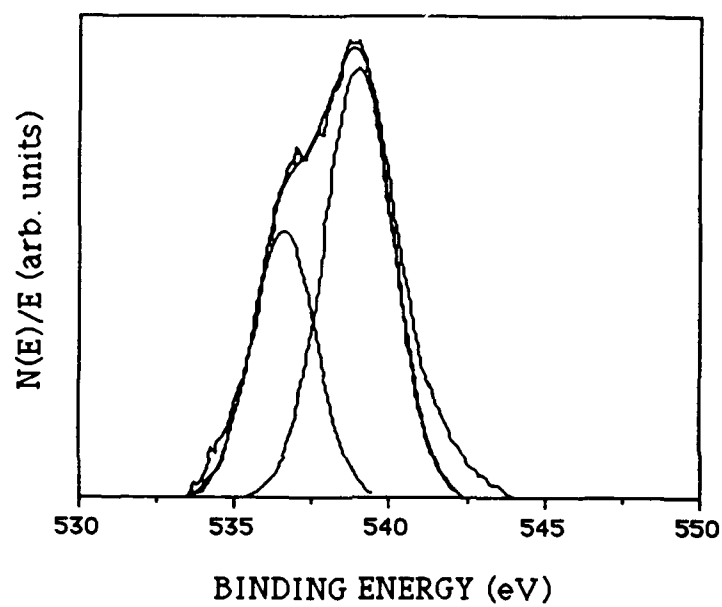


Figure 6-10. Oxygen 1s XPS peak for an IAD LaF_3 film bombarded with $60 \mu\text{A}/\text{cm}^2$ of 300 eV argon ions showing the deconvolution of the peak into two Gaussians.

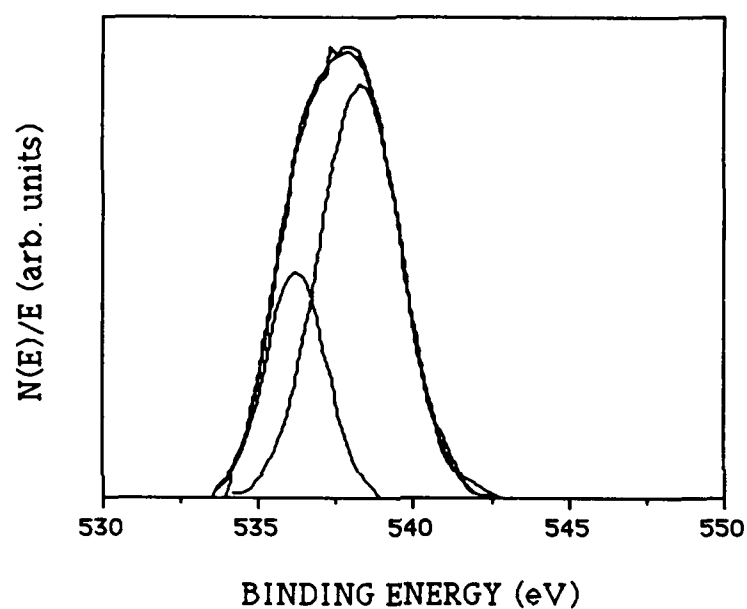


Figure 6-11. Oxygen 1s XPS peak for an IAD LaF_3 film bombarded with $100 \mu\text{A}/\text{cm}^2$ of 300 eV argon ions showing the deconvolution of the peak into two Gaussians.

Infrared Water Absorption Band

The amount of water present in a film is a good measure of its packing density. Allen (1982) has previously employed the magnitude of the $3\text{ }\mu\text{m}$ water absorption band as a qualitative measure of the densification caused by ion-assisted deposition. The infrared transmittance of films deposited on germanium substrates was measured with a Perkin-Elmer 983 FTIR spectrometer at OCLI. All of these films were deposited in the same batches as the fused silica samples used to calculate the refractive indices of the films and are thus approximately 500 nm thick.

These measurements show that the water content of the films decreases drastically as the ion beam current density increases (Figure 6-12). There is still a slight absorption band present in the 300 eV, $100\text{ }\mu\text{A}/\text{cm}^2$ and 500 eV, $60\text{ }\mu\text{A}/\text{cm}^2$ samples. From Figure 6-3, the packing densities of the identical films on fused silica were greater than 90%.

Multilayer Coatings

Once single-layer coatings had been characterized, two multilayer coatings were deposited to demonstrate the utility of the IAD process. These coatings were $(\text{HL})^{11}\text{H}$ stacks with $\text{H}=\text{LaF}_3$ and $\text{L}=\text{MgF}_2$ and a design wavelength of 400 nm. The bombardment parameters for the IAD multilayer are given in Table 6-1. The conventionally-deposited coating contained cracks from the cumulative tensile stress of both coating materials, while the IAD coating contained no cracks because of the previously observed tensile stress reduction associated with ion-assisted deposition (Jacobs et al. 1986). We then

Table 6-1. Deposition Conditions of an IAD LaF_3 / MgF_2 Stack.

Material	Dep. Rate (nm/sec)	Ion beam species	Ion beam energy (eV)	Ion current density ($\mu\text{A}/\text{cm}^2$)
MgF_2	0.6	Ar	300	40
LaF_3	0.6	Ar	300	100

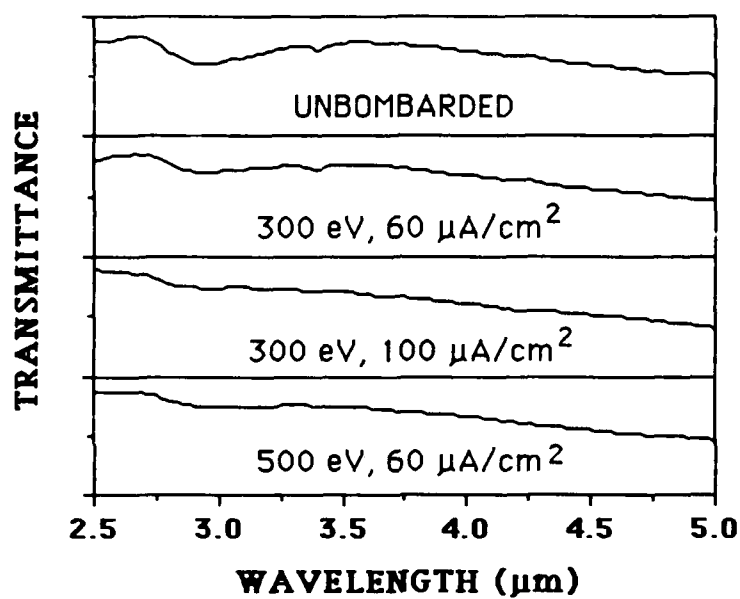


Figure 6-12. Transmittance of IAD LaF_3 films in the 3 μm water absorption band for varying argon ion beam energies and current densities. The transmittance scale is 45%-65% for each film.

measured the air-to-vacuum shift of these coatings using a specially constructed vacuum cell in the Cary 14 spectrophotometer. The transmittance spectrum of the conventionally-deposited coating shifted 5 nm between atmosphere and 15 mtorr as the adsorbed water was pumped from the coating (Figure 6-13), while the transmittance of the IAD coating showed no measurable shift (Figure 6-14), suggesting that the IAD process resulted in a near-unity packing density. In addition, the width of the reflectance band and peak reflectance of the IAD coating are both larger than for the conventional coating because the index contrast between the two materials has increased with bombardment. Indeed, the index of the LaF_3 layers increases more with bombardment than that of the MgF_2 layers. The IAD coating does, however, have approximately 2% absorption at peak reflectance.

Conclusions

Ion-assisted deposition has increased the packing density of lanthanum fluoride thin films to near-unity values with little or no increase in film absorption, even with large ion fluxes. The films do, however, begin to show an oxyfluoride component as the ion flux is increased. It appears that individual crystalline grains within the films undergo this phase transition, with the ratio of oxyfluoride grains to fluoride grains increasing with ion flux. Bombardment with oxygen ions, besides causing the fluoride-to-oxyfluoride transition at lower ion fluxes, also results in the expected oxide-like absorption edge in the near ultraviolet.

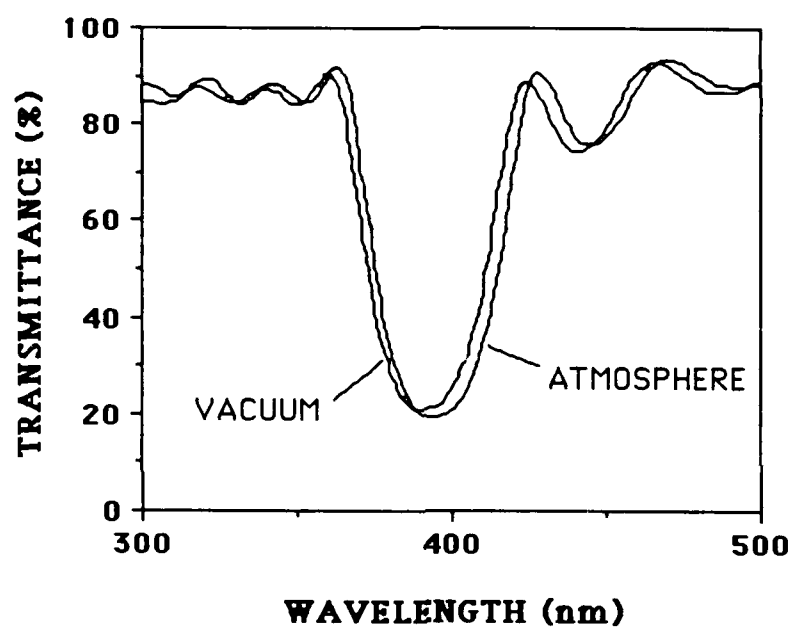


Figure 6-13. Air-to-vacuum shift of a 23-layer conventionally deposited $\text{LaF}_3/\text{MgF}_2$ stack.

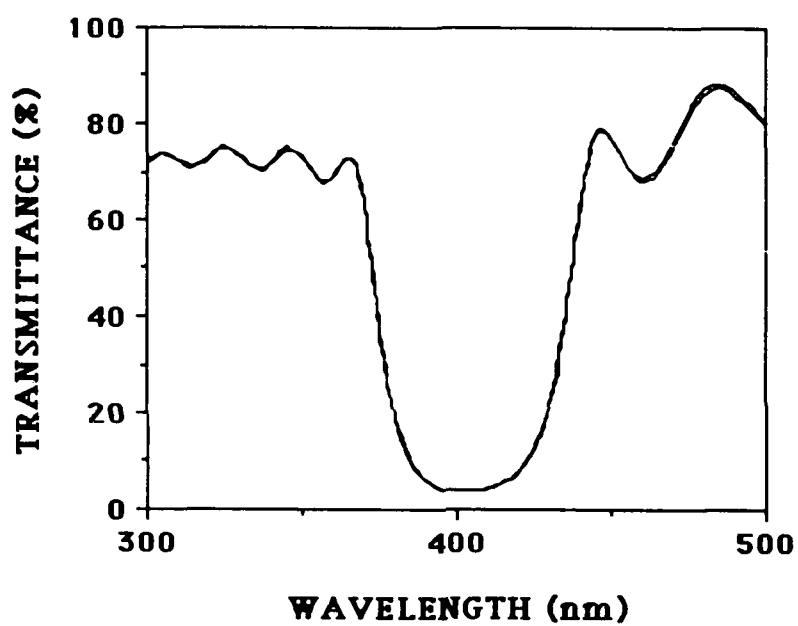


Figure 6-14. Air-to-vacuum shift of a 23-layer IAD $\text{LaF}_3/\text{MgF}_2$ stack deposited with the ion beam parameters of Table 1. The shift is less than 1 nm.

The films deposited by ion-assisted deposition show a slight fluorine deficiency due to the preferential sputtering of lighter atoms out of the films. These anion vacancies are filled by oxygen atoms or complexes (such as water or OH^-) and therefore do not contribute to absorption at wavelengths longer than 300 nm under our bombardment conditions. Extra fluorine could be added to the films to fill these vacancies by bombarding the films with fluorine (which raises obvious safety concerns) or a fluorine-rich gas such as freon (Gibson and Kennemore 1986).

Ion-Assisted Deposition of Lanthanide Fluorides

Because of the success we had with the ion-assisted deposition of lanthanum fluoride, we felt it worthwhile to investigate other lanthanide fluoride materials as candidates for IAD. The lanthanide trifluorides MeF_3 ($\text{Me} = \text{Ce}, \dots, \text{Lu}$) are chemically similar to LaF_3 because they share the same valence electron configuration, and the available information (Pulker 1979; Heaps, Elias, and Yen 1976) suggested that these materials are all highly transparent in the visible and near ultraviolet. We therefore decided to investigate several representative compounds to see if we could draw any general conclusions about the IAD of lanthanide fluorides.

CeF_3 , NdF_3 , DyF_3 , and PrF_3 have all previously been investigated as optical coating materials in the visible and ultraviolet (Pulker 1979; Hass et al. 1959). The latter three materials have similar optical properties; we chose to investigate NdF_3 . CeF_3 is known to have a strong optical absorption band between 200 and 300 nm, but we

investigated it anyway in the hope that the material would still be useful at 353 nm, the XeF laser wavelength.

The ultraviolet and vacuum ultraviolet optics of the lanthanide fluorides are known to be dependent on the allowable transitions of the Me^{3+} ion. These transition atoms have a $6s^2$ valence shell, with the additional electrons going into the 4f or 5d states. Lanthanum, which should have one 4f electron, instead has one 5d because of a quirk in the energy levels of the 57-electron configuration. The optical band edge of the lanthanide fluorides results from the 4f-5d electron transition of the lanthanide cation, which is well known. In addition, there are a number of 4f-4f transitions between crystal field split states present from the infrared to the ultraviolet which cause very weak absorption bands. LaF_3 has no such transitions. CeF_3 , with two 4f electrons, has only two 4f-4f transitions which are both in the infrared. NdF_3 , with four 4f electrons, has a very complicated 4f electron manifold, and a number of possible electron transitions (Dieke 1968). As we shall see, however, only three of these transitions have been observed in our thin films.

Cerium Fluoride

Cerium fluoride films were deposited by evaporating 99.9% pure CERAC material from molybdenum boats at a rate of 6 Å/sec. The only chamber heating was provided by the source, raising the temperature at most to 50 °C by the end of three depositions. The optical samples were 800-900 nm thick. We immediately observed

that these films were under intense stress, with some of the films showing microscopic cracking.

Unbombarded CeF_3 films have a refractive index which is just above that of glass in the visible (Figure 6-15), but they are also highly transparent in the visible and near ultraviolet, with the 4f-5d absorption band starting very abruptly at 300 nm (Figure 6-16). The shape of this absorption band matches that reported by Hass et al. (1959) for CeF_3 films, with absorption bands at 210 nm, 220 nm, 235 nm, and 250 nm corresponding to transitions between the 4f and 5d doublets (Dieke 1968).

We next attempted to improve the packing density of the CeF_3 films with argon bombardment. Figures 6-15 and 6-16 show the refractive indices and transmittances of CeF_3 films bombarded with 20 and 50 $\mu\text{A}/\text{cm}^2$ of argon ions. The index did indeed increase, but this ion flux was not sufficient to raise the index near the bulk value. The ultraviolet absorption, however, is greatly increased, with the long-wavelength tail of the fundamental absorption edge extending into the visible. Because we were interested in this material at 353 nm, we concluded that the ion flux required to achieve bulk density would make the films optically unacceptable at this wavelength and decided not to pursue this investigation further. We are unsure of the exact nature of this band broadening, although a disordering of the film by the ion bombardment could expose the Ce^{3+} ions to a greater variety of local environments, thereby broadening the absorption band. Also, the formation of an oxide or oxyfluoride component in the films with

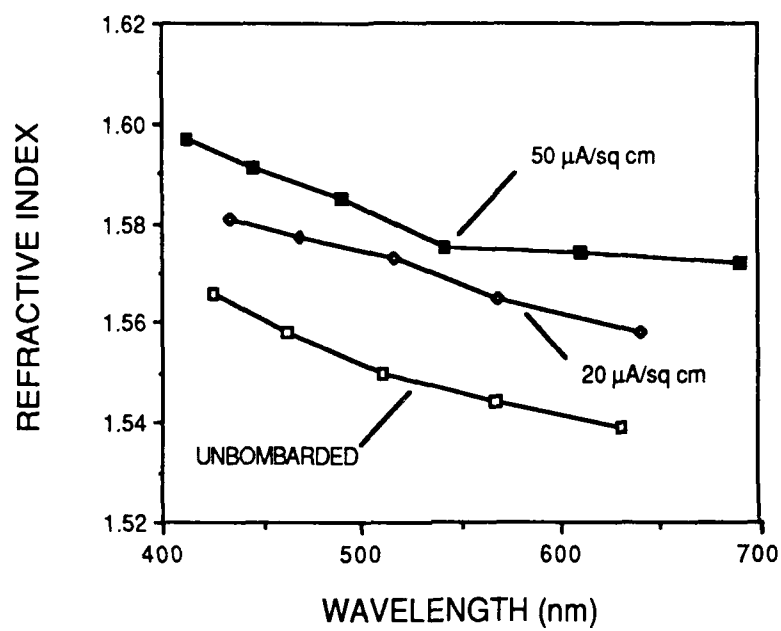


Figure 6-15. Refractive index of unbombarded and 300 eV argon-bombarded CeF_3 films as a function of wavelength.

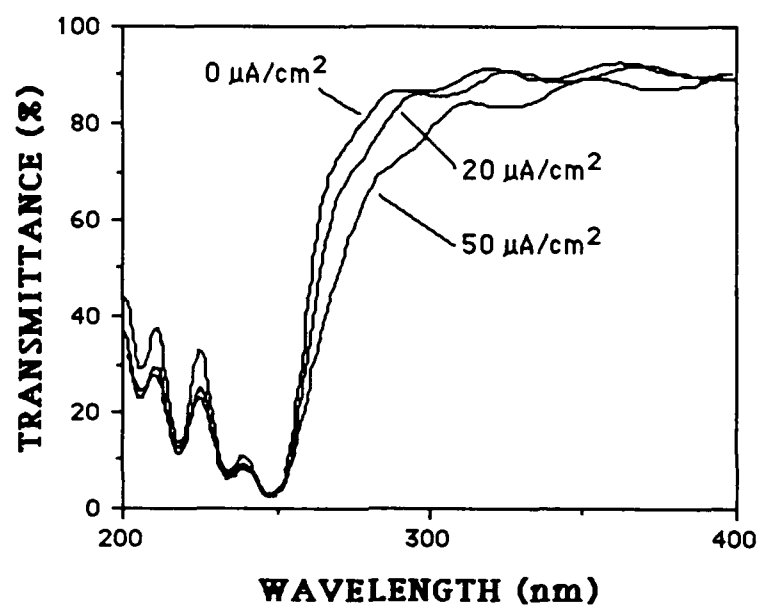


Figure 6-16. Ultraviolet transmittance of unbombarded and 300 eV argon-bombarded CeF_3 films showing the 4f-5d absorption band.

increasing bombardment (as will be discussed below) could cause increased absorption below 400 nm (Pulker 1979).

Oxygen bombardment was investigated briefly in case the additional absorption was due to anion vacancies, which implanted oxygen would then fill. The refractive indices of these films are above the bulk CeF_3 values (Figure 6-17), suggesting that oxygen is indeed being incorporated into the lattice. This conclusion is strengthened by the presence of increased absorption between 300 and 400 nm (Figure 6-18) typical of CeO_2 (Pulker 1979). Oxygen bombardment is thus incompatible with ultraviolet CeF_3 coatings. This result highlights an obvious point-- oxygen bombardment should only be used with metal fluorides if the associated metal oxide does not absorb strongly in the wavelength region of interest. Oxygen bombardment is thus normally acceptable in the visible, but can be detrimental in the ultraviolet.

The Rutherford backscattering measurements (Figure 6-19) show that the unbombarded CeF_3 film is stoichiometric to within the accuracy of the measurement and that the fluorine is preferentially sputtered during the bombardment, as expected. The oxygen in the films more than compensates for the fluorine deficiency, suggesting that water or OH^- radicals are being trapped interstitially or are strongly bonded to film surfaces. These oxygen complexes in anion vacancies could cause absorption similar to that present in CeO_2 .

X-ray diffraction shows that CeF_3 thin films, like LaF_3 films, are highly crystalline with the same tysonite crystalline structure (Dieke 1968). Argon

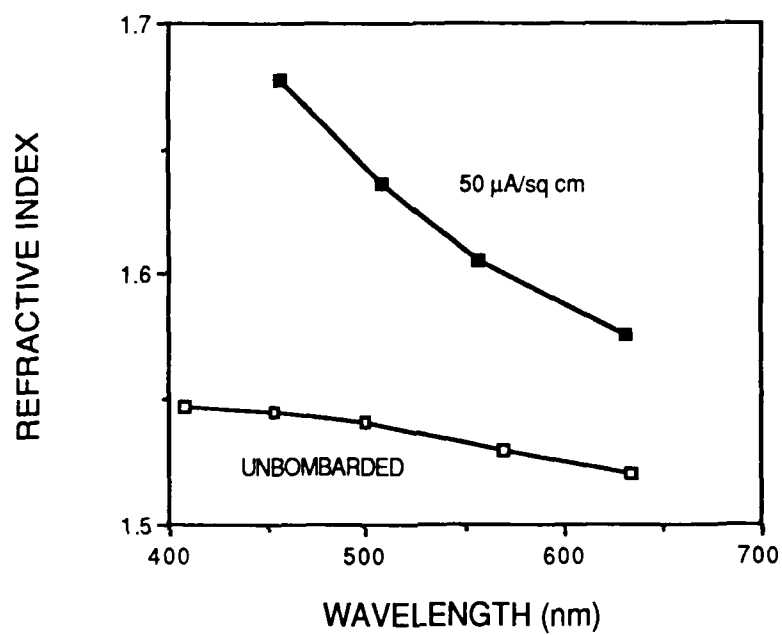


Figure 6-17. Refractive index of unbombarded and 300 eV oxygen-bombarded CeF_3 films as a function of wavelength.

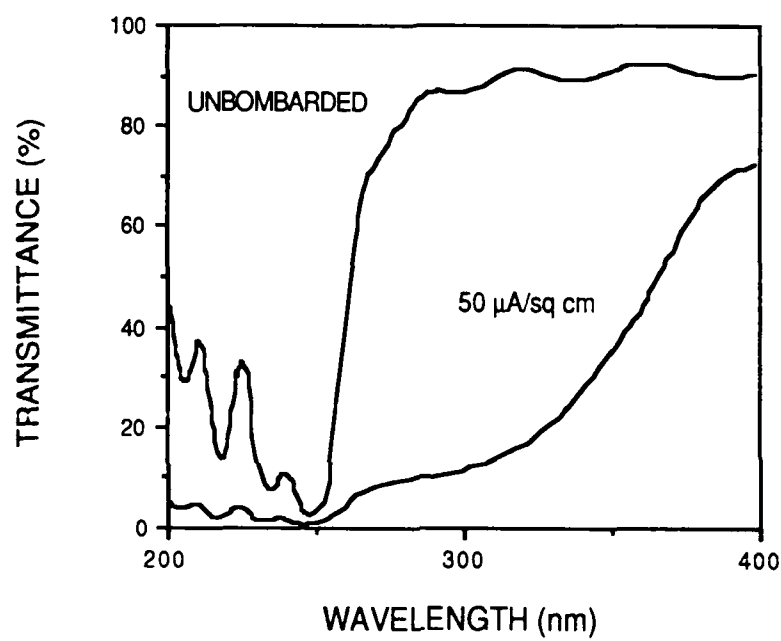


Figure 6-18. Ultraviolet transmittance of unbombarded and 300 eV oxygen-bombarded CeF_3 films showing the 4f-5d absorption band.

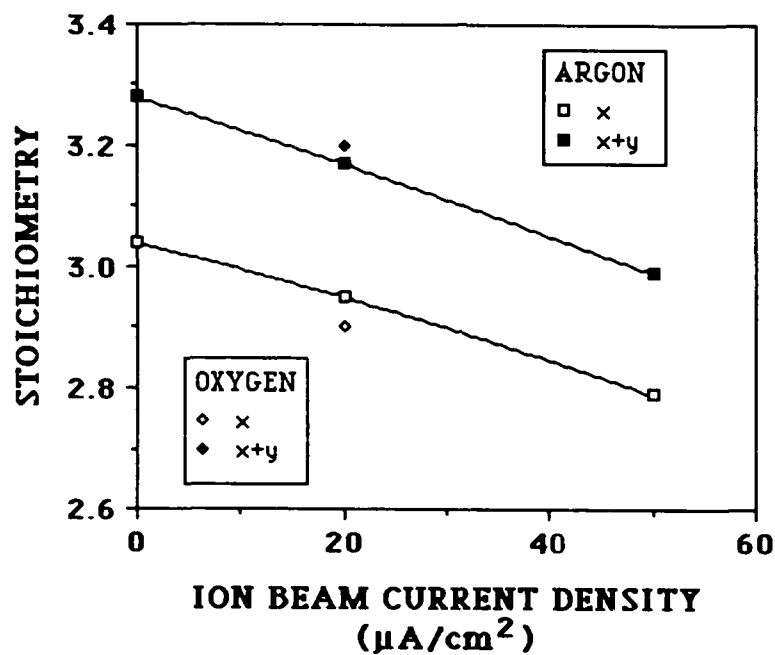


Figure 6-19. Fluorine to cerium ratio x and anion to cation ratio $x+y$ of 300 eV argon-bombarded CeF_3 films, with the stoichiometry expressed in the form CeF_xO_y .

bombardment with increasing ion flux causes the same disappearance of the (111) CeF_3 orientation (Figure 6-20), but the ion fluxes are not large enough to create the oxyfluoride phase. The similarity of this x-ray diffraction trend for argon bombardment to that of LaF_3 supports the conclusions drawn from the optical and RBS measurements that oxygen causes the troublesome absorption between 300 and 400 nm with argon bombardment. This also suggests that a better vacuum could alleviate the problem by eliminating the residual water vapor in the chamber. This water vapor is incorporated into the anion vacancies caused by ion bombardment, as Gibson and Kennemore (1986) have demonstrated for MgF_2 .

Neodymium Fluoride

After our lack of success with CeF_3 , we decided to examine another lanthanide fluoride with a shorter wavelength absorption edge. Neodymium fluoride (NdF_3) was chosen because its absorption edge is well below 200 nm. The deposition conditions were identical to those used for CeF_3 . No oxygen bombardment was attempted because of the 400 nm absorption edge of Nd_2O_3 (Pulker 1979).

Conventional NdF_3 coatings were unusual in two respects. First, we observed three very weak absorption bands at 353, 520, and 575-580 nm which, as mentioned above, correlate with 4f-4f transitions (Dieke 1968) (Figure 6-21). Hass et al. (1959) previously reported on the optical properties of NdF_3 films, but did not mention

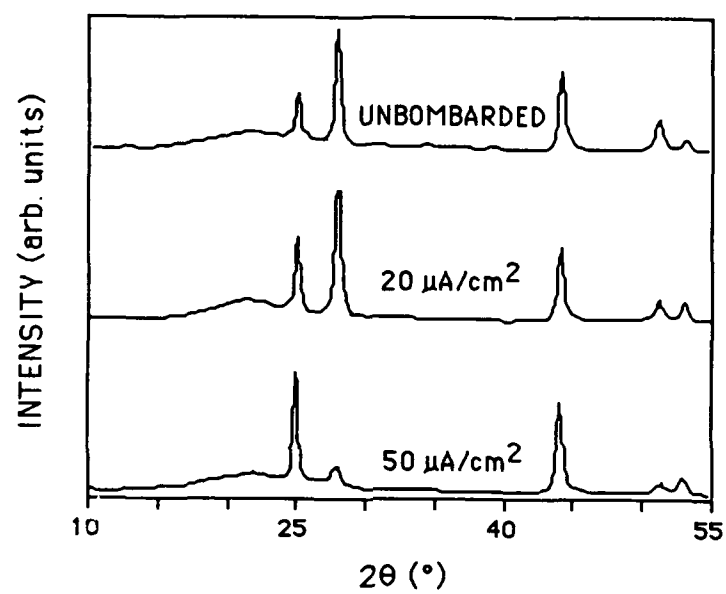


Figure 6-20. X-ray diffraction scans of unbombarded and 300 eV argon-bombarded CeF_3 films.

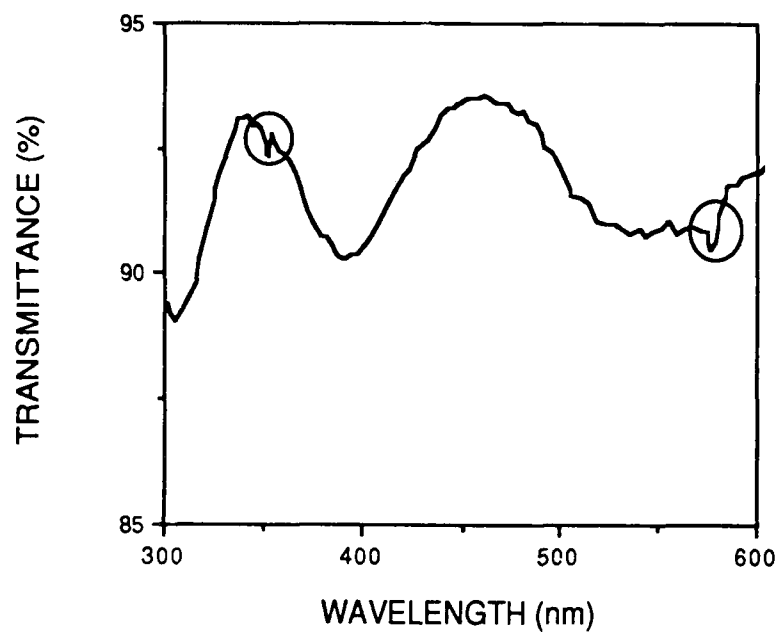


Figure 6-21. Transmittance of a NdF_3 thin film showing two 4f-4f absorption bands. There is also a band at 520 nm which is lost in the noise of the figure, but which is evident in the original trace.

these bands. We have more recently observed 4f-4f absorption bands in most of the lanthanide trifluorides (Lingg et al. 1986). Second, these coatings were surprisingly fluorine deficient. Three unbombarded samples showed fluorine to neodymium ratios of 2.88, 2.88, and 2.94. A slight fluorine deficiency is normal, but these deficiencies are surprisingly large. We have no good explanation for this result.

Argon bombardment was much more successful with NdF_3 than with CeF_3 . Figures 6-22 and 6-23 show the refractive indices of films bombarded with 300 and 500 eV argon ions, respectively. The refractive index was significantly increased in both cases but did not quite reach bulk values. The bulk ordinary and extraordinary refractive indices (NdF_3 is a uniaxial crystal) are taken from Laiho and Lakkisto (1983). We of course also raised the ion fluxes further to attempt to increase the refractive index further; however, Figure 6-24 shows that larger ion fluxes cause measurable absorption, and we are thus limited to a refractive index slightly below bulk unless this absorption is acceptable. It is interesting to note that the onset of absorption occurs for NdF_3 at an ion current density approximately $20 \mu\text{A}/\text{cm}^2$ lower than for LaF_3 , but we must remember that $20 \mu\text{A}/\text{cm}^2$ is a rather small shift. Our work with CeF_3 and NdF_3 , however, does suggest that LaF_3 is more resistant than the lanthanide (Ce...Lu) fluorides to additional absorption caused by ion bombardment.

The high packing density of some of the more heavily bombarded IAD NdF_3 films was verified by infrared transmittance measurements for films on silicon substrates.

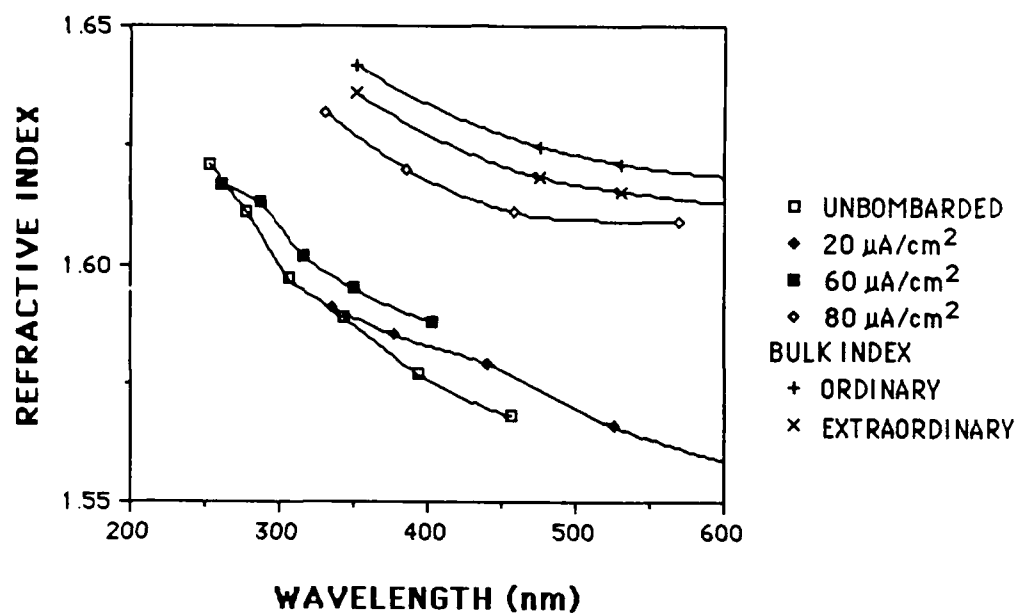


Figure 6-22. Refractive index of 300 eV argon-bombarded NdF_3 films as a function of wavelength.

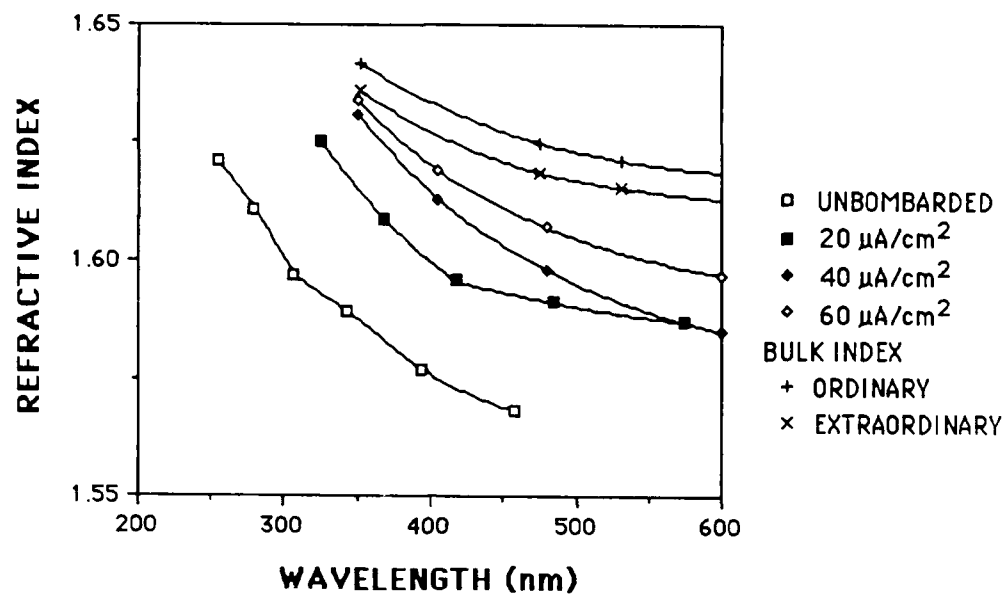


Figure 6-23. Refractive index of 500 eV argon-bombarded NdF_3 films as a function of wavelength.

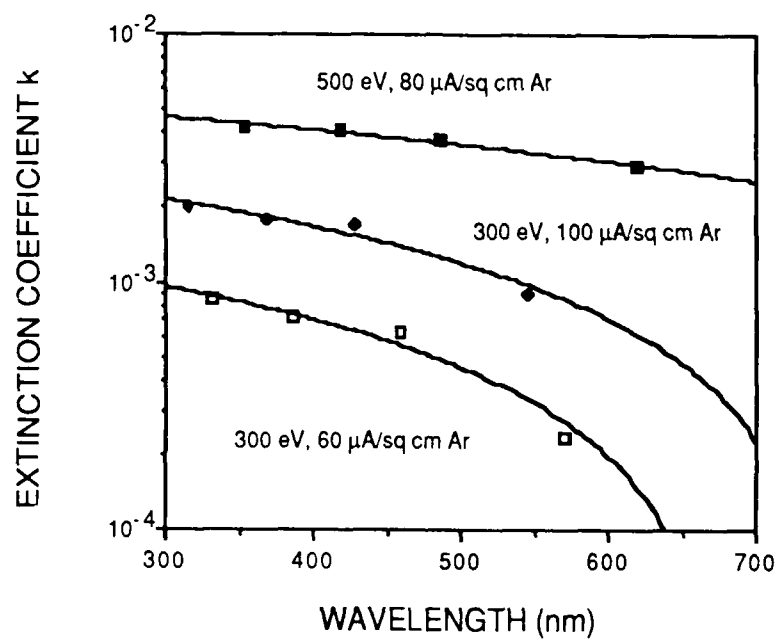


Figure 6-24. Extinction coefficient k vs. wavelength for the three NdF_3 films with measurable absorption. All films with smaller ion fluxes have extinction coefficients below the sensitivity of the measurement.

These films show a rather low transmittance which conflicts with the high transmittance of films deposited simultaneously onto fused silica substrates. Figure 6-25 shows that the film bombarded with $80 \mu\text{A}/\text{cm}^2$ of 300 eV argon ions has a very slight absorption band approximately 1% deep near $2.8 \mu\text{m}$ which is probably due to water, but which could be caused by OH^- radicals. Bombardment by $100 \mu\text{A}/\text{cm}^2$ of 300 eV argon ions eliminates the $3 \mu\text{m}$ water absorption band, leaving a minor OH^- absorption which is detectable by viewing Figure 6-25 at grazing incidence. The $80 \mu\text{A}/\text{cm}^2$ film has a very small absorption, a very high refractive index and an extinction coefficient below 10^{-3} across the visible and near ultraviolet (Figures 6-19 and 6-21); $80 \mu\text{A}/\text{cm}^2$ of 300 eV argon ions is therefore a very attractive bombarding flux if this minimal amount of absorption is acceptable. The elimination of the OH^- band in the $100 \mu\text{A}/\text{cm}^2$ film is a very strange result, as we have observed that NdF_3 films, like LaF_3 films, appear to acquire more of an oxyfluoride nature as the ion beam current density is increased. Unfortunately, this larger ion flux results in an extinction coefficient $k > 2 \times 10^{-3}$ in the visible. If water removal is more important than maximum transmittance, however, $100 \mu\text{A}/\text{cm}^2$ of 300 eV argon ions could be an effective set of beam parameters. No films with 500 eV argon ion bombardment were deposited onto IR transparent substrates; we will merely conjecture that similar results would be achieved.

Conclusions

We can now compare the ion-assisted deposition of the lanthanide fluorides with the IAD of LaF_3 . We are of course generalizing from a sampling of only two compounds,

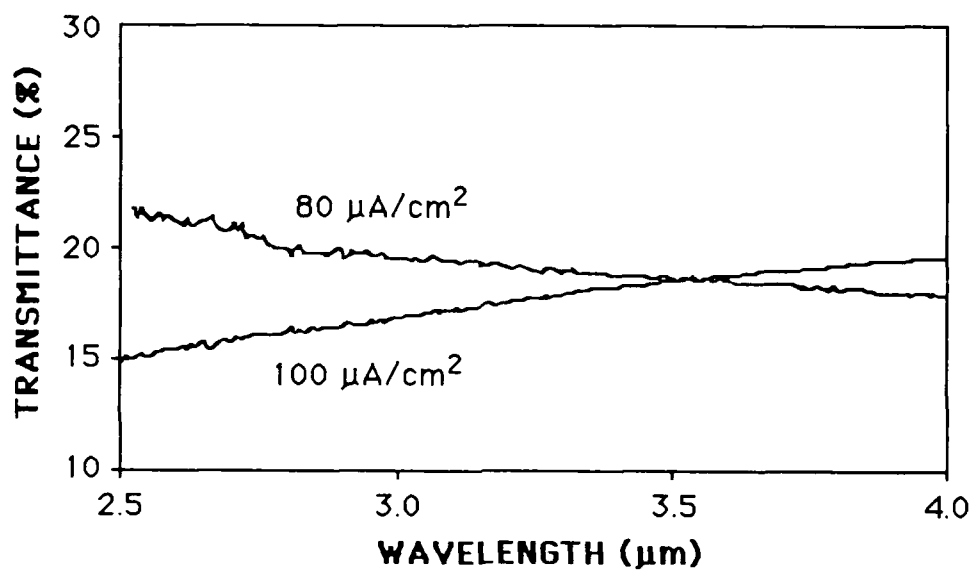


Figure 6-25. Infrared transmittance of 300 eV argon-bombarded NdF₃ films in the 3 μm water absorption band.

CeF_3 and NdF_3 . These conclusions are almost certainly applicable to PrF_3 as well. The lanthanide fluorides with heavier cations require further investigation, as our preliminary experiments show that these materials do not show the strong hexagonal (or trigonal) crystallinity of LaF_3 , CeF_3 , and NdF_3 (Lingg et al. 1986).

The IAD of NdF_3 and CeF_3 is similar to that of LaF_3 in the following ways:

(1) Fluorine is preferentially sputtered in all cases, leaving anion vacancies which are filled by oxygen atoms or complexes. It appears that optical absorption becomes severe when a significant number of these vacancies can no longer be filled by the oxygen.

(2) These materials form highly crystalline films, even when deposited conventionally onto ambient temperature substrates. Portions of the films undergo a phase change from fluoride to oxyfluoride as the ion flux increases. This suggests that the increasing amount of oxygen in the crystal lattice distorts the lattice more and more until it is energetically favorable to undergo the phase transformation.

(3) The refractive index and packing density of these materials is increased by IAD. Away from fundamental absorption edges, such as the ultraviolet edge in CeF_3 , this improvement is accompanied by little additional absorption. It is still uncertain whether the increase in absorption observed for CeF_3 is due to a broadening of the 4f-5d Ce^{3+} absorption band or to the formation of oxyfluoride crystallites in the films.

There are also differences, however:

(1) The lanthanide fluorides, once the ion flux is increased sufficiently to cause optical absorption in the visible, seem to show a quicker onset of absorption than LaF_3 .

This could be due to the relatively short-wavelength absorption edge of La_2O_3 (300 nm) in comparison to NdF_3 (400 nm) and CeO_2 (400 nm) (Pulker 1979).

(2) The lanthanide fluorides suffer from weak 4f-4f absorption bands from the ultraviolet to the infrared, with the number and location of the bands depending on the cation. These bands are probably not significant unless these narrow wavelength intervals are crucial in a particular design. Since not all of the bands are strong enough to be measurable in thin films, a trial deposition is required to determine if a tabulated band will actually be a problem.

CHAPTER 7

THE ION-ASSISTED DEPOSITION OF ALUMINUM OXIDE

Aluminum oxide (Al_2O_3) is an attractive material for laser coatings and hard protective coatings. Packing densities of nearly one are achievable using conventional electron beam evaporation (Ogura 1975) and impressive laser damage thresholds (Rainer et al. 1985) have been reported. Ebert, however, has reported that Al_2O_3 coatings deposited in a low energy negatively-ionized oxygen atmosphere have greater absorption than similar films deposited in neutral oxygen, with an increase of the absorption coefficient from 6 to 10 cm^{-1} at a wavelength of 514 nm (Ebert 1982). We therefore decided to investigate the ion-assisted deposition of Al_2O_3 to determine whether the optical and mechanical properties of Al_2O_3 coatings could be improved without a significant increase in absorption. Such an improvement had previously been reported in ZrO_2 (Martin et al. 1984a) and TiO_2 (McNeil et al. 1984), so we hoped that similar results could be achieved with Al_2O_3 . Our early work involved argon bombardment in an oxygen atmosphere, because this allowed us simplify the study by eliminating oxygen ion implantation. We later attempted oxygen bombardment as well when we discovered that argon ion bombardment was only marginally effective.

It should be mentioned at this point that Al_2O_3 is one of the worst possible a priori choices for ion-assisted deposition. It was shown in Chapter 2 that the most dramatic IAD results have been achieved with materials that show marked improvement when deposited at elevated temperatures. Al_2O_3 is reported to have a packing density of almost one even when deposited onto ambient temperature substrates (Ogura 1975), suggesting that IAD may not have much effect on the film properties. As mentioned above, however, it was decided to investigate this material for other reasons.

Preliminary investigations of Al_2O_3 were reported by Saxe (1985). All of the results reported here involve studies conducted subsequent to Saxe's work.

Deposition Conditions

The Al_2O_3 was evaporated with an 11 kV electron beam source using a molybdenum crucible liner. The starting material was CERAC 99.8% pure 1/8" pieces and the typical deposition rate was 6 Å/sec. A series of unbombarded and IAD films were simultaneously deposited on glass, fused silica, and graphite substrates. An oxygen backfill was used for most of the depositions, with the oxygen pressure varying from 4×10^{-5} to 4×10^{-4} mbar. In addition, an argon partial pressure of 8×10^{-5} mbar was present during argon bombardment as a result of the gas passing through the ion gun. Some oxygen obviously diffuses into the ion gun during these experiments and is subsequently accelerated, but the high pressure (roughly 10^{-3} mbar) inside the ion gun ensures that the ion beam contains very little oxygen. The initial experiments were

conducted with the chamber heated only by the electron-beam source. By the end of the runs, however, the chamber temperature had risen to over 100 °C. We therefore decided to heat the chamber to 100 °C before each deposition with the quartz heating lamps mounted above the substrate dome. The chamber temperature then typically rose to approximately 135 °C by the end of the depositions. This change should be much less important than the rise from room temperature to 100 °C.

It was observed earlier (Saxe 1985) that the source material from CERAC outgassed significantly during the early stages of source heating, raising the chamber pressure considerably. Similar behavior has also been observed by another group using material from a different vendor (Suits 1987). RBS results show that films deposited with fresh material without a suitable outgassing period showed a large surplus of oxygen in the first 1500 Å of deposited material. These films have unusually low values of refractive index and are quite inhomogeneous. This drop in index with excess oxygen has been observed previously (Pelletier 1985). After this problem was detected, data was taken only from samples deposited with properly aged source material.

Unbombarded Films

The optical constants of the Al_2O_3 films were found to be highly dependent on the oxygen partial pressure during deposition. We conducted a series of runs to determine the best conditions for conventional deposition so that IAD samples could be compared to optimized conventional films. Table 7-1 shows the results of these runs for both pure

O₂ and Ar/O₂ atmospheres. For the pure oxygen backfill, the index is lowered for either a deficit or excess of oxygen. The optimal pressure is on the order of 1.2×10^{-4} mbar. When argon is added, as required for argon ion bombardment, a backfill of 8×10^{-5} mbar Ar/ 1.2×10^{-4} mbar O₂ was optimal. Therefore, these parameters were chosen for the argon bombardment experiments.

X-ray diffraction measurements were carried out on a number of the unbombarded films. None of the films showed any measurable crystalline peaks and it was therefore assumed that the coatings were amorphous.

The crystallinity of the Al₂O₃ films was then examined more closely with transmission electron microscopy (TEM) by Drs. Claude Boulesteix and Françoise Varnier of the University of Aix-Marseille III at Saint Jérôme. A 400 Å thick film was deposited with a 2×10^{-4} mbar oxygen backfill onto glass precoated with a thin layer of carbon. The film was then covered with a layer of collodion and peeled off the substrate. The resulting micrographs showed that the films were indeed amorphous (Figure 7-1). After several minutes of electron bombardment in the microscope, however, the film began to show a slight crystallization (Figure 7-2), suggesting that the amorphous phase is unstable.

Bombarded Films

Al₂O₃ films were next deposited with argon ion bombardment: This allows the bombardment process to be investigated without the complication of oxygen ion

Table 7-1. Optical Constants of Unbombarded Al_2O_3 Films at 350 nm

Partial Pressures (10^{-5} mbar)		n	k x 10^4
Ar	O ₂		
0	8	1.68	5
0	12	1.68	4
0	20	1.62	7
0	40	1.65	3
8	4	1.65	25
8	12	1.66	2
8	22	1.64	7
8	32	1.63	5

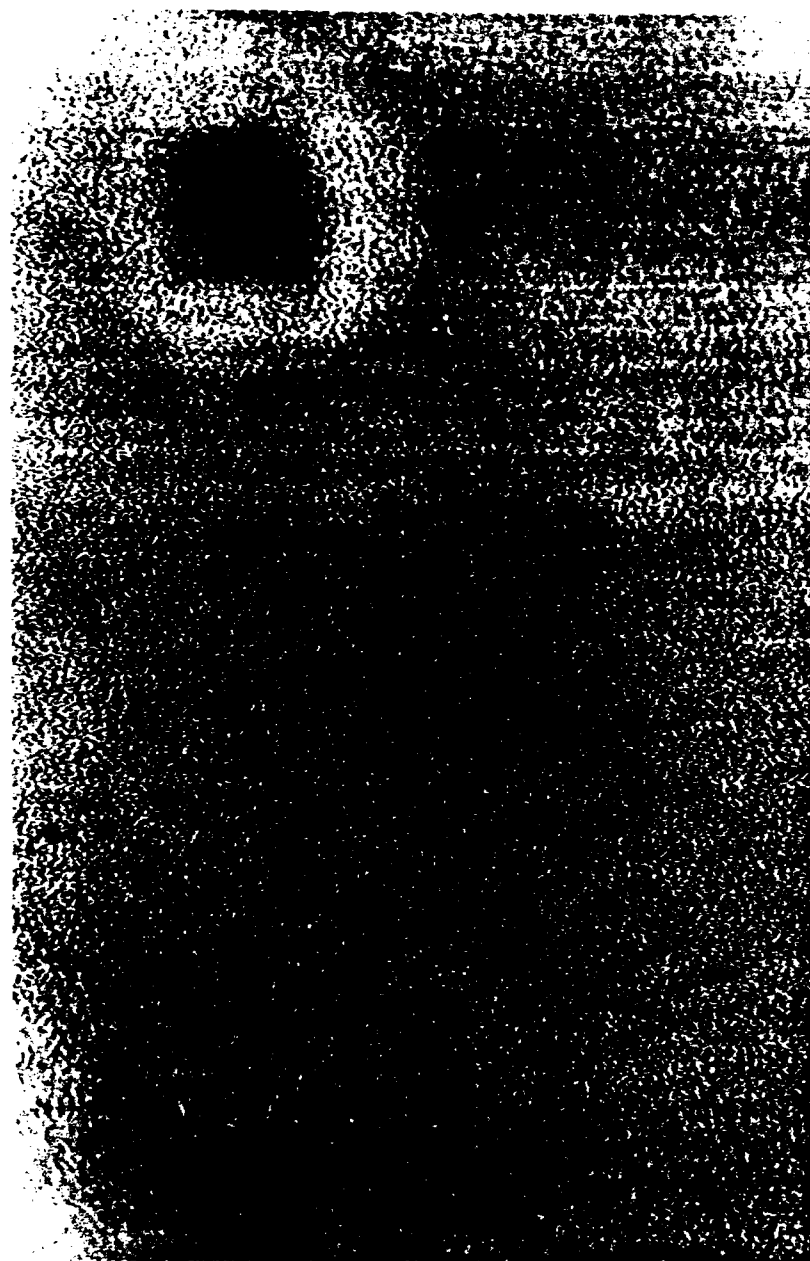


Figure 7-1. Transmittance electron micrograph of an unbombarded Al₂O₃ film as deposited (400,000x magnification).

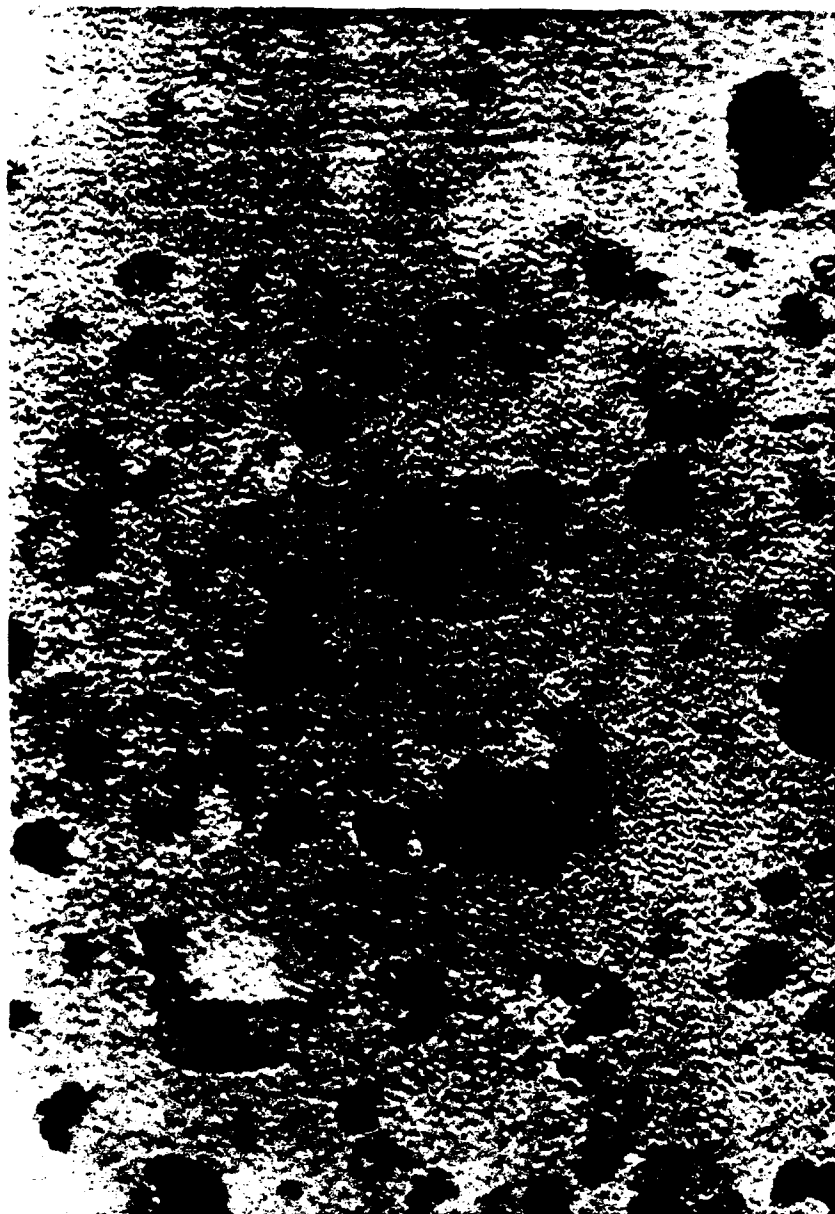


Figure 7-2. Transmittance electron micrograph of an unbombarded Al_2O_3 film after several minutes of electron bombardment in the electron microscope (400,000x magnification).

implantation, although argon trapping in the film is a consideration. A gas mixture of 8×10^{-5} mbar Ar/ 1.2×10^{-4} mbar O_2 was chosen, since this mixture resulted in the best unbombarded film. Only the argon passed through the ion source, so that the ion beam consisted almost entirely of argon ions (some oxygen undoubtedly diffuses into the source). The refractive index increased only slightly under argon bombardment (Table 7-2).

For the deposition of oxides, oxygen bombardment should be highly advantageous. Implanted oxygen can fill anion vacancies in the growing film and does not introduce impurities, although interstitial oxygen atoms are still to be expected. We therefore performed several experiments using oxygen as a bombarding species. We have not investigated the relative percentages of O^+ and O_2^+ ions in the ion beam. Previous studies (McNeil et al. 1984) have shown that a similar Kaufman-type ion gun produced an O_2^+ to O^+ ratio of approximately two to one. We have assumed that our ion source produces a similar beam.

Table 7-3 shows the effect on the optical constants of a 50% Ar/50% O_2 ion beam. This one to one ratio refers to the gas flow into the ion gun rather than the ionized beam exiting it. In this experiment, the O_2 backfill was not sufficient to yield a good conventional film; however, the ion bombardment raised the refractive index at 350 nm to 1.70. In addition, the absorption decreased when the films were bombarded. This suggests that implanted oxygen ions are filling anion vacancies in the films. The ion bombardment thus allowed the films to be deposited at a lower pressure than would have

Table 7-2. Optical Constants of IAD Al_2O_3 Films at 350 nm
(500 eV Argon Ion Bombardment)

(1.2×10^{-4} mbar O_2 /8 $\times 10^{-4}$ mbar Ar)

Ion current density ($\mu\text{A}/\text{cm}^2$)	n	k $\times 10^4$
0	1.66	2
20	1.68	2
40	1.67	2
50	1.68	4
50	1.67	2
100	1.66	7
125	1.66	3

Table 7-3. Optical Constants of Al_2O_3 Films at 350 nm with 50% Ar/50% O_2 Bombardment

P(Ar) (10^{-5} mbar)	P(O_2)	ION ENERGY (eV)	ION FLUX ($\mu\text{A}/\text{cm}^2$)	n	k x 10^4
0	4	---	0	1.65	10
4	4	300	20	1.69	3
4	4	500	75	1.70	2

been possible otherwise, and to raise the refractive index to the levels previously reported for sputtered films (Martin 1986).

Pure oxygen ion bombardment was next performed with an oxygen pressure of 2×10^{-4} mbar. The unbombarded film under these conditions had a very low index, but the ion bombardment increased the index to 1.70 at 350 nm for an ion current density of $140 \mu\text{A}/\text{cm}^2$ (Table 7-4). This value agrees well with the indices reported for other ion-based deposition methods (Martin 1986). Oxygen bombardment does not cause the drop in refractive index for large ion current densities noted above for argon ion bombardment. The main difference between the two processes is the addition of oxygen ion implantation as a major factor in the film growth. These ions can fill oxygen vacancies caused by ion sputtering and create less network disruption than implanted argon.

The high packing density of these films was confirmed by measuring the infrared transmittance of films deposited onto silicon substrates. An unbombarded film deposited with 2×10^{-4} mbar of oxygen has a weak absorption band at $2.7 \mu\text{m}$ due to OH^\cdot radicals, while oxygen-bombarded films appear to have no measurable absorption in this region (Figure 7-3). The small residual absorption between 2.5 and $2.9 \mu\text{m}$ is due to atmospheric water vapor in the spectrometer sample chamber.

Films with a refractive index of 1.69 to 1.70 at 350 nm thus appear to have a packing density very close to unity. In addition, the unbombarded film has a surprisingly high packing density in relation to its low refractive index. We investigated this anomaly further by measuring the air-to-vacuum shift of an unbombarded coating deposited on

Table 7-4. Optical Constants of IAD Al_2O_3 Films at 350 nm
(500 eV Oxygen Ion Bombardment)

(2×10^{-4} mbar O_2)

Ion current density ($\mu\text{A}/\text{cm}^2$)	n	k $\times 10^4$
0	1.61	7
20	1.66	5
50	1.69	3
100	1.69	4
140	1.70	2

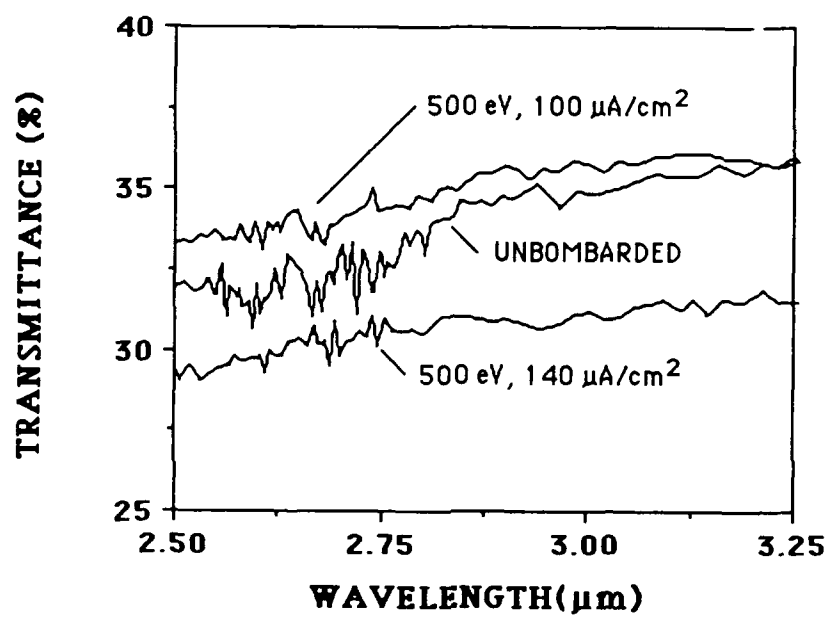


Figure 7-3. Infrared transmittance of unbombarded and IAD Al_2O_3 films in the 3 μm water absorption band.

fused silica with a refractive index of 1.61--the lowest value measured in this study--in the Cary 14 using a special vacuum cell attachment. The film showed a shift of less than 1 nm upon pumping from atmospheric pressure down to 10 mtorr. This confirms the high packing density observed in the infrared measurements.

X-ray diffraction of IAD films again showed no signs of crystallinity. TEM of an IAD film bombarded with $100 \mu\text{A}/\text{cm}^2$ of 500 eV oxygen ions by Dr. Boulesteix showed that this film was also truly amorphous.

With ion-assisted deposition, we have thus been able to deposit aluminum oxide coatings at a relatively low temperature with a high refractive index, near-unity packing density, and very little absorption. In addition, very good films can be deposited without ion bombardment with the proper choice of oxygen pressure. The wide range of refractive indices observed for films with very high packing densities is extremely unusual. Since both the conventional and IAD films are amorphous, the only plausible explanation for this effect is a change in the amorphous networking of the films with IAD. Of course, this is a supposition: EXAFS studies are currently being conducted to characterize the nature of the amorphous networking in the films.

CHAPTER 8

PREPARATION OF ALUMINUM NITRIDE AND OXYNITRIDE THIN FILMS BY ION-ASSISTED DEPOSITION

Aluminum nitride (AlN) is a very versatile coating material. Its mechanical strength and chemical stability allow it to protect machine tools and to serve as an insulating layer in microelectronic applications. More recently, its relatively wide bandgap (6.5 eV) has led to its consideration as an optical coating material for use in the visible and near-ultraviolet regions (Pawlewicz et al. 1986; Koshigoe et al. 1984).

Aluminum nitride films have been deposited by many methods, including chemical vapor deposition (Noreika and Ing 1968), reactive ion sputtering (Holmes 1986), ion implantation (Lieske and Hezel 1981), and dual-beam ion sputtering (Harper, Cuomo, and Hentzell 1985; Allen 1985). In this work a growing aluminum film, thermally evaporated from an electron-beam source, was bombarded with a nitrogen ion beam. We hoped that the thermal source could provide a large aluminum deposition rate and allow the deposition of AlN over a wide area in a system where only one ion source was available. Martin and Netterfield have recently reported the successful ion-assisted deposition of Si_3N_4 (Netterfield, Martin, and Sainty 1986), suggesting that aluminum nitride deposition should be feasible by IAD as well. We have

also deposited aluminum oxynitride films by adding oxygen to the chamber backfill during the depositions.

Deposition Conditions

All coating runs were performed at 100 °C with a residual pressure of 1×10^{-6} mbar or less. Aluminum starting material of 99.999% purity was evaporated by an electron beam source from an intermetallic crucible at a deposition rate of 2 to 7 Å/sec, as measured by a quartz crystal rate monitor shielded from the ion beam. In most of the depositions, the chamber was filled with 8×10^{-5} mbar of nitrogen gas through the ion gun. Aluminum nitride films were deposited by bombarding the growing aluminum films with a nitrogen ion beam with ion energies of 250, 500, 750, or 1000 eV.

Rutherford Backscattering Spectrometry

We first deposited an aluminum film at a rate of 2 Å/sec in a nitrogen backfill of 8×10^{-5} mbar to determine if (a) this nitrogen would be incorporated into the films and (b) whether our base vacuum was sufficiently free of oxygen and water vapor to prevent significant oxidation of the films. The nitrogen content of these films was less than 2 at. %. The bulk of the film contained 1.1 ± 0.2 at. % oxygen, with greater oxidation observed near both the substrate-film and film-air interfaces.

Table 8-1 shows the stoichiometries of aluminum nitride films as determined by RBS. The stoichiometries are expressed in the form AlN_xO_y . This is simply a convenient notation, and does not imply the formation of a compound with the indicated

Table 8-1. Stoichiometries of AlN Films (AlN_xO_y)

Al dep. rate ($\text{\AA}/\text{sec}$)	Ion Beam		γ (N atoms/Al atom)	Stoichiometry	
	Energy (eV)	Current Density ($\mu\text{A}/\text{cm}^2$)		x	y
2	250	90 \pm 20	0.9 \pm .3	0.89 \pm .01	.04 \pm .006
2	250	100 \pm 20	1.0 \pm .4	1.01 \pm .01	.03 \pm .01
2	250	140 \pm 20	1.5 \pm .5	1.21 \pm .02	.04 \pm .01
2.5	250	130 \pm 20	1.2 \pm .4	0.81 \pm .02	.06 \pm .01
2	500	190 \pm 20	2.0 \pm .5	1.24 \pm .02	.03 \pm .003
4	500	100 \pm 20	0.5 \pm .1	0.58 \pm .01	.03 \pm .01
4	500	150 \pm 20	0.8 \pm .2	1.04 \pm .02	.03 \pm .01
4.5	500	190 \pm 20	0.9 \pm .2	1.15 \pm .02	.024 \pm .006
2	750	100 \pm 20	1.0 \pm .3	1.03 \pm .02	.05 \pm .01
2	750	190 \pm 20	2.0 \pm .5	1.23 \pm .03	.12 \pm .03
2	750	210 \pm 20	2.2 \pm .5	1.17 \pm .02	.09 \pm .02
4	750	145 \pm 20	0.8 \pm .2	0.82 \pm .01	.02 \pm .01
4.5	750	100 \pm 20	0.4 \pm .1	0.55 \pm .01	.023 \pm .004
4.5	750	200 \pm 20	0.9 \pm .2	1.27 \pm .02	.03 \pm .003
6	750	380 \pm 20	1.3 \pm .2	1.11 \pm .02	.08 \pm .02
6.5	750	290 \pm 20	0.9 \pm .2	1.26 \pm .02	.027 \pm .003
2.5	1000	200 \pm 20	1.8 \pm .5	1.29 \pm .03	.21 \pm .01
2.5	1000	300 \pm 20	2.7 \pm .6	1.58 \pm .10	.52 \pm .04

stoichiometry. The ratio of incident nitrogen atoms to aluminum atoms γ at the substrate has been calculated under the assumption that the ion beam consists of N_2^+ ions. The number of nitrogen "atoms" is thus twice the number of N_2^+ ions impinging on the substrate.

Most of the films have a stoichiometry between $AlN_{0.8}$ and $AlN_{1.2}$, with a large number of the films having $x > 1.0$ (Figure 8-1). Harper, Cuomo, and Hentzell (1985) have previously reported that dual-beam sputtered films with several hundred eV ions bombarding the substrate are stoichiometric if the nitrogen-to-aluminum arrival rate at the substrate is greater than one. They hypothesize that this self-limiting effect in the stoichiometry is due to diffusion of nitrogen to the surface of the films followed by desorption of N_2 from the surface. We observed no such self-limiting effect with IAD. A 1:1 ratio is achieved only for particular sets of deposition conditions rather than for whole regions of the deposition parameter space as observed with dual-beam sputtering. Since the only significant difference between the two methods is the aluminum source, it is possible that highly energetic sputtered aluminum atoms are responsible for the diffusion of excess nitrogen atoms to the surface of the films where they could be desorbed. Bombardment by the nitrogen beam alone presumably does not promote sufficient mobility within the growing film for nitrogen diffusion and desorption. The RBS results also show that the films have very high packing densities: The majority of the films show little oxygen below the surface oxidation layer, suggesting that most of the oxygen adsorbed from the residual chamber atmosphere during deposition

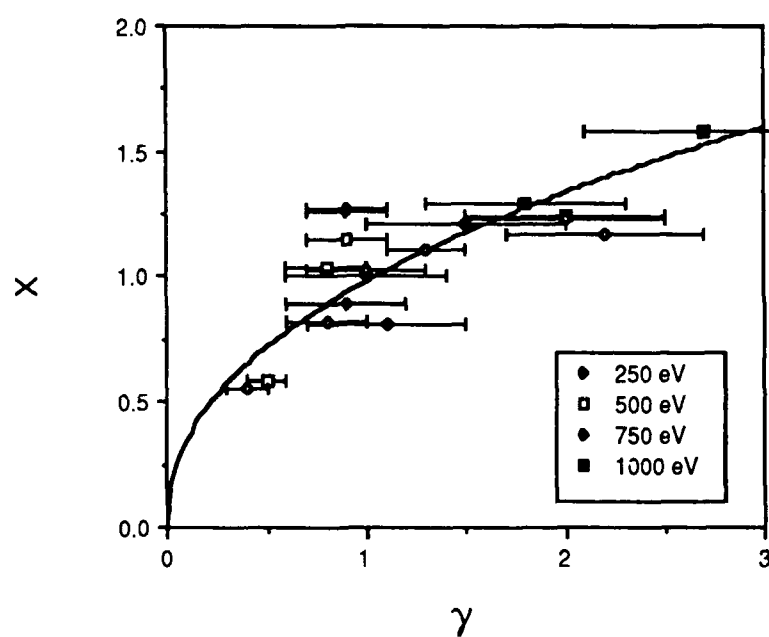


Figure 8-1. Stoichiometry of aluminum nitride films, expressed in the form AlN_x , as a function of the ratio of nitrogen to aluminum arrival rates.

is resputtered, and that the films are too dense for water to migrate through the films after venting the system to atmosphere. There is an oxidized layer at the surface of the films with a thickness of 150 ± 75 nm. The oxygen-to-aluminum ratios y in Table 8-1 are averages through the total film thickness, including this surface layer.

Based on the RBS analysis, we also observe that the film deposition rate can be increased if a sufficient ion flux is available. We have shown that $300 \mu\text{A}/\text{cm}^2$ of 750 eV ions is sufficient to produce a film with $x > 1.0$ for an aluminum deposition rate of 0.65 nm/sec.

The RBS results indicate several sets of deposition conditions which yield a 1:1 Al:N ratio. For example, evaporating aluminum at a rate of 0.2 nm/sec while bombarding with a 750 eV, $100 \mu\text{A}/\text{cm}^2$ ion beam should result in a stoichiometric film. However, we shall show in the next section that films deposited with similar parameters are optically absorbing.

Optical Measurements

We performed transmittance and reflectance measurements on films deposited on fused silica substrates over a wavelength range of 0.2 to $2.0 \mu\text{m}$. Films deposited with an insufficient ion beam flux are opaque with a shiny or dull gray appearance depending on the deposition conditions. The sheet resistance of these films has been measured with a four-point probe, which shows that the resistance of films rises above the 3000 Ω/square upper limit of our instrument when the films begin to show any visible transmittance. As the films approach the correct stoichiometry, the transmittance increases. In even the best case, however, the films absorb at wavelengths shorter than

500 nm (Figure 8-2). Holmes (1986) has observed similar behavior with reactive ion beam sputtered films, which he attributed to nitrogen vacancies or defect states, although his films showed no absorption above 450 nm. Our films are in general nonabsorbing at wavelengths longer than 1 μm ; we have therefore used the quarter-wave transmittance in the 1 to 2 μm region to calculate a refractive index for these films. As the dispersion curve of AlN is essentially flat over this wavelength region, calculations made at slightly different wavelengths are still comparable. Table 8-2 gives the refractive indices of these films; these values are slightly lower than the literature values of 1.90 to 1.95 (Pawlewicz et al. 1986).

Annealing Studies

In an attempt to improve the optical properties of the films, we annealed a number of AlN films in a tube furnace at 500 °C. Dry nitrogen flowed through the tube to reduce the oxygen and water vapor content in the furnace, but the tube was not sealed. Table 8-3 shows the effect of annealing on three RBS samples with widely varying stoichiometries. We see that the nitrogen content of the films remained the same or decreased after 210 minutes, and that the oxygen content of the films increased slightly. The oxygen in the original films was concentrated in a surface layer which became thicker during annealing as oxygen penetrated the films.

The annealing of thicker samples on fused silica substrates showed that the optical properties of the films were improved substantially (Figure 8-3), with no absorption observed at wavelengths longer than 500 nm, and the absorption edge shifted below 350 nm. Additional annealing at 500 °C did not affect the transmittance of the

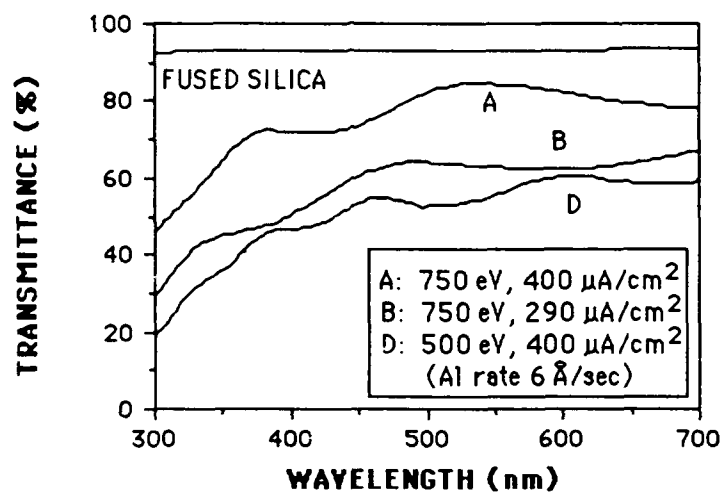


Figure 8-2. Transmittance of typical AlN films deposited by ion-assisted deposition.

Table 8-2. Near Infrared Refractive Indices of AlN Films

Al dep. rate (Å/sec)	Ion Beam		γ (N atoms/Al atoms)	Refractive index n (± 0.02)
	Energy (eV)	Current Density ($\mu\text{A}/\text{cm}^2$)		
2	750	185	$1.9 \pm .6$	1.87
3	500	190	$1.3 \pm .3$	1.82
3	500	150	$1.0 \pm .3$	1.89
4	750	290	$1.5 \pm .2$	1.86
6	750	400	$1.4 \pm .2$	1.84

Table 8-3. Effect of Annealing on Stoichiometry of AlN_xO_y Films

Al dep. rate ($\text{\AA}/\text{sec}$)	Ion Beam		Stoichiometry			
	Energy (eV)	Current Density ($\mu\text{A}/\text{cm}^2$)	Unannealed x	Unannealed y	Annealed x	Annealed y
4.5	750	100	$.55 \pm .01$	$.023 \pm .004$	$.56 \pm .01$	$.068 \pm .004$
2.5	250	130	$.81 \pm .02$	$.06 \pm .01$	$.74 \pm .02$	$.15 \pm .01$
6.5	750	290	$1.26 \pm .02$	$.027 \pm .003$	$1.15 \pm .02$	$.054 \pm .005$

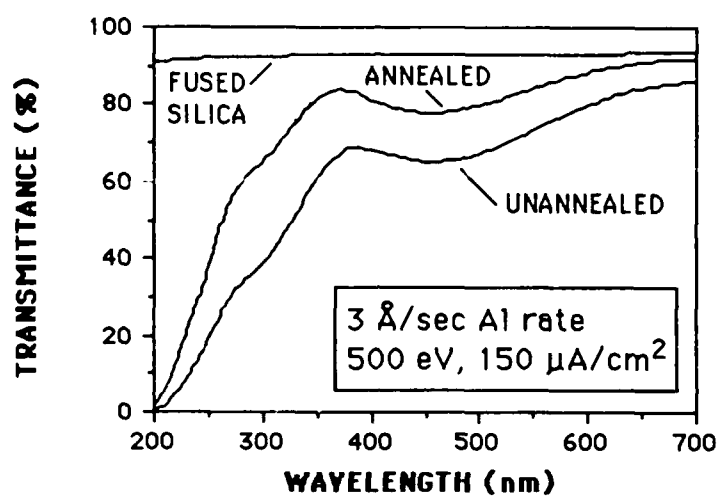


Figure 8-3. Transmittance of an AlN film deposited by IAD before and after annealing for 210 minutes at 500 °C.

films, although additional oxygen is certainly diffusing into the films. This suggests that unsatisfied bonds in the films are filled quickly by oxygen atoms or complexes, eliminating the absorption related to dangling bonds. The cause of the remaining absorption is still not positively identified.

Oxynitride Deposition

Mixed compounds of oxides and nitrides can tailor the refractive index of coating materials. Aluminum oxynitrides should span the refractive index range between 1.65 and 1.9 in the visible. We have deposited aluminum oxynitride films by adding 4×10^{-5} mbar of oxygen to the vacuum chamber during the deposition. This oxygen then occupies adsorption sites created by the nitrogen ion bombardment. Figure 8-4 shows the transmittance of two films deposited with an aluminum deposition rate of 0.6 nm/sec and bombarded by 750 eV nitrogen ions. Both films have significantly better optical properties than the aluminum nitride films discussed above. This is presumably due to adsorbed oxygen atoms filling vacancies created by the ion bombardment. The films will show an absorption edge more typical of nitride material. The $200 \mu\text{A}/\text{cm}^2$ sample has a refractive index of 1.93 while the $300 \mu\text{A}/\text{cm}^2$ film has an index of 1.82 because of its greater oxygen content. Thus, we can vary the refractive index by changing the ion beam current density. An alternative method would be to pass oxygen through the ion gun. This oxygen would be more effectively implanted into the films, resulting in a larger oxygen content for the same ion beam current density. The refractive index of 1.93 is surprisingly high, and may suggest that the amount of adsorbed oxygen in the film is quite small.

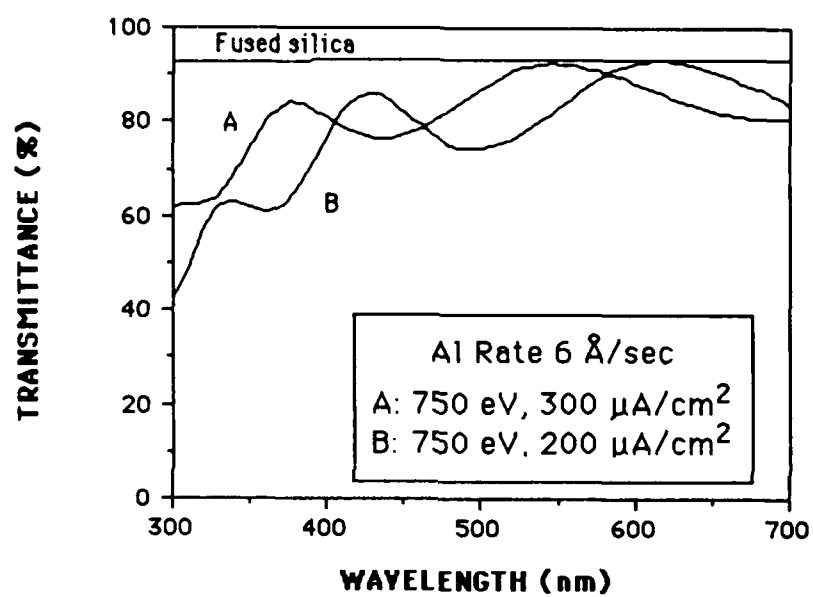


Figure 8-4. Transmittance of aluminum oxynitride films deposited by IAD.

Conclusions

Aluminum nitride thin films can be deposited by ion-assisted deposition; however, the diffusion and desorption of excess nitrogen observed for dual-beam ion sputtering is not evident with ion-assisted deposition. An excess of nitrogen is clearly present in many of the films. A nitrogen deficiency results in opaque conducting films, while a nitrogen excess produces insulating films with absorption in the visible. This absorption can be decreased by annealing in a predominantly nitrogen atmosphere at 500 °C, suggesting that the absorption is due to nitrogen vacancies, despite the excess of nitrogen in the films. Absorption is still present below 500 nm, but the films now possess a greatly increased transmittance in the near ultraviolet.

Aluminum oxynitride films can be deposited by adding oxygen to the chamber during deposition, probably allowing the deposition of films with refractive indices between those of Al_2O_3 and AlN . These films have significantly better optical properties than the nitride films.

CHAPTER 9

CONCLUSIONS

We have investigated the ion-assisted deposition of a wide range of materials. In virtually all cases, some film property was improved by IAD. It is also fair to say, however, that it is impossible to deposit by IAD the perfect film with unity packing density, low absorption, and exceptional environmental stability. The IAD process is a compromise of conditions to optimize coatings for a particular application.

Ion-Assisted Deposition of Metal Fluorides

While there are obviously differences in the effect of IAD on the various fluorides investigated, we can draw some very general conclusions:

- 1) The different masses and coordination numbers of the metal and fluorine atoms in the films result in a preferential sputtering of fluorine from the films. The IAD films are thus substoichiometric.
- 2) The vacancies in the film lattice created by the preferential sputtering are filled when possible with oxygen atoms or complexes (OH^- , for example) if the oxygen is available. The oxygen comes from the residual chamber pressure largely in the form of water vapor or, when oxygen ions are used, from oxygen ion implantation.
- 3) When sufficient oxygen is available to fill the anion vacancies, the films have negligible optical absorption in the visible spectrum. As the oxygen content increases, however, an ultraviolet absorption edge typical of the metal oxide appears.

4) When the preferential sputtering is so severe that there is no longer sufficient oxygen present to fill the anion vacancies, the films begin to absorb in the visible as well as the ultraviolet.

5) For materials which form crystalline films (in our case LaF_3 , CeF_3 , and NdF_3), the increasing oxygen content of the films eventually triggers a phase transition in some crystallites from the tysonite phase of the fluoride to the pseudo-fluorite phase of the oxyfluoride. As the stable oxyfluoride requires a larger oxygen content than that present in our films, individual crystallites with larger oxygen contents are apparently undergoing the phase transition. The similarity of the grain sizes of the fluoride and oxyfluoride phases also suggests that entire crystallites are being transformed.

6) Ion-assisted deposition increases the packing density of metal fluoride thin films. This densification has manifested itself in many film properties: increased density, decreased vacuum-to-air shifts and water absorption bands, and increased refractive index. These properties can often be improved almost to their optimal values, but often at the expense of absorption levels which may be unacceptable for some applications. The computer simulations of Müller (1986b) suggest that this densification is due to the recoil implantation of atoms from the surface of the growing film into the body of the film, where they fill vacancies. This conflicts with the earlier suggestions that the ion bombardment simply increased the mobility of condensing atoms, allowing them to migrate further before being trapped into the lattice.

7) The excessive tensile stress of the fluorides when deposited onto ambient temperature substrates is greatly reduced by IAD. We have not quantified this effect, but have observed that the critical thickness at which the coatings crack is significantly increased by ion bombardment.

8) When a Kaufman ion source is used, the hot filaments lead to heavy-metal contamination of the films. Using tungsten filaments, we have typically seen tungsten levels of 0.01-0.1 at. % in IAD films. These levels are too low to effect optical absorption, but McNally has shown (McNally 1986) that switching from tungsten to tantalum filaments significantly increased the laser damage threshold of 351 nm $\text{Al}_2\text{O}_3/\text{SiO}_2$ laser mirrors. For such applications, filamentless ion sources should therefore be considered.

Ion-Assisted Deposition of Aluminum Oxide

Aluminum oxide is a very unusual material. This is not surprising, since we chose to investigate it because of its unusual behavior in a previous study (Ebert 1982). For this reason, our conclusions concerning the ion-assisted deposition of aluminum oxide should not be extrapolated to other refractory oxides. This difference in behavior is most likely due to the unusually high packing density of Al_2O_3 films even when deposited onto ambient temperature substrates (Ogura 1975). We have deposited Al_2O_3 films by IAD using both argon and oxygen ions, reaching the following conclusions:

1) The optical properties of unbombarded Al_2O_3 films are strongly dependent on deposition conditions. We have observed an extremely strong dependence on oxygen pressure. The effect of IAD is in turn dependent on these process parameters.

2) Even our lowest index unbombarded films show no measurable vacuum-to-air shift, and have virtually no $3\text{ }\mu\text{m}$ water absorption band. The films are therefore very dense, even without IAD.

3) The refractive index of the Al_2O_3 films is increased by IAD. An index of 1.70 has been obtained at a wavelength of 350 nm, consistent with the values achieved by sputtering methods (Martin 1986). High index IAD films have been deposited under conditions which resulted in extremely low-index unbombarded films.

4) This increase in refractive index does not correlate with an increase in density. In fact, argon bombardment does not significantly alter the density of the films.

5) All of the Al_2O_3 films show no structure in x-ray diffraction: TEM shows that the films are indeed amorphous. The refractive index of 1.70 is presumably the value for a dense amorphous network with a packing density of one. If lower index films have near-unity packing densities and the index change is not due to changes in crystallinity, then the most logical explanation is that the films undergo a change in their amorphous networking. EXAFS analysis is currently underway to verify this hypothesis.

6) Argon ion bombardment increases the absorption of the films, but oxygen bombardment in general reduces the absorption if the unbombarded films made with the same deposition conditions have a measurable amount of absorption. In this way, oxygen

bombardment of oxides has a significant advantage, since the implanted oxygen can fill a vacancy in the Al_2O_3 network without the addition of an impurity.

7) The wire filaments in Kaufman ion sources have a short operating lifetime when operated with oxygen, due to the oxidation of the filaments. This limitation may make the traditional Kaufman source unacceptable for production of multilayer oxide designs. Cold cathode ion sources or the more recent filamentless Kaufman sources may be preferable in these circumstances.

Ion-Assisted Deposition of Aluminum Nitride

We have demonstrated that a nitride compound can be deposited by ion-assisted deposition by bombarding thermally evaporated aluminum with a nitrogen ion beam, with the following results:

1) Aluminum evaporated thermally in a nitrogen atmosphere shows no measurable nitrogen incorporation. Any nitrogen incorporated into the IAD films can probably be attributed to nitrogen ion implantation or ion-stimulated sorption, although it is possible that some of the plasma products from the ion source are more reactive than the neutral N_2 molecules.

2) Sufficient nitrogen can be incorporated into the films to make a stoichiometric nitride. In fact, the films just as easily exhibit N:Al ratios greater than 1.0, with stoichiometries above $\text{AlN}_{1.5}$ observed. This is rather surprising, since similar experiments with dual-beam sputtering (Harper, Hentzell, and Cuomo 1985) discovered a self-limiting stoichiometry effect which resulted in stoichiometric films

when the nitrogen-to-aluminum arrival rate became one or greater. This effect was attributed to the diffusion of excess nitrogen to the surface, followed by desorption. The only difference between the two experiments is the absence of energetic aluminum atoms in the IAD case, suggesting that the ion bombardment does not by itself supply enough energy to the films to promote nitrogen diffusion.

3) Substoichiometric films with a stoichiometry of approximately $\text{AlN}_{0.5}$ display a two-phase structure, with opaque and transparent regions on the order of several microns across alternating through the film. This suggests that the films do not nitridize uniformly. These films are dull gray to the naked eye; when the stoichiometry increases to the $\text{AlN}_{0.8}$ range, the films become a shiny gray.

4) Films with a stoichiometry of $\text{AlN}_{1.0}$ or greater are dielectric; however, they generally exhibit excessive absorption in the visible. Annealing at 500 °C reduces the absorption significantly, with the absorption edge now starting in the 400-500 nm wavelength range. This improvement is probably due to diffusion of interstitial nitrogen out of the film and/or the diffusion of oxygen into nitrogen vacancies in the films.

5) This project stretched the capabilities of a 3 cm Kaufman source. A larger source would be necessary to supply the required current densities over a large region for practical applications.

Suggestions for Further Research

Our group and others are now coming to grips with the details of ion-assisted deposition. In particular, the computer modelling of Karl Heinz Müller (1986a,

1986b) has greatly improved our understanding of the microscopic processes involved in IAD. However, there are still many important questions which remain to be addressed before the process is truly understood:

1) The majority of IAD work to date has been carried out with argon or oxygen ion bombardment, with the exception of Gibson and Kennemore's (1986) work with freon. There is great scope for experimentation; the use of other noble gases may verify the kinetic nature of the IAD process. Helium should be particularly interesting in this respect because its low mass will allow a comparative study over a wide range of ion momentums. Nitrogen is also interesting since it is not incorporated into fluorides to any significant degree. It can also be used to make gradient index layers in oxides. Finally, other fluorine compounds should be investigated.

2) Sputter yields are known to be highly angle dependent. We expect that the angle of ion incidence should also have a significant effect on the ability of the ions to cause recoil implantation into the film. It has recently been demonstrated (Yu et al. 1986) that preferred orientations of niobium films can be achieved by ion bombardment at certain angles of incidence. Similar effects may be observable with dielectric materials.

3) Ion-assisted deposition is well suited to the deposition of graded index structures, with the ion current density varied to modify the refractive index. Rugate filters are an obvious example.

4) Some binary systems, such as the vanadium oxides, have phases with different stoichiometries. Kelly and Naguib (1970) have shown that particular

crystalline phases can be driven by bombardment of bulk material--it may therefore be possible to deposit the preferred phases of binary systems by IAD

5) IAD with a rotating substrate has barely been investigated. If IAD is to become a viable commercial process, much work will be required in this area. In particular, the monitoring problem is difficult with bombardment of a planetary or double planetary rack since a monitor chip will not see the same ion beam as the substrates.

6) Filamentless Kaufman ion sources which can run indefinitely with oxygen are just coming onto the market. These sources will allow the deposition of multilayer oxide coatings with beam parameters not previously possible because of concern over the filament lifetime. Laser damage measurements should also be performed on coatings deposited with these sources to determine if the lower contamination levels lead to higher damage thresholds.

LIST OF ACRONYMS

CVD	Chemical Vapor Deposition
EXAFS	Extended X-Ray Absorption Fine Structure Spectroscopy
FTIR	Fourier Transform Infrared
IAD	Ion-Assisted Deposition
JCPDS	Joint Committee on Powder Diffraction Standards
PVD	Physical Vapor Deposition
RBS	Rutherford Backscattering Spectrometry
UV	Ultraviolet
TEM	Transmission Electron Microscopy
VUV	Vacuum Ultraviolet
XPS	X-Ray Photoelectron Spectroscopy
XRD	X-Ray Diffraction

LIST OF REFERENCES

- Allen, Thomas H. (1982) "Properties of Ion Assisted Deposited Silica and Titania Films," Proc. Soc. Photo-Opt. Instrum. Eng., Vol. 325, pp. 93-100.
- Allen, Thomas H. (1985) "Optical materials deposited using ion beam sputtering," J. Opt. Sci. Amer. A, Vol. 2, p. P92.
- Arndt, D. P., Azzam, R. M. A., Bennett, J. M., Borgogno, J. P., Carniglia, C. K., Case, W. E., Dobrowolski, J. A., Gibson, U. J., Hart, T. Tuttle, Ho, F. C., Hodgkin, V. A., Klapp, W. P., Macleod, H. A., Pelletier, E., Purvis, M. K., Quinn, D. M., Strome, D. H., Swenson, R., Temple, P. A., and Thonn, T. F. (1984) "Multiple determination of the optical constants of thin-film coating materials," Applied Optics, Vol. 23, pp. 3571-3596.
- Baumeister, Philip (1985) "Optical Coating Trivia," Optics News, Vol. 11, pp. 19,28.
- Betz, Gerhard and Wehner, Gottfried K. (1983) "Sputtering of Multicomponent Materials," in Behrisch, R., Editor, Sputtering by Particle Bombardment II, Springer-Verlag: Berlin.
- Biersack, J. P. and Eckstein, W. (1984) "Sputtering Studies with the Monte Carlo Program TRIM.SP," Appl. Phys. A, Vol. 34, pp. 73-94.
- Borgogno, J. P., Lazarides, B., and Pelletier, E. (1982) "Automatic determination of the optical constants of inhomogeneous thin films," Applied Optics, Vol. 21, pp. 4020-4029.
- Bourg, Marcel (1962) "Détermination de la Structure de Couches Minces Transparentes par des Méthodes Optiques; Étude Théorique de leur Formation," Ann. Phys., Vol. 7, pp. 623-658.
- Bradford, A. P., Hass, G., and McFarland, M. (1972) "Optical Properties of Evaporated Magnesium Oxide Films in the 0.22-8 μm Wavelength Region," Applied Optics, Vol. 11, pp. 2242-2244.
- Brinkman, John A. (1954) "On the Nature of Radiation Damage in Metals," J. Appl. Phys., Vol. 25, pp. 961-970.
- Catlow, C. R. A., James, R., and Norgett, M. J. (1976) "The Defect Structure of Compounds with the Rutile Structure," Journal de Physique, Vol. 37, Colloque C7, pp. 443-448.

Chu, Wei-Kan, Mayer, James W., and Nicolet, Marc-A. (1978) Backscattering Spectrometry, Academic Press: New York.

Dieke, Gerhard Heinrich (1968) Spectra and Energy Levels of Rare Earth Ions in Crystals, Interscience: New York.

Driscoll, Walter G., Editor (1978) Handbook of Optics, McGraw-Hill: New York, p. 7-94.

Ebert, J. (1982) "Activated Reactive Evaporation," Proc. Soc. Photo-Opt. Instrum. Eng., Vol. 325, pp. 29-38.

Garcia, Marie Frances (1986) "Three Techniques for Determining the Optical Constants of Dielectric Thin Films," Master's Thesis, University of Arizona.

Gibson, Ursula J. (1987) "Ion Beam Processing of Optical Thin Films," To be published in Vossen, J., Editor, Physics of Thin Films, Vol. 13, Academic Press: New York.

Gibson, U. J. and Kennemore III, C. M. (1986) "Ambient temperature deposition of MgF_2 with noble and chlorofluorocarbon ion assistance," Proc. Soc. Photo-Opt. Instrum. Eng., Vol. 678, pp. 130-133.

Greis, Ortwin, and Haschke, John M. (1982) "Rare Earth Fluorides," in Gschneidner, K. A. and Eyring, L., Editors, Handbook on the Physics and Chemistry of Rare Earths, North-Holland: Amsterdam.

Grigorov, G. I., and Martev, I. N. (1986) "Ion-Stimulated Sorption: An Ion-Assisted Technology with New Possibilities," Thin Solid Films, Vol. 143, pp. 177-185.

Guenther, K. H., and Pulker, H. K. (1976) "Electron microscopic investigations of cross sections of optical thin films," Applied Optics, Vol. 15, pp. 2992-2997.

Hacman, D. (1970) "Optical and partial pressure analysis during deposition of MgF_2 films in ultra high vacuum," Optica Acta, Vol. 17, pp. 659-666.

Harper, James M. E., Cuomo, Jerome J., Gambino, Richard J., and Kaufman, Harold R. (1984) "Modification of Thin Film Properties by Ion Bombardment During Deposition," in Auciello, Orlando and Kelly, Roger, Editors, Ion Bombardment Modification of Surfaces, Elsevier: Amsterdam.

Harper, J. M. E., Cuomo, J. J., and Hentzell, H. T. G. (1985) "Synthesis of compound thin films by dual ion beam deposition. I. Experimental approach," J. Appl. Phys., Vol. 58, pp. 550-555.

Hass, G., Ramsey, J. B., and Thun, R. (1959) "Optical Properties of Various Evaporated Rare Earth Oxides and Fluorides," J. Opt. Soc. Amer., Vol. 49, pp. 116-120.

Heaps, Wm. S., Elias, L. R., and Yen, W. M. (1976) "Vacuum-ultraviolet absorption bands of trivalent lanthanides in LaF_3 ," Phys. Rev. B, Vol. 13, pp. 94-104.

Heitmann, Walter (1970) "Vacuum Evaporated Films of Aluminum Fluoride," Thin Solid Films, Vol. 5, pp. 61-67.

Herrmann Jr., W. C. and McNeil, J. R. (1982) "Ion Beam Applications for Optical Coating," Proc. Soc. Photo-Opt. Instrum. Eng., Vol. 325, pp. 101-104.

Holmes, Sam (1986) "Ion Beam Sputtering for Optical Coatings," Proc. Soc. of Vacuum Coaters 29th Annual Technical Conference, pp. 11-24.

Hirsch, E. H. and Varga, I. K. (1978) "The Effect of Ion Irradiation on the Adherence of Germanium Films," Thin Solid Films, Vol. 52, pp. 445-452.

Hirsch, E. H. and Varga, I. K. (1980) "Thin Film Annealing by Ion Bombardment," Thin Solid Films, Vol. 69, pp. 99-105.

Jacobs, S. D., Hrycin, A. L., Cerqua, K. A., Kennemore III, C. M., and Gibson, U. J. (1986) "Adhesion Enhancements and Internal Stress in MgF_2 Films Deposited with Ion Beam Assistance," Thin Solid Films, Vol. 144, pp. 69-76.

Jacobson, Michael Ray (1987) Coating, Monitoring, and Anti-Contamination Techniques, Society of Photo-Opt. Instrum. Eng. Short Course Notes.

Jacobsson, R. (1975) "Inhomogeneous and coevaporated homogeneous films for optical applications," Physics of Thin Films, Vol. 8, p. 51.

Joint Committee on Powder Diffraction Standards (JCPDS) (1976) Inorganic File, American Society for Testing and Materials: Swarthmore, Pa.

Kaufman, H. R., Cuomo, J. J. and Harper, J. M. E. (1982) "Technology and applications of broad-beam ion sources used in sputtering: Part I. Ion source technology," J. Vac. Sci. Technol., Vol. 21, pp. 725-736.

Kaufman, Harold R. (1984) Fundamentals of Ion-Source Operation, Commonwealth Scientific Corporation: Alexandria, Va.

Kennemore III, Charles M. and Gibson, Ursula J. (1984) "Ion beam processing for coating MgF_2 onto ambient temperature substrates," *Applied Optics*, Vol. 23, pp. 3608-3611.

Kinosita, Koreo, and Nishibori, Mineo (1969) "Porosity of MgF_2 Films--Evaluation based on Changes in Refractive Index due to Adsorption of Vapors," *J. Vac. Sci. Technol.*, Vol. 6, pp. 730-733 (1969).

Kittel, Charles (1976) Introduction to Solid State Physics, Wiley: New York.

Klein, Miles V. (1970) Optics, Wiley: New York.

Koshigoe, L. G., Johnson, L. F., Donovan, T. M., and Marrs, C. D. (1984) "Characterization of Aluminum Nitride/Aluminum Oxide Reactively Sputtered Antireflection Coatings," in Laser Induced Damage in Optical Materials: 1984, NBS Spec. Pub. 727, pp. 233-252.

Laiho, R., and Lakkisto, M. (1983) "Investigation of the refractive indices of LaF_3 , CeF_3 , PrF_3 , and NdF_3 ," *Philosophical Magazine B*, Vol. 48, pp. 203-207.

Langford, J. I. and Wilson, A. J. C. (1978) "Scherrer after sixty Years: A survey and Some New Results in the Determination of Crystallite Size," *J. Appl. Cryst.*, Vol. 11, pp. 102-113.

Lauer, James L., and Miller Jr., P. H. (1947) "An Instrument for the Measurement of the Index of Refraction of Liquids in the Wavelength Range 200 $\text{m}\mu$ to 1000 $\text{m}\mu$," *J. Opt. Soc. Amer.*, Vol. 37, p. 664.

Lieske, N. and Hezel, R. (1981) "Formation of Al-nitride films at room temperature by nitrogen ion implantation into aluminum," *J. Appl. Phys.*, Vol. 52, pp. 5806-5810.

Lingg, L. J., Targove, J. D., Weng, C. C., and Jacobson, M. R. (1986) "Rare Earth Fluorides for Ultraviolet Coatings," *J. Opt. Soc. Amer. A*, Vol. 3, p. P20.

Macleod, H. A. (1982) "Microstructure of optical thin films," *Proc. Soc. Photo-Opt. Instrum. Eng.*, Vol. 325, pp. 21-28.

Macleod, H. A. (1986) "Ion and photon-beam assisted deposition of thin films," *Proc. Soc. Photo-Instrum. Eng.*, Vol. 652, pp. 222-234.

Malitson, I. H. (1965) "Interspecimen Comparison of the Refractive Index of Fused Silica," *J. Opt. Soc. Amer.*, Vol. 55, pp. 1205-1209.

Manifacier, J. C., Gasiot, J., and Fillard, J. P. (1976) "A simple Method for the Determination of the Optical Constants N , k and the Thickness of a Weakly Absorbing Thin Film," J. Phys. E, Vol. 9, pp. 1002-1003.

Martin, P. J. (1986) "Ion-based methods for optical thin film deposition," J. Mat. Sci., Vol. 21, pp. 1-25.

Martin, P. J., Macleod, H. A., Netterfield, R. P., Pacey, C. G. and Sainty, W. G. (1983) "Ion-Beam-Assisted Deposition of Thin Films," Applied Optics, Vol. 22, pp. 178-184.

Martin, Philip J. and Netterfield, Roger P. (1985) "Ion assisted deposition of magnesium fluoride films on substrates at ambient temperature," Applied Optics, Vol. 24, pp. 1732-1733.

Martin, P. J. and Netterfield, R. P. (1986) "Optical Films Produced by Ion-based Techniques," in E. Wolf, Editor, Progress in Optics XXIII, Elsevier: Amsterdam.

Martin, P. J., Netterfield, R. P., and Sainty, W. G. (1984a) "Modification of the optical and structural properties of dielectric ZrO_2 films by ion-assisted deposition," J. Appl. Phys., Vol. 55, pp. 235-241.

Martin, P. J., Netterfield, R. P., Sainty, W. G. and Pacey, C. G. (1984b) "The preparation and characterization of optical thin films produced by ion-assisted deposition," J. Vac. Sci. Technol. A., Vol. 2, pp. 341-345.

Martin, Philip J., Sainty, Wayne G., Netterfield, Roger P., McKenzie, David R., Cockayne, David J. H., Sie, Soey H., Wood, Obert R., and Craighead, Harold G. (1987) "Influence of ion assistance on the optical properties of MgF_2 ," Applied Optics, Vol. 26, pp. 1235-1239.

McNally, James J., Williams, F. L., and McNeil, J. R. (1986) "Properties of optical thin films deposited using ion-assisted deposition," Proc. Soc. Photo-Opt. Instrum. Eng., Vol. 678, pp. 151-160.

McNally, James J. (1986) University of New Mexico, Private Communication.

McNeil, John R., Al-Jumaily, G. A., Jungling, K. C., and Barron, A. C. (1985) "Properties of TiO_2 and SiO_2 thin films deposited using ion assisted deposition," Applied Optics, Vol. 24, pp. 486-489.

McNeil, John R., Barron, Alan C., Wilson, S. R. and Herrmann Jr., W. C. (1984) "Ion-Assisted Deposition of Optical Thin Films: Low Energy vs High Energy Bombardment," Applied Optics, Vol. 23, pp. 552-559.

Messerly, Michael J. (1987) "Ion-Beam Analysis of Optical Coatings," Ph. D. Dissertation, University of Arizona.

Movchan, B. A. and Demchishin, A. V. (1969) "Study of the Structure and Properties of Thick Vacuum Condensates of Nickel, Titanium, Tungsten, Aluminum Oxide and Zirconium Dioxide," *Fiz. Metal Metalloved*, Vol. 28, pp. 653-660.

Müller, Karl-Heinz (1986b) "Model for ion-assisted thin film densification," *J. Appl. Phys.*, Vol. 59, pp. 2803-2807.

Müller, Karl-Heinz (1986a) "Monte Carlo calculation for structural modifications in ion-assisted thin film deposition due to thermal spikes," *J. Vac. Sci. Technol. A*, vol. 4, pp. 184-188.

Naguib, H. M., and Kelly, Roger (1970) "The Crystallization of Amorphous ZrO_2 by Thermal Heating and by Ion Bombardment," *J. Nuc. Mat.*, Vol. 35, pp. 293-305.

Netterfield, R. P. (1986) "Ion-assisted processes in thin-film deposition," *Proc. Soc. Photo-Opt. Instrum. Eng.*, Vol. 678, pp. 14-23.

Netterfield, Roger P., Sainty, W. G., Martin, P. J., and Sie, S. H. (1985) "Properties of CeO_2 thin films prepared by oxygen-ion-assisted deposition," *Applied Optics*, Vol. 24, pp. 2267-2272.

Netterfield, R. P., Martin, P. J., and Sainty, W. G. (1986) "Synthesis of silicon nitride and silicon oxide films by ion-assisted deposition," *Applied Optics*, Vol. 25, pp. 3808-3809.

Noreika, A. J., and Ing, D. W. (1968) "Growth Characteristics of AlN Films Pyrolytically Deposited on Si," *J. Appl. Phys.*, Vol. 39, pp. 5578-5581.

Ogura, S. (1975) "Some Features of the Behaviour of Optical Thin Films," Ph. D. Thesis, Newcastle upon Tyne Polytechnic.

Pawlewicz, W. T., Martin, P. M., Knoll, R. W., and Mann, I. B. (1968) "Multilayer optical coating fabrication by dc magnetron reactive sputtering," *Proc. Photo-Opt. Instrum. Eng.*, Vol. 678, pp. 134-140.

Pelletier, Emile (1985) University of Aix-Marseilles III, Private Communication.

Pulker, H. K. (1979) "Characterization of Optical Thin Films," *Applied Optics*, Vol. 18, pp. 1969-1977.

Pulker, Hans K. (1982) "Stress, adherence, hardness, and density of optical thin films," Proc. Soc. Photo-Opt. Instrum. Eng., Vol. 325, pp. 84-92.

Pulker, H. K., and Zaminer Ch. (1970) "Composition and Structure of Vapour-Deposited Cryolite Films," Thin Solid Films, Vol. 5, pp. 421-428.

Rainer, Frank, Lowdermilk, W. Howard, Milam, David, Carniglia, Charles K., Hart, Trudy Tuttle, and Lichtenstein, Terri L. (1985) "Materials for optical coatings in the ultraviolet," Applied Optics, Vol. 24, pp. 496-500.

Ritter, Elmar (1976) "Optical film materials and their applications," Applied Optics, Vol. 15, pp. 2318-2327.

Saxe, Steven Gary (1986) "Ion-Induced Processes in Optical Coatings," Ph. D. Dissertation, University of Arizona.

Seitz, Frederick, and Koehler, J. S. (1956) Solid State Physics, Vol. 2, p. 307.

Sibley, W. A., and Facey, O. E. (1968) "Color Centers in MgF_2 ," Phys. Rev., Vol. 174, pp. 1076-1082.

Sigmund, Peter (1969) "Theory of Sputtering. I. Sputtering Yield of Amorphous and Polycrystalline Targets," Phys. Rev., vol. 184, pp. 383-416.

Sigmund, Peter (1981) "Sputtering by Ion Bombardment: Theoretical Concepts," in Behrisch, R., Editor, Sputtering by Particle Bombardment I, Springer-Verlag: New York.

Sigmund, P. and Claussen, C. (1981) "Sputtering from elastic-collision spikes in heavy-ion-bombarded metals," J. Appl. Phys, Vol. 52, pp. 990-993.

Smith, David and Baumeister, Philip (1979) "Refractive Index of some Oxide and Fluoride Coating Materials," Applied Optics, Vol. 18, pp. 111-115.

Suits, Frank (1987) University of Arizona, Private Communication.

Swenson, Rick (1987) University of Arizona, Private Communication.

Targove, James D., Lehan, John P., Lingg, Linda J., Macleod, H. Angus, Leavitt, J. A., and McIntyre Jr., L. C. (1987) "Ion-assisted deposition of lanthanum fluoride thin films," To be published in Applied Optics.

Thornton, John A. (1974) "Influence of apparatus geometry and deposition conditions on the structure and topography of thick sputtered coatings," J. Vac. Sci. Technol., Vol. 11, pp. 666-670.

Townsend, P. D., Kelly, J. C., and Hartley, N. E. W. (1976) Ion Implantation, Sputtering, and their Applications, Academic Press: New York.

Van Milligen, Fred J., Bovard, Bertrand, Jacobson, Michael R., Mueller, James, Potoff, Ross, Shoemaker, Richard L., and Macleod, H. Angus (1985) "Development of an automated scanning monochromator for monitoring thin films," Applied Optics," Vol. 24, pp. 1799-1802.

Van Vechten, D., Hubler, G. K., and Donovan, E. P. (1986) "Characterization of a 3 cm Kaufman ion source with nitrogen feed gas," Vacuum, Vol. 36, pp. 841-845.

Weast, Robert C., Editor (1978) CRC Handbook of Chemistry and Physics, CRC Press: West Palm Beach.

Yu, Lock See, Harper, James M. E., Cuomo, Jerome J., and Smith, David A. (1986) "Control of thin film orientation by glancing angle ion bombardment during growth," J. Vac. Sci. Technol. A, Vol. 4, pp. 443-447.

Zachariasen, W. H. (1951) "Crystal Chemical Studies of the 5f-series of Elements. XIV. Oxyfluorides, XOF," Acta Cryst., Vol. 4, pp. 231-236.